# Investigation and evaluation of neuroprotective and regenerative strategies in experimental models of Multiple Sclerosis

Inaugural-Dissertation

zur Erlangung des Doktorgrades der Mathematisch-Naturwissenschaftlichen Fakultät der Heinrich-Heine-Universität Düsseldorf

Vorgelegt von

**Mustafa Sindi** 

aus Bedburg

Düsseldorf, 22.01.2025

Aus der Klinik für Neurologie und des Instituts für Molekulare Medizin III des Universitätsklinikums Düsseldorf

Gedruckt mit der Genehmigung der Mathematisch-
Naturwissenschaftlichen Fakultät der Heinrich-Heine-Universität
Berichterstatter:
Prof. Dr. Philipp Albrecht
Prof. Dr. Bodo Levkau
Tag der mündlichen Prüfung: 16.09.2025

# **Table of Contents/Inhaltsverzeichnis**

Su	mma	ary			
Zu	samı	menfassung			
1.	Introduction				
,	1.1.	Multiple sclerosis	1		
•	1.2.	Translational MS models	2		
•	1.3.	Readout methodology	3		
,	1.4.	Aims of the thesis	5		
2.	Pul	blications as first author	6		
3.	Dis	scussion	7		
	3.1. of ch	.1. Longitudinal, translational in-vivo readouts of the visual system and models f choice			
,	3.2.	A multifaceted disease requires multifaceted therapeutically strategies	8		
,	3.3.	Future directions in the field of MS therapeutic interventions	10		
4.	Oth	her publications	13		
4	4.1.	Publications as co-author	13		
4	4.2.	Review articles publications as first author	13		
5.	Ref	ferences	14		
6.	Appendix20				
7.	Acknowledgement/Danksagung22				
8.	Declaration/Erklärung23				

# **Summary**

This thesis focuses on neuroprotective and regenerative strategies in experimental models of Multiple Sclerosis (MS), a complex autoimmune disease characterized by demyelination, axonal damage, and neuronal loss, affecting approximately 2.8 million people globally. This research aims to address the limitations of current disease-modifying therapies (DMTs), which, while effective in modulating immune responses and reducing relapse rates, do not halt disease progression or reverse existing neurological damage.

Utilizing rodent models, the study explores novel neuroprotective strategies within inflammatory (EAE), degenerative (LI-PRL), and demyelinating (Cuprizone) contexts. These models provide a comprehensive analysis of the disease's multifaceted nature, encompassing inflammation, degeneration, and demyelination. Key methodologies include Optical Coherence Tomography (OCT), Optomotor Response (OMR), and Confocal Scanning Laser Ophthalmoscopy (cSLO), which facilitate longitudinal, non-invasive assessments correlating well with clinical, histological, immunological, and molecular evaluations.

The research investigates several promising neuroprotective agents: a selective agonist of S1P1 and S1P5 receptors, an AMPA-positive allosteric modulator (AMPA-PAM), MAO-B inhibitors, and sodium channel blockers. Notably, the S1PR-1/5 modulator RP-101074 demonstrated significant neuroprotective effects in a model of central nervous system degeneration, with an intermediate dose offering pronounced protection against visual function loss, indicating potential benefits beyond immunomodulation, including neural protection. The AMPA-PAM PF4778574 mitigated clinical disability and reduced demyelination. However, it did not affect microglial activity, suggesting limited anti-inflammatory effects. Furthermore, sodium channel blockers, particularly flecainide, showed beneficial outcomes in enhancing blood-brain barrier (BBB) integrity and reducing lymphocyte infiltration into the CNS.

Overall, this work underscores the necessity of a multifaceted therapeutic approach for MS, combining immunomodulation with strategies that promote neuroprotection, remyelination, and regeneration. These findings significantly contribute to the understanding of neuroprotective interventions in MS and emphasize the importance of continued research to develop treatments addressing both the inflammatory and neurodegenerative aspects of the disease, ultimately aiming to improve the quality of life for patients with MS.

# Zusammenfassung

Diese Arbeit widmet sich neuroprotektiven und regenerativen Strategien in experimentellen Modellen der Multiplen Sklerose (MS), einer komplexen Autoimmunerkrankung, die durch Demyelinisierung, axonale Schädigungen und neuronalen Verlust gekennzeichnet ist und weltweit etwa 2,8 Millionen Menschen betrifft. Ziel dieser Arbeit ist es gewesen, die Limitationen der aktuellen krankheitsmodifizierenden Therapien, so genannten DMTs, zu einem gewissen Grad entgegenzuwirken. Die bereits zugelassenen Therapien sind zwar effektiv in der Modulation der Immunantwort bzw. Depletion überschießender Immunzellen, und somit der Reduktion der Rückfallrate, verhindern jedoch nicht gänzlich das Fortschreiten der Erkrankung und können bestehende neurologische Schäden nicht rückgängig machen.

In den folgend erläuterten Experimenten verwendeten wir MS Mausmodelle, um neuartige neuroprotektive Strategien in verschiedenen Zuständen der Erkrankung zu erforschen: in entzündlichen (EAE), degenerativen (LI-PRL) und demyelinisierenden (Cuprizone) Modellen. Diese Modelle ermöglichen eine umfassende Evaluation der vielschichtigen Ausprägungen dieser Erkrankung, die Aspekte wie Entzündung, Degeneration und Demyelinisierung umfasst. Wichtige Evaluationsmethoden beinhalten die Optische Kohärenztomographie (OCT), die Optomotorische Reaktion (OMR) und die Konfokale Scanning Laser Ophthalmoskopie (cSLO), allesamt Modelle des visuellen Systems. Diese nicht-invasiven, longitudinalen Untersuchungsmethoden korrelieren gut mit klinischen, histologischen, immunologischen und molekularen Analysen.

Untersucht werden mehrere vielversprechende neuroprotektive Substanzen: selektive Agonisten der S1P1- und S1P5-Rezeptoren, AMPA-positive allosterische Modulatoren (AMPA-PAM), MAO-B-Hemmer und Natriumkanalblocker. Besonders hervorzuheben ist der S1PR-1/5-Modulator RP-101074, der in einem Modell der zentralnervösen Degeneration signifikante neuroprotektive Effekte zeigte. Eine mittlere Dosis bot dabei einen ausgeprägten Schutz gegen den Verlust der Sehfunktion und deutet somit auf mögliche Vorteile über die Immunmodulation hinaus hin, einschließlich neuronaler Schutzmechanismen. Der AMPA-PAM PF4778574 reduzierte die klinische Behinderung und die Demyelinisierung, beeinflusste jedoch nicht die Aktivität der Mikroglia, was auf begrenzte entzündungshemmende Effekte hinweist. Zudem zeigten Natriumkanalblocker, insbesondere Flecainid, positive Effekte auf den klinischen Verlauf der EAE, was laut unseren Analysen höchstwahrscheinlich auf einen

Effekt auf die Integrität der Blut-Hirn-Schranke und damit verbunden auf eine reduzierte Lymphozyteninfiltration in das zentrale Nervensystem zurückzuführen ist.

Insgesamt betont diese Arbeit die Notwendigkeit eines vielschichtigen therapeutischen Ansatzes bei MS, der die Immunmodulation bzw. Depletion mit Strategien kombiniert, die Neuroprotektion, Remyelinisierung und/oder Regeneration fördern. Die gewonnenen Erkenntnisse dieser Arbeit tragen wesentlich zum Verständnis neuroprotektiver Interventionen bei MS bei und unterstreichen die Bedeutung fortlaufender Forschung, um Behandlungen zu entwickeln, die sowohl die entzündlichen als auch die neurodegenerativen Aspekte der Erkrankung adressieren, mit dem Ziel, die Lebensqualität der Patienten zu verbessern.

# 1. Introduction

# 1.1. Multiple sclerosis

Multiple sclerosis (MS) is an autoimmune disorder characterized by demyelination, which leads to axonal damage and subsequent neuronal loss. Affecting approximately 2.8 million people globally (Walton et al., 2020), the etiology of MS remains incompletely understood. MS symptoms encompass a broad spectrum due to the diverse areas of the central nervous system it can affect. Common symptoms include fatigue, walking difficulties, numbness or tingling, muscle weakness, spasticity, vision problems such as optic neuritis and double vision, and bladder and bowel dysfunction. Cognitive impairments, including difficulties with memory, attention, and processing speed, are also prevalent. Additionally, MS can lead to emotional changes, such as depression and anxiety, and less commonly, speech and swallowing difficulties, tremor, seizures, and breathing problems. The variability and unpredictability of these symptoms make MS a particularly challenging condition to manage. Potential causes include genetic predisposition, environmental factors, and infectious agents, among others (Disanto et al., 2012). MS manifests in various forms, namely relapsing-remitting MS (RRMS), secondary progressive MS (SPMS), primary progressive MS (PPMS), and progressiverelapsing MS (PRMS). In recent years, numerous disease-modifying therapies (DMTs) have been approved for the treatment of MS (Edinger & Habibi, 2024). Despite the efficacy of these DMTs in modulating immune responses and reducing relapse rates, they fall short in halting overall disease progression and relapse-independent disability progression (Manouchehri et al., 2022). Additionally, they do not reverse existing neurological damage. Therefore, there is an urgent need for neuroprotective and regenerative therapies to address these unmet clinical challenges.

The pathology of MS begins with an autoimmune reaction wherein autoreactive T cells, activated in the periphery to a yet unidentified antigens, proliferate and differentiate into effector T cells, preparing the immune system for an attack (Liu et al., 2022; Markovic-Plese et al., 2004). Upon activation, these cells traverse the blood-brain barrier (BBB), a critical step facilitated by the upregulation of adhesion molecules on the endothelial cells of the BBB and the secretion of matrix metalloproteinases (MMPs) that degrade the BBB's extracellular matrix components (Buhler et al., 2009; Guo et al., 2004; Werner et al., 2008). Once within the central nervous system (CNS), these T cells re-encounter their specific antigens presented by antigen-

presenting cells (APCs) such as microglia and macrophages, leading to further activation and proliferation (Szpakowski et al., 2021). This immune activation results in the release of proinflammatory cytokines, chemokines, and other mediators, creating an inflammatory milieu. In this environment, B cells also play a crucial role, producing antibodies against myelin components, thereby exacerbating the immune attack (Nikbin et al., 2007). The inflammatory process targets the myelin sheath, leading to demyelination. This stripping of myelin disrupts the normal saltatory conduction of electrical impulses along axons, resulting in conduction block or slowed nerve transmission, which manifests as the various neurological symptoms of MS (Smith & McDonald, 1999). Additionally, chronic inflammation leads to the formation of sclerotic plaques and direct axonal damage, contributing to neurodegeneration (Haines et al., 2011; Kaufmann et al., 2022; Popescu et al., 2013). The loss of myelin and subsequent axonal injury culminate in a progressive loss of neuronal conductivity and overall neuronal death, further impairing CNS function. This complex interplay of immune-mediated damage, inflammation, and neurodegeneration underpins the multifaceted and debilitating nature of MS (Hauser & Oksenberg, 2006).

# 1.2. Translational MS models

To study various aspects of MS, researchers utilize a multitude of models, primarily in rodents. For investigating the primary inflammatory components of the disease, experimental autoimmune encephalomyelitis (EAE) is a widely used model. Active EAE can be induced using different myelin proteins, with specific combinations for different strains such as (Terry et al., 2016): C57BL/6 mice can be induced with MOG or PLP (Mendel et al., 1995; Tompkins et al., 2002), SJL/J mice with PLP or MBP (Greer et al., 1996; L. J. Tan et al., 1992), BALB/c mice with PLP (Lyons et al., 2002), Lewis rats with MBP (Shin et al., 2012), Brown Norway rats with MOG (Stefferl et al., 1999), Sprague Dawley rats with MOG (Kwilasz et al., 2022), and Dark Aguti rats with spinal cord homogenate (STOSIC-GRUJICIC et al., 2004). Passive EAE is another approach, involving the adoptive transfer of myelin-specific lymphocytes into various mouse or rat strains (McPherson et al., 2014). This model helps in studying immune cell behavior and interaction in the absence of the initial sensitizing antigen. Genetic or spontaneous EAE models provide insights into hereditary and spontaneous autoimmune responses. The 2D2/C57BL/6 mouse has a MOG-specific T-cell receptor (TCR), while the 2D2xTH C57BL/6 mouse combines MOG-specific TCR (2D2) and MOG-specific B cell

receptor (TH). The 2D2/SJL/J mouse has a MOG-specific TCR in the SJL/J strain. Additionally, the T/R+ H-2u mouse has an MBP-specific TCR, the HLA-DR15 + MBP-TCR model expresses human HLA-DR15 and MBP-specific TCR, and the PLPmut C57BL/6 mouse is a transgenic model with a human PLP1 mutation (Glatigny & Bettelli, 2018). To explore the demyelination and remyelination processes, models like the cuprizone model are extensively used. Cuprizone, a copper chelator, induces reversible demyelination in rodents. Other demyelination models include the lysolecithin injection model, causing focal demyelination via lysolecithin injection, and the ethidium bromide model, which similarly induces local demyelination through toxin injection. For studying neurodegeneration without primary immune involvement, models such as the light-induced photoreceptor loss (LI-PRL) and optic nerve crush (ON-Crush) are employed. These models focus on specific neuronal populations and axonal injury, respectively, facilitating the study of neurodegenerative and direct neuroprotective mechanisms and potential therapeutic strategies. Each of these models offers unique insights into different facets of MS, enabling a comprehensive understanding of the disease and the development of targeted treatments (Dedoni et al., 2023).

# 1.3. Readout methodology

Crucial for preclinical evaluation methodology is the use of readout methods that are easily transferable to clinical settings, straightforward to apply, and efficient. In this context, we utilize the visual system as a gate to other parts of the CNS such as the brain and spinal cord. It allows non-invasive, longitudinal evaluation with minimal stress and provides a reliable prediction of the CNS condition, correlating well with general CNS pathology, as supported by numerous recent publications (Albrecht et al., 2012; Dietrich et al., 2019; Krämer et al., 2024). Our primary readout method is optical coherence tomography (OCT). OCT is a non-invasive imaging technique that captures high-resolution cross-sectional images of retinal structures. It provides detailed visualization of the retinal nerve fiber layer (RNFL) and ganglion cell layer (GCL), essential for detecting neurodegenerative changes. Human and rodent OCT are translationally relevant; the anatomical and functional similarities allow for the extrapolation of preclinical findings to human conditions, making OCT a robust tool for both research and clinical diagnostics. This method's ability to monitor disease progression and therapeutic responses makes it a logic choice for preclinical MS research.

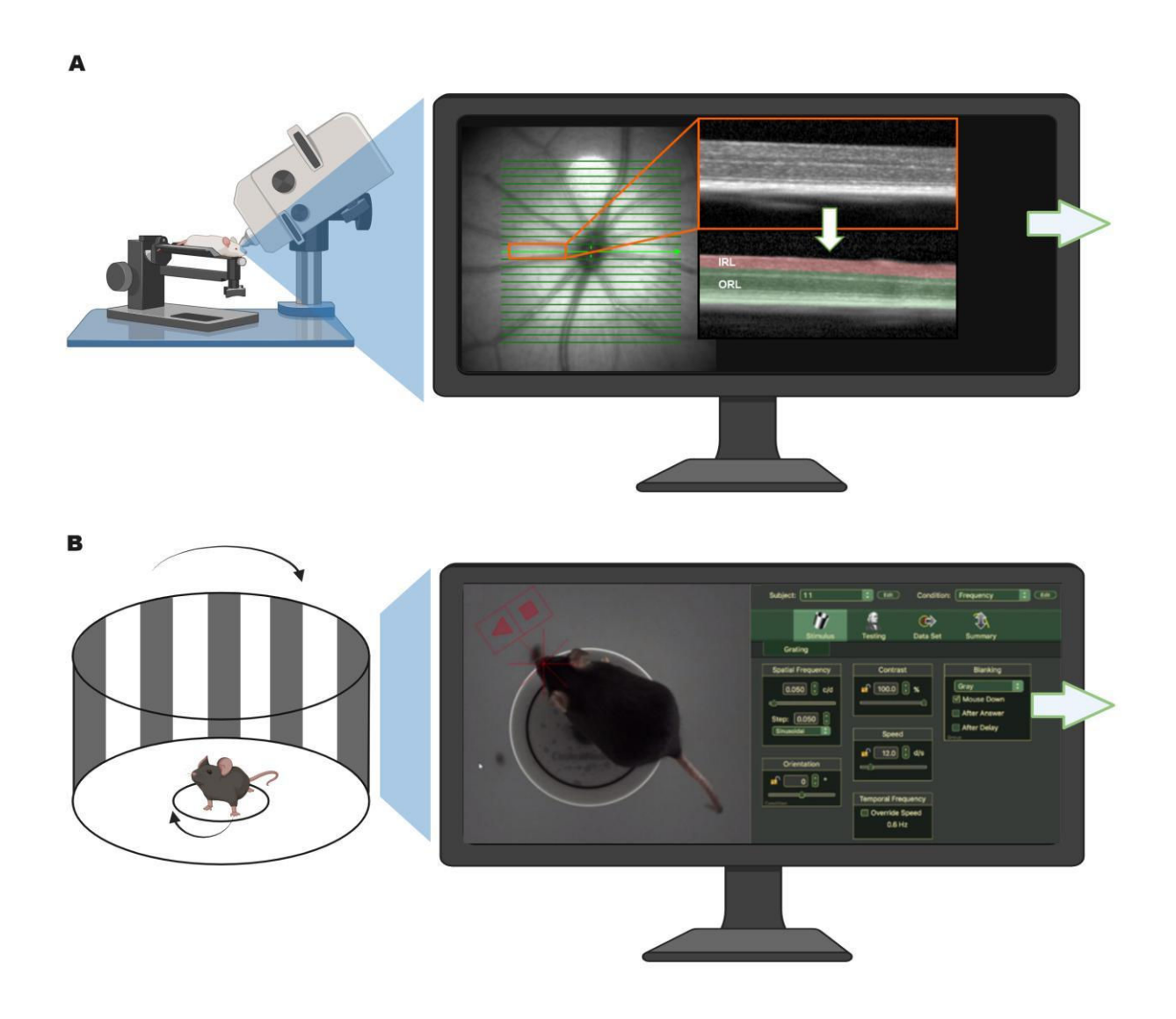


**Figure 1: Sketch of OCT and OMR Measurement Apparatuses.** (A) Schematic view of an OCT measurement with the primary output of a retinal cross-section, followed by machine segmentation of the inner retinal layers (IRL) and outer retinal layers (ORL). (B) Schematic representation of an OMR measurement with the depiction of the measurement software used to determine the contrast threshold. Created with BioRender.com

Further, we utilize the optomotor response (OMR) as a key method to evaluate on a functional level. OMR is a non-invasive behavioral assay that assesses visual acuity and contrast sensitivity by measuring an animal's reflexive head and neck movements in response to moving visual stimuli (Hecker et al., 2020). OMR's translational relevance lies in its simplicity and efficiency. It provides valuable insights into the functional integrity of the visual system, correlating well with CNS pathology (Hecker et al., 2020). The findings from OMR in rodent models can be extrapolated to human visual acuity and/or contrast sensitivity testing, facilitating the development of therapeutic interventions and monitoring disease progression.

The ease of application and the ability to conduct longitudinal studies make OMR a powerful addition to OCT readouts.

# 1.4. Aims of the thesis

The aim of this thesis was to evaluate strategies for neuroprotection in MS, focusing on the degenerative processes that lead to ongoing clinical disability and are unresponsive to standard immunosuppressive and most immunomodulatory treatments. By utilizing rodent models of MS, specifically the inflammatory (EAE), degenerative (LI-PRL), and demyelinating (Cuprizone) models, this research aimed to evaluate the efficacy of these novel strategies. We employed translational longitudinal in vivo readout methods such as OCT, OMR and cSLO, alongside ex vivo analyses including Blood-Brain Barrier (BBB) permeability assays, immune phenotyping by flow cytometry, gene expression analyses by qPCR and histological evaluation of neuronal, immune, and myelination markers. Using these comprehensive approaches, we aimed to advance our understanding of neuroprotective interventions in MS.

# 2. Publications as first author

Sindi, M., Hecker, C., Issberner, A., Ruck, T., Meuth, S. G., Albrecht, P., & Dietrich, M. (2023). S1PR-1/5 modulator RP-101074 shows beneficial effects in a model of central nervous system degeneration. Frontiers in Immunology, 14, 1234984. https://doi.org/10.3389/fimmu.2023.1234984

**Status: Published** 

**Contribution to the work:** First authorship, Study design, performing most of the in vivo and in vitro experiments, analyzing the data, creating the graphs, writing the manuscript.

Sindi, M., Dietrich, M., Klees, D., Gruchot, J., Hecker, C., Silbereis, J., Issberner, A., Hartung, H.-P., Ruck, T., Stark, H., Kurz, T., Küry, P., Meuth, S. G., & Albrecht, P. (2025). Positive allosteric modulation of AMPA receptors via PF4778574 leads to reduced demyelination and clinical disability in experimental models of multiple sclerosis. Frontiers in Immunology, 16. https://doi.org/10.3389/fimmu.2025.1532877

Status: Published

**Contribution to the work:** First authorship, Study design, performing most of the in vivo and in vitro experiments, analyzing the data, creating the graphs, writing the manuscript.

Sindi, M., Klees, D., Dobelmann, V., Disse, P., Weigel, H., Lichtenberg, S., Ricci, R., Thewes, L., Deniz-Köseoglu, G., Hecker, C., Müntefering, T., Issberner, A., Gruchot, J., Hartung, H.-P., Ruck, T., Berndt, C., Kurz, T., Stark, H., Küry, P., ... Albrecht, P. (2025). Flecainide mediated sodium channel blockade enhances blood brain barrier integrity and promotes neuroprotection in neuroinflammation. Scientific Reports, 15(1), 31032. https://doi.org/10.1038/s41598-025-15430-w

**Status: Published** 

**Contribution to the work:** First authorship, Study design, performing most of the in vivo and in vitro experiments, analyzing the data, creating the graphs, writing the manuscript.

6



### **OPEN ACCESS**

EDITED BY Ingo Kleiter, Marianne-Strauss-Klinik, Germany

REVIEWED BY Volker Siffrin, Charité University Medicine Berlin, Germany Sabrina Reinehr, Ruhr-University Bochum, Germany

\*CORRESPONDENCE
Philipp Albrecht

phil.albrecht@gmail.com

<sup>†</sup>These authors have contributed equally to this work and share senior authorship

RECEIVED 05 June 2023 ACCEPTED 18 July 2023 PUBLISHED 09 August 2023

### CITATION

Sindi M, Hecker C, Issberner A, Ruck T, Meuth SG, Albrecht P and Dietrich M (2023) S1PR-1/5 modulator RP-101074 shows beneficial effects in a model of central nervous system degeneration. *Front. Immunol.* 14:1234984. doi: 10.3389/fimmu.2023.1234984

### COPYRIGHT

© 2023 Sindi, Hecker, Issberner, Ruck, Meuth, Albrecht and Dietrich. This is an open-access article distributed under the terms of the Creative Commons Attribution License (CC BY). The use, distribution or reproduction in other forums is permitted, provided the original author(s) and the copyright owner(s) are credited and that the original publication in this journal is cited, in accordance with accepted academic practice. No use, distribution or reproduction is permitted which does not comply with these terms.

# S1PR-1/5 modulator RP-101074 shows beneficial effects in a model of central nervous system degeneration

Mustafa Sindi<sup>1</sup>, Christina Hecker<sup>1</sup>, Andrea Issberner<sup>1</sup>, Tobias Ruck<sup>1</sup>, Sven G. Meuth<sup>1</sup>, Philipp Albrecht<sup>1,2\*†</sup> and Michael Dietrich<sup>1†</sup>

<sup>1</sup>Department of Neurology, Medical Faculty of the Heinrich-Heine University, Düsseldorf, Germany,

**Introduction:** In multiple sclerosis (MS), chronic disability primarily stems from axonal and neuronal degeneration, a condition resistant to conventional immunosuppressive or immunomodulatory treatments. Recent research has indicated that selective sphingosine-1-phosphate receptor S1PR-1 and -5 modulators yield positive effects in progressive MS and mechanistic models of inflammation-driven neurodegeneration and demyelination.

**Methods:** In this study, the S1PR-1/-5 modulator RP-101074 was evaluated as a surrogate for ozanimod in the non-inflammatory, primary degenerative animal model of light-induced photoreceptor loss (LI-PRL) in CX3CR1-GFP mice to assess potential neuroprotective effects, independent of its immunomodulatory mechanism of action.

**Results:** Prophylactic administration of RP-101074 demonstrated protective effects in the preclinical, non-inflammatory LI-PRL animal model, following a bell-shaped dose-response curve. RP-101074 treatment also revealed activity-modulating effects on myeloid cells, specifically, CX3CR1+ cells, significantly reducing the marked infiltration occurring one week post-irradiation. Treatment with RP-101074 produced beneficial outcomes on both retinal layer thickness and visual function as evidenced by optical coherence tomography (OCT) and optomotor response (OMR) measurements, respectively. Additionally, the myelination status and the quantity of neural stem cells in the optic nerve suggest that RP-101074 may play a role in the activation and/or recruitment of neural stem cells and oligodendrocyte progenitor cells, respectively.

**Conclusion/Discussion:** The data from our study suggest that RP-101074 may have a broader role in MS treatment beyond immunomodulation, potentially offering a novel approach to mitigate neurodegeneration, a core contributor to chronic disability in MS.

KEYWORDS

S1PR-1, S1PR-5, RP-101074, neuroprotection, multiple sclerosis, microglia, CX3CR1

<sup>&</sup>lt;sup>2</sup>Department of Neurology, Maria Hilf Clinics, Mönchengladbach, Germany

# 1 Introduction

Multiple Sclerosis (MS) is an inflammatory autoimmune disorder characterized by demyelination, oligodendrocyte loss, subsequent axonal damage, and eventual neuronal degeneration within the central nervous system (1). This degeneration primarily accounts for the persistent clinical disability in MS patients, which remains unresponsive to conventional immunosuppressants and most immunomodulatory therapies. MS-related pathological alterations are typically marked by the infiltration of lymphocytes and macrophages into the CNS parenchyma, instigating the upregulation of adhesion molecules and promoting immune cell recruitment via inflammatory cytokines. This cascade results in glial and neuronal injury through a not yet fully elucidated mechanism. Increased oxidative stress has been hypothesized to play a significant role in neuronal damage (2), as activated immune cells may release reactive oxygen or nitrogen species.

Ozanimod, siponimod, and ponesimod are oral sphingosine-1phosphate (S1P) receptor modulators with varying selectivities for different S1P receptor sub-types and have been the focus of extensive research in recent years (3-5). Ozanimod and siponimod selectively target S1P receptor sub-types 1 and 5, while ponesimod is selective for S1P receptor sub-type 1. These selective S1P receptor modulators have demonstrated promising efficacy in the treatment of relapsing-remitting multiple sclerosis (RRMS) (6) and secondary progressive multiple sclerosis (SPMS) (5). Presently, research is being conducted to understand the brain-protecting effects of these selective S1P receptor modulators during the later stages of multiple sclerosis. This could potentially provide new treatment alternatives for patients suffering from progressive forms of the disease. Within this comprehensive framework for, we are increasingly incorporating state-of-the-art technologies to enhance our monitoring capabilities. Optical coherence tomography (OCT), for instance, is proving to be instrumental due to its non-invasive nature and ability to provide high-resolution, detailed images of the retina within the eye, thereby enabling a more precise understanding of disease progression and response to treatment. Previous research has demonstrated a notable reduction in the

Abbreviations: BW, Body weight; CC, Cell count; CNS, Central nervous system; CSLO, Confocal scanning laser ophthalmoscopy; CX3CR1, CX3C chemokine receptor 1; CX3CL1, Chemokine (C-X3-C motif) ligand 1; EAE, Experimental autoimmune encephalomyelitis; ELM, External limiting membrane; (E)GFP, (Enhanced) green fluorescent protein; GCL, Ganglion cell layer; HHI-LI-PRL, High-intensity light induced photoreceptor loss; INL, Inner nuclear layer; IPL, Inner plexiform layer; IRL, Inner retinal layer; IS, Inner segment; LI, Light induced; LWI-LI-PRL, Low-intensity light induced photoreceptor loss; MD, Mean Difference; MOG, Myelin oligodendrocyte glycoprotein; MBP, Myelin basic protein; MP, Mega pixels; MS, Multiple sclerosis; mOL's, Myelinating oligodendrocytes; NFL, Nerve fiber layer; OCT, Optical coherence tomography; OMR, Optomotor response; ONL, Outer nuclear layer; OPC's, Oligodendrocytes progenitor cells; OPL, Outer plexiform layer; ORL, Outer retinal layer; OS, Outer segment; P.i., Post irradiation; PRL, Photoreceptor loss; RPE, Retinal pigment epithelium; Sox-2, Sex determining region Y (SRY) - box 2; TRT, Total retinal thickness; IRL, Inner retinal layer.

thickness of the retinal nerve fiber layer (RNFL) and the ganglion cell layer-inner plexiform layer complex (GCIP) in MS patients as a consequence of optic neuritis, as well as in the eyes of MS patients without optic (7–9). Retinal degeneration in MS patients not only serves as a morphological correlate of functional visual deficits but also reflects overall disability, such as that assessed by the Expanded Disability Status Scale (EDSS) (7, 9, 10), and brain atrophy measured by MRI (10–12). This renders OCT an ideal tool for visualizing neurodegeneration, neuroprotection, and neuro-repair processes in both clinical and preclinical settings.

Our study revolves around the murine light-induced photoreceptor loss (LI-PRL) model, which represents a primarily non-inflammatory neurodegenerative condition. The aim was to assess the effectiveness of the compound RP-101074 in the chronic stages of degenerative CNS disease. This also applies to the chronic phases of MS, where lymphocyte and monocyte infiltration and inflammation play a less significant role in driving pathology, while neurodegeneration and activation of microglia emerge as the dominant characteristics. Unfortunately, there is not an ideal animal model to perfectly mimic this condition. However, the LI-PRL model induces CNS damage and subsequently inflammation and degeneration in the retina that is independent of T cell activity, thus making it a valuable model for our investigation. Although LI-PRL provokes retinal inflammation, it is not chronic as in the experimental autoimmune encephalomyelitis (EAE) model, but rather undergoes rapid remission. This period of remission of inflammation presents a critical window for us to observe neurodegeneration and to evaluate the potential neuroprotective effects of the compound. This model has been instrumental in our previous investigations, where we explored the neuroprotective effects of dimethyl fumarate, an immunomodulatory substance with potential neuroprotective capabilities (13). Building upon this previous work, we further extended our research to examine the protective capabilities of various doses of the S1PR-1/-5 modulator and ozanimod surrogate RP-101074 on retinal degeneration and visual function within the same LI-PRL model. The objective was to investigate if RP-101074 exhibits neuroprotective properties that could signify potential benefits in disorders characterized by primary neurodegeneration.

# 2 Material and methods

### 2.1 Animals

Six-week-old, female C57Bl/6J mice and CX3CR1-GFP transgenic mice were utilized in this study. For the CX3CR1-GFP mice, B6.129P2(Cg)-Cx3cr1tm1Litt/J mice (CX3CR1-GFP) were originally obtained from "The Jackson Laboratory" and fully backcrossed into the C57BL/6J strain at the animal facility at Heinrich Heine University in Düsseldorf, Germany. Additionally, we ensured the absence of the RD8 mutation, which is associated with hereditary macular degeneration. C57Bl/6J mice were purchased from Janvier Labs, France. In LWI-LI-PRL, n=5 animals (10 eyes) per group were used in two independently performed experiments. In HHI-LI-PRL, n=6 animals (12 eyes) per group were used in two independently performed experiments.

# 2.2 Light-induced photoreceptor loss and treatment

Prior to irradiation using an LED light source (cold temperature), the pupils were dilated with a combination of 0.5% Tropicamide and 2.5% Phenylephrine. To prevent dehydration and cataract formation during irradiation, the eyes were treated with eye gel. Both eyes were exposed to irradiation for 45 minutes at maximum intensity and with the fully opened shutter. The distance between the light source and the eye was set at 10 mm for weak degenerative conditions (Low Intensity, LWI) and 5 mm for strong degenerative conditions (High Intensity, HHI).

Mice were treated daily, from the day of irradiation until the end of the experiment after either 5 or 6 weeks, with RP-101074 at doses of 0.1 mg/kg, 0.3 mg/kg, 1 mg/kg, and 5 mg/kg body weight (BW), administered via oral gavage. The vehicle control group was subjected to the same procedures as the treatment group, including anesthesia and eye preparation, but without irradiation. Animals of the vehicle group were administered with a vehicle solution of PBS/DMSO (1%).

# 2.3 OCT measurements

Periodic OCT measurements were conducted using the Spectralis HRA + OCT device (Heidelberg Engineering, Germany) with several adaptations for rodents, as previously described (14). Segmentation of retinal volume scans was performed using the Heidelberg Eye Explorer software, with manual control for segmentation errors. The volume of the para-papillary region was assessed using the ETDRS grid, excluding the center with the disc, as published previously (15). Inner retinal layer (IRL) thickness, outer retinal layer (ORL) thickness, and total retinal thickness (TRT) were examined at defined intervals after irradiation and compared with baseline measurements (IRL: NFL, GCL, and IPL layers; ORL: INL, OPL, ONL, ELM, IS/OS, RPE, Choroid; TRT: IRL + ORL).

# 2.4 Confocal scanning laser ophthalmoscopy measurements

CSLO was performed periodically (Figure 1) using the 480 nm laser and the fluorescence angiography filter of the Spectralis<sup>®</sup> device (as described in 2.3) for imaging retinal microglia in CX3CR1-GFP transgenic mice. The number of GFP-positive cells in a predefined oval mask around the optic disc was counted using a modified automated algorithm developed by 16 (Figure 2). By employing the CX3CR1-GFP mouse line, the activity of CX3CR1+ myeloid cells was longitudinally analyzed in the retina to draw conclusions about the effects of RP-101074 treatment on microglial cells.

# 2.5 Anesthesia

For the photoreceptor loss (PRL) treatment and Optical Coherence Tomography (OCT)/confocal Scanning Laser

Ophthalmoscopy (cSLO) measurements, the animals were anesthetized using isoflurane (Vaporizer from Harvard Apparatus Anesthetic Vaporizors; Isofluran from Piramal critical care). Specifically, induction was carried out at 3.5% isoflurane, followed by maintenance at 2% isoflurane, with a flow rate of 0.6 L/minute of oxygen.

# 2.6 Optomotor response measurements

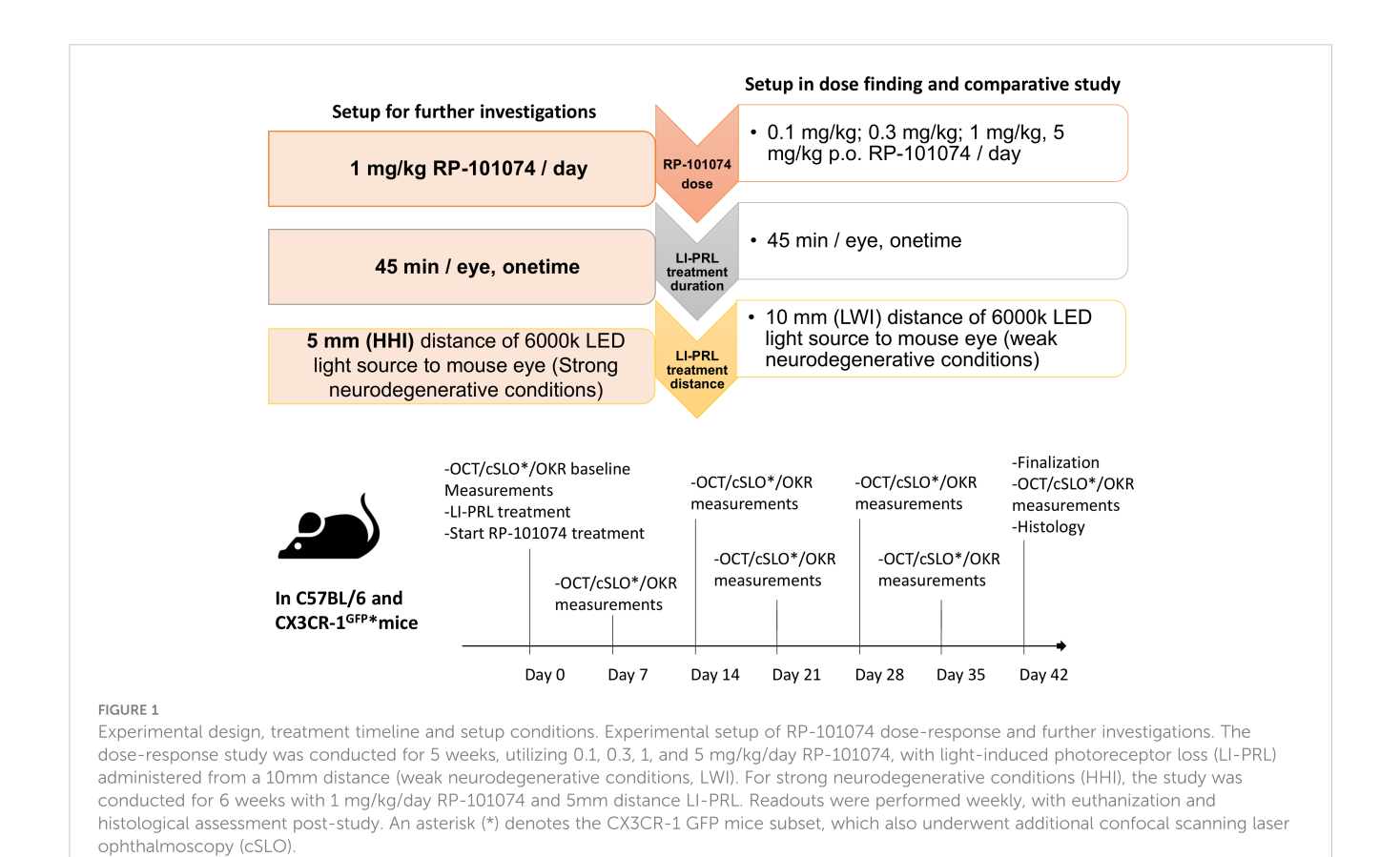
OMR measurements were performed periodically (Figure 1) using the OptoMotry<sup>®</sup> device from Cerebral Mechanics, in parallel with OCT and cSLO measurements. Spatial frequency was monitored as a parameter for visual function. The spatial frequency threshold was determined by randomly changing the spatial frequency to identify the threshold at which the mouse could track, as previously described (15, 17).

# 2.7 Histology

Mice were anesthetized with Ketamine/Xylazine, euthanized using an overdose of isoflurane (Piramal critical care), and cardiac perfusion was performed using phosphate-buffered saline (Gibco, Carlsbad, USA). The optic nerves were then isolated and fixated in 4% paraformaldehyde (Carl Roth, Karlsruhe, Germany) overnight. After fixation, the optic nerves were subjected to a sucrose gradient for dehydration and subsequently embedded in O.C.T. compound (Sakura TM Finetek, Alphen aan den Rijn, The Netherlands). Longitudinal sections of five micrometers were cut and prepared for fluorescence staining. Longitudinal sections of the optic nerves were used for quantifying neural stem cells (Sox2, (Clone E-4) Santa Cruz Biotechnology, 1:200), assessing the state of myelination (MBP (Clone 12), Merck Millipore, 1:200), and evaluating neuronal survival (βIII-tubulin (Clone TUJ1), Biolegend, 1:200) using Leica HyD detector attached to a Leica DMi8 confocal microscope (63x objective lens magnification). Cy5 rat antimouse, Cy5 rabbit anti-mouse (1:500, Millipore) and Alexa Fluor TM 488 rabbit anti-mouse (1:500, Invitrogen) were used as secondary antibodies. The numbers of cells stained with Sox2 were analyzed using ImageJ software, applied by blinded raters, and expressed as a ratio to DAPI staining. The overall signal for MBP and BIII-tubulin (positive total area in the red channel) was analyzed using ImageJ software as shown in Figure 2.

# 2.8 Statistics

Statistical analysis was performed using Prism (version 9, GraphPad® Software, Inc.) and IBM SPSS Statistics (version 20, IBM Corporation, USA). Total and percent changes of the acquired retinal parameters (OCT, OMR, and cSLO) were analyzed using generalized estimation equation (GEE) models, accounting for within-subject inter-eye correlations, to test for differences between the two groups. For non-paired data, group means



analyses were compared using a one-way ANOVA with the Dunnett *post hoc* test, utilizing one optic nerve per animal for the histological investigations.

3 Results

# 3.1 Retinal structural and visual function analysis after LI-LWI-PRL treatment (weak neurodegenerative conditions)

To mimic the range of damage severity seen in multiple sclerosis, we conducted a longitudinal investigation on C57BL/6J mice, applying two levels of light-induced damage. The rationale behind this approach was to simulate both mild and severe forms of retinal degeneration that occur in the disease course. Therefore, we weekly evaluated the potential of RP-101074 in protecting against retinal degeneration following 45 minutes of irradiation per eye. The results obtained in this study could help us better understand the dose-dependent effects of RP-101074, and its potential utility in clinical settings.

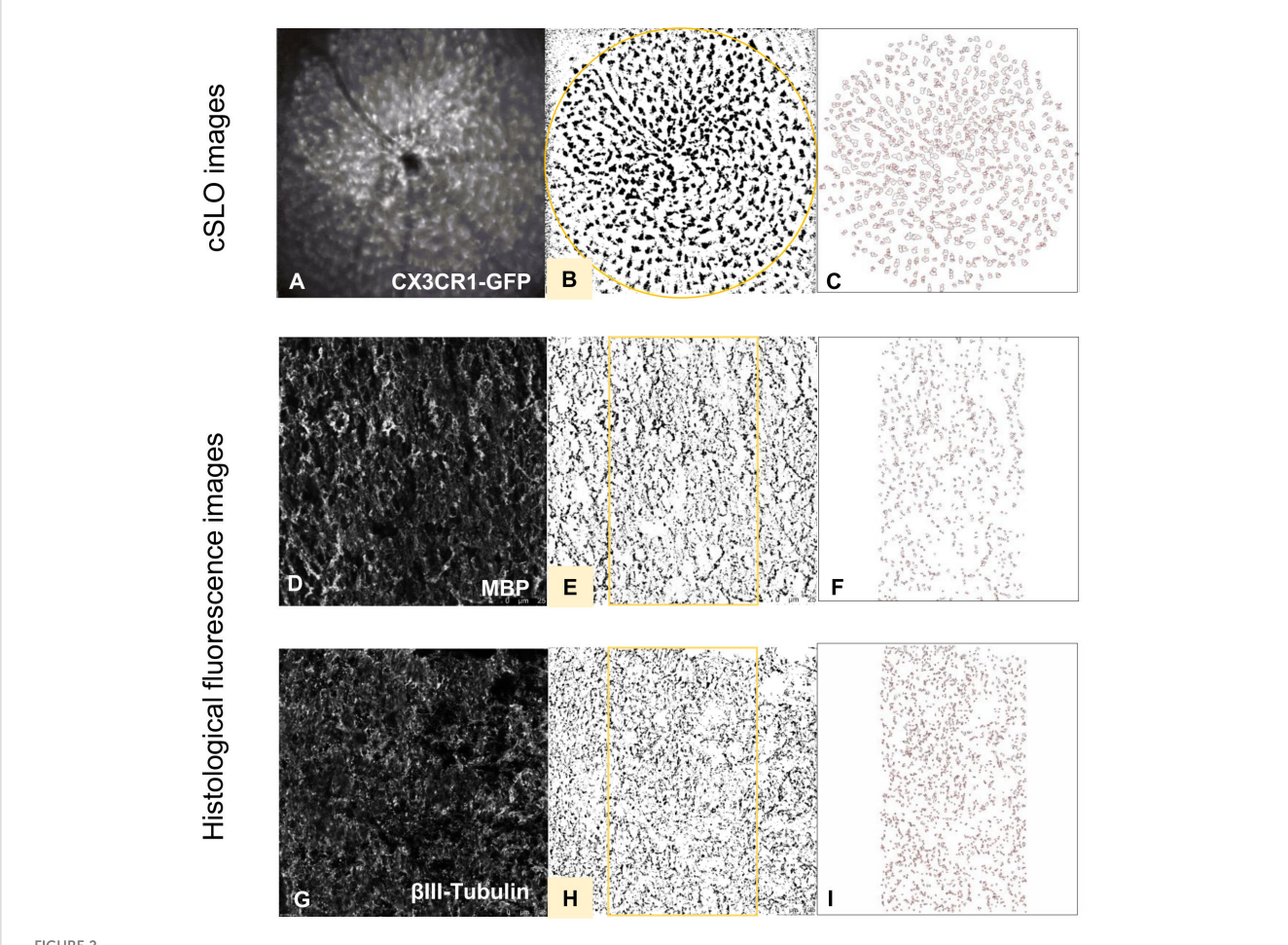
Under weak degenerative conditions, specifically LWI-LI-PRL (10 mm distance from eye to light source), no statistically significant changes were observed in the retinal layer's structural analysis by OCT (Figures 3A–C) in all treatment groups, including vehicle treatment. On the functional level, prophylactic treatment with 1 mg/kg and 5 mg/kg body weight (BW) RP-101074 provided robust protective effects, preventing visual function loss after LWI-LI-PRL.

These effects followed a bell-shaped dose-response curve, as the 1 mg/kg (Week 5: P=<0.0001, MD=0.1365) dose was more effective than the 5 mg/kg dose (Week 5: P=0.0066, MD=0.09651). Other doses did not lead to improved visual acuity (Figure 3D).

# 3.2 Retinal structural analysis and visual function analysis after HHI-LI-PRL treatment (strong neurodegenerative conditions)

After identifying the most effective dose of 1 mg/kg BW of RP-101074 for improving visual function in LWI conditions, the mice's eyes were irradiated with high-intensity light, here, HHI-LI-PRL (5 mm distance from eye to light source), to analyze the effect of 1 mg/kg BW RP-101074 in strong neurodegenerative conditions.

The structural analysis of the retinal layers and visual function measurement after HHI-LI-PRL revealed beneficial effects of RP-101074 when applied at a dose of 1 mg/kg BW (Figures 4–C). A prominent degeneration of all retinal layers occurred already 1 week after irradiation. The neurodegenerative process was significantly reduced when treating the animals prophylactically with 1 mg/kg BW of RP-101074, starting on the day of irradiation. The reduction of the IRL thickness (B) (Week 1: P=<0.0001, MD=-3.971) reached its maximum already 1 week after irradiation, followed by a recovery phase, while total retinal (C) (Week 4: P=<0.0001, MD=-12.50) and ORL (A) (Week 4: P=<0,0004, MD=-12.28) thickness showed increasing degeneration until week 4. Even 6



Histological evaluation process of fluorescence and cSLO images. cSLO: Initially, (A) CX3CR1-GFP labeled cells in the retina were captured by cSLO. Then, a (B) calibrated oval mask section was placed around the optic disc, followed by a (C) automated cell count using Fiji-ImageJ2 software, as per the protocol developed by Frenger et al. (16). Fluorescence images: Fluorescence-stained tissues with different markers were captured and processed (D, G). Then, a (E, H) calibrated rectangle mask section was applied in the middle of the optic nerve, followed by a (F, I) automated total area measurement using Fiji-ImageJ2 software.

weeks after irradiation, the effect of RP-101074 regarding TRT and ORT change was still significant compared to untreated control mice (Week 6 ORL: P=<0.0011, MD=-9.576), (Week 6 TRT: P=<0.0003, MD=-11.09).

The visual function was reduced after HHI-LI-PRL treatment, initially in both the RP-101074 treated (Week 2: P=<0.0001, MD=-0.07077) and the untreated group (Week 2: P=<0.0001, MD=-0.09965). However, after 3 weeks, the visual function was restored almost completely in the RP-101074 treated group (Week 3: Mean=0.2787 (Vehicle control) vs. Mean=0.2654 (treated)), while the vehicle + PRL group showed continuous loss of function until week six compared to vehicle control (Week 6: P=<0.0001, MD=-0.1066).

# 3.3 Effect of RP-101074 on microglial infiltration in the CNS of CX3CR1<sup>GFP</sup> mice after HHI-LI-PRL

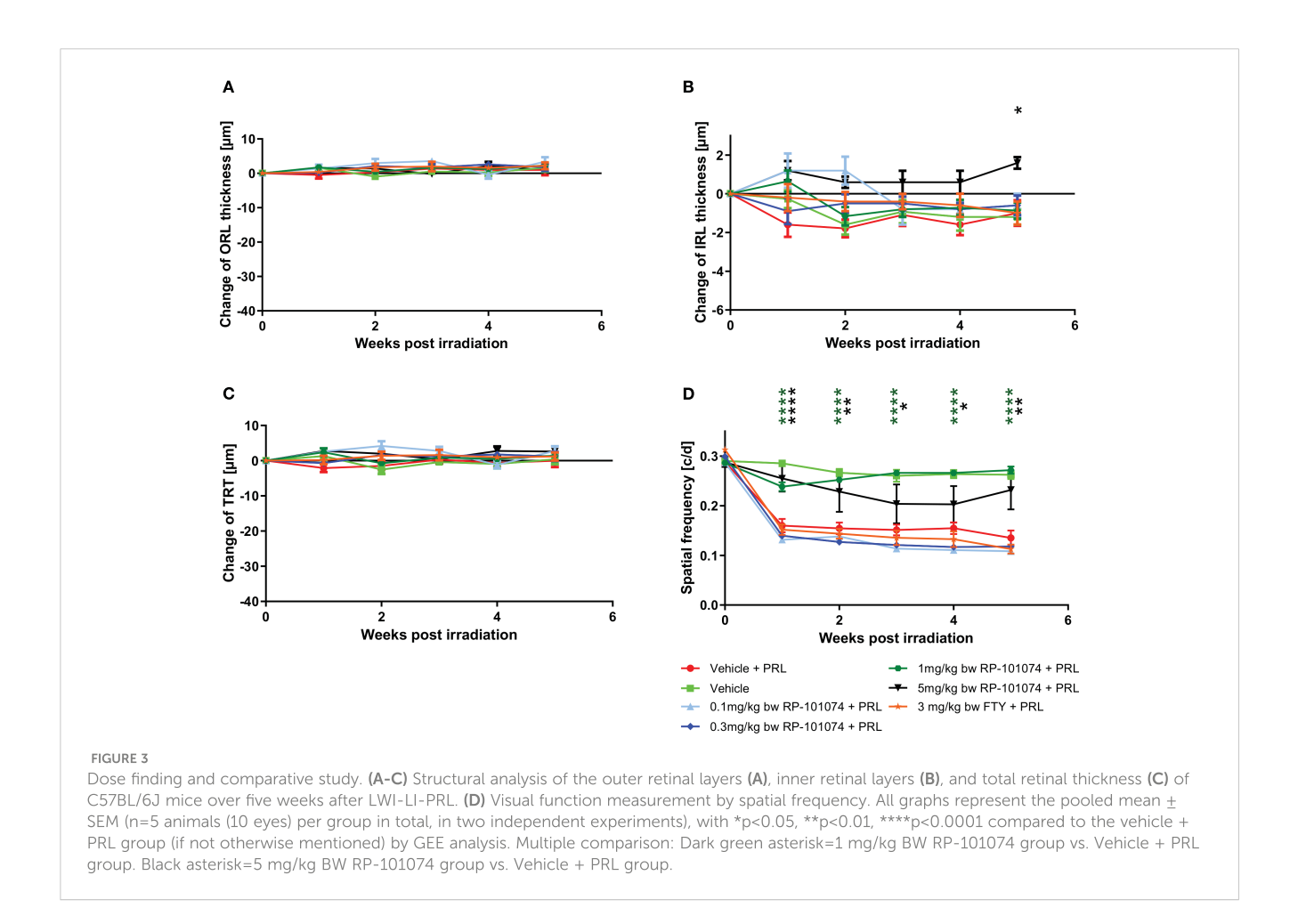
To study the effects of 1 mg/kg BW RP-101074 on myeloid cells after HHI-LI-PRL irradiation, confocal scanning laser

ophthalmoscopy (cSLO) was used to investigate the infiltration of GFP expressing myeloid cells in the CNS, specifically in the retina around the optic disc, using the CX3CR1-GFP transgenic mouse line, which expresses GFP under the CX3C chemokine receptor 1 (CX3CR1) promotor.

As shown in Figure 5, a significant infiltration of myeloid cells in the CNS was observed 1 week after HHI-LI-PRL (Mean=796.9) compared (P=<0.0001) to vehicle control (Mean=402.1), while the infiltration was significantly reduced in the RP-101074 treated group (Mean=576.6, P=<0.0001). At week 4 post irradiation and henceforth, the number of myeloid cells in the CNS was similar in the vehicle + PRL and RP-101074 + PRL group, converging to the cell number counted at the baseline measurement before HHI-LI-PRL treatment.

# 3.4 Histological analyzes of optic nerve longitudinal sections after HHI-LI-PRL

To address the question whether HHI-LI-PRL treatment impacts myelination status and whether RP-101074 exhibits a



prophylactic effect, longitudinal sections of optic nerves were subjected to immunohistochemical staining for myelin basic protein (MBP) and Sex determining region Y (SRY) - box 2 (Sox2). MBP serves as a myelin marker, while Sox2 is a marker for neural stem cells and newly differentiated myelinating oligodendrocytes (mOLs).

As evidenced in Figure 6, HHI-LI-PRL led to a decrease in MBP-positive myelin within the optic nerve sections (Mean=498.6). In contrast (P=<0.0018), prophylactic treatment with RP-101074 significantly increased the amount of myelin (Mean= (Mean=629.3), suggesting its protective role in maintaining myelination status.

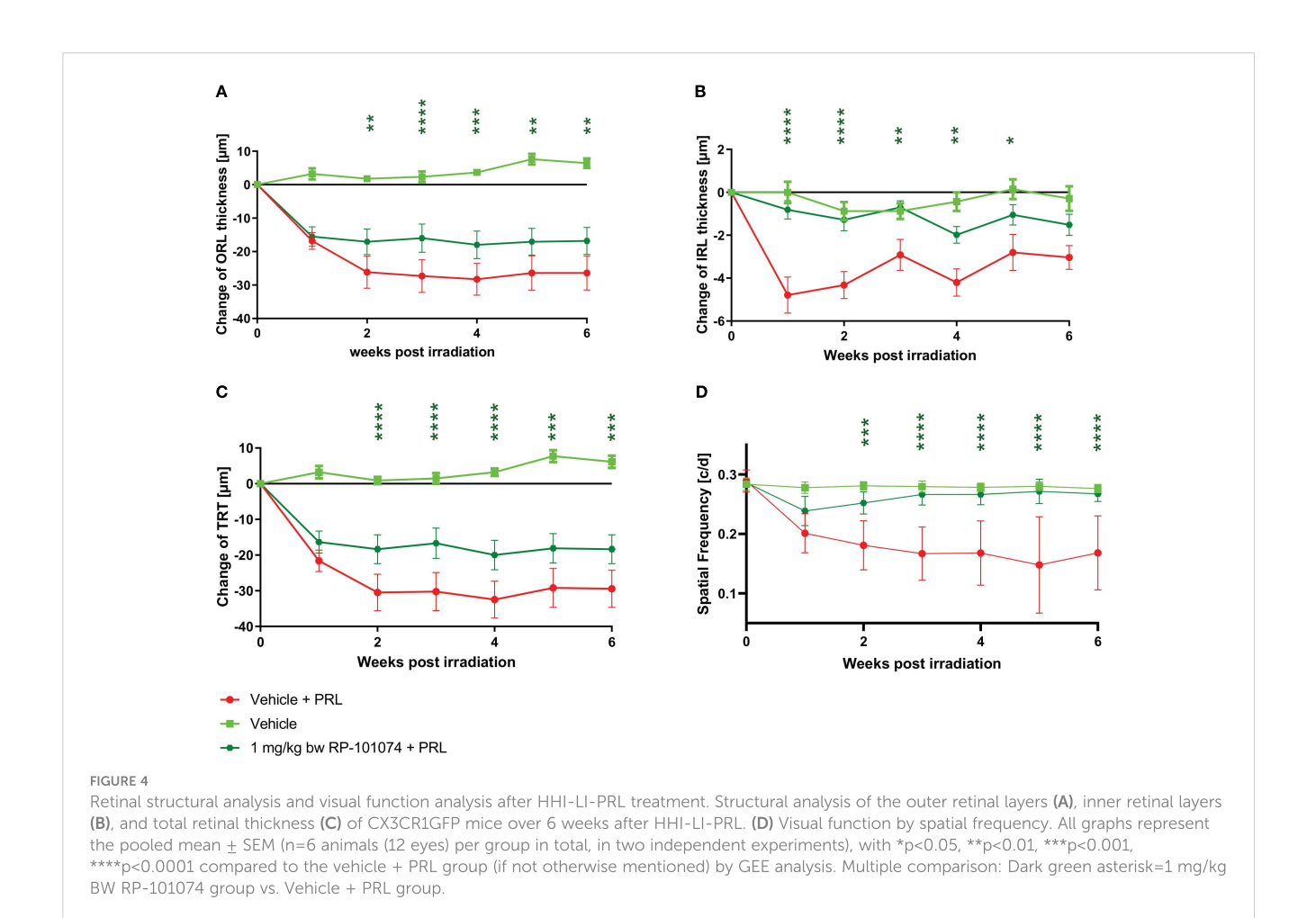
HHI-LI-PRL administration led to a decrease in  $\beta$ III-Tubulin-positive axons within the optic nerves. The representative images of optic nerves post-HHI-LI-PRL treatment depict instances with completely damaged axonal structures (Figure 7C) and others with milder axonal damage, as evidenced by reduced  $\beta$ III-Tubulin expression (Figure 7F). Prophylactic RP-101074 treatment, initiated on the day of irradiation, resulted in diminished axonal damage, as demonstrated by increased (Mean=429.8)  $\beta$ III-Tubulin abundance in the optic nerves (Figures 7D, G) in comparison (P=<0.0247) to the vehicle-treated group (Mean=290.7) (Figures 7B, E).

The outcomes displayed in Figure 8 (Sox2 expression) follow a similar pattern to those of MBP expression (Figure 6). HHI-LI-PRL treatment led to a reduced number of Sox2-positive neural stem cells (Mean=3.1). Prophylactic RP-101074 treatment (Mean=14.67)

resulted in a significant (P=<0.0001) increase in Sox2-positive cell numbers within the HHI-LI-PRL model.

To further elucidate the potential protective impact of RP-101074, we evaluated its influence on oligodendrocyte progenitor cell (OPC) markers, NG2 and PDGFRα. Longitudinal optic nerve sections were subjected to immunohistochemical staining for these markers. Figure 9A reveals the relative expression of NG2 in the different experimental groups. Remarkably, we observed a significant upregulation of NG2 in the RP-101074-treated group (Mean=1.481), compared to both the vehicle group (P=0.0005, Mean=0.325) and the HHI-LI-PRL group (P=<0.0001, Mean=0.239). This indicates a potential role of RP-101074 in promoting OPC proliferation or survival following PRL treatment. The representative images of NG2 immunostaining across the experimental groups are illustrated in Figure 9C.

The effects of RP-101074 treatment on PDGFR $\alpha$  expression, another OPC marker, are depicted in Figure 9B. Consistent with the NG2 expression trend, there was a notable increase in PDGFR $\alpha$  levels in the RP-101074-treated group (Mean=0.819) compared to both the vehicle group (P=0.0001, Mean=0.071) and the HHI-LI-PRL group (P=<0.0001, Mean=0.069). This finding further corroborates the proposed protective and promyelinating role of RP-101074 in the context of PRL. Representative images of PDGFR $\alpha$  immunostaining in the different experimental conditions are shown in Figure 9D.



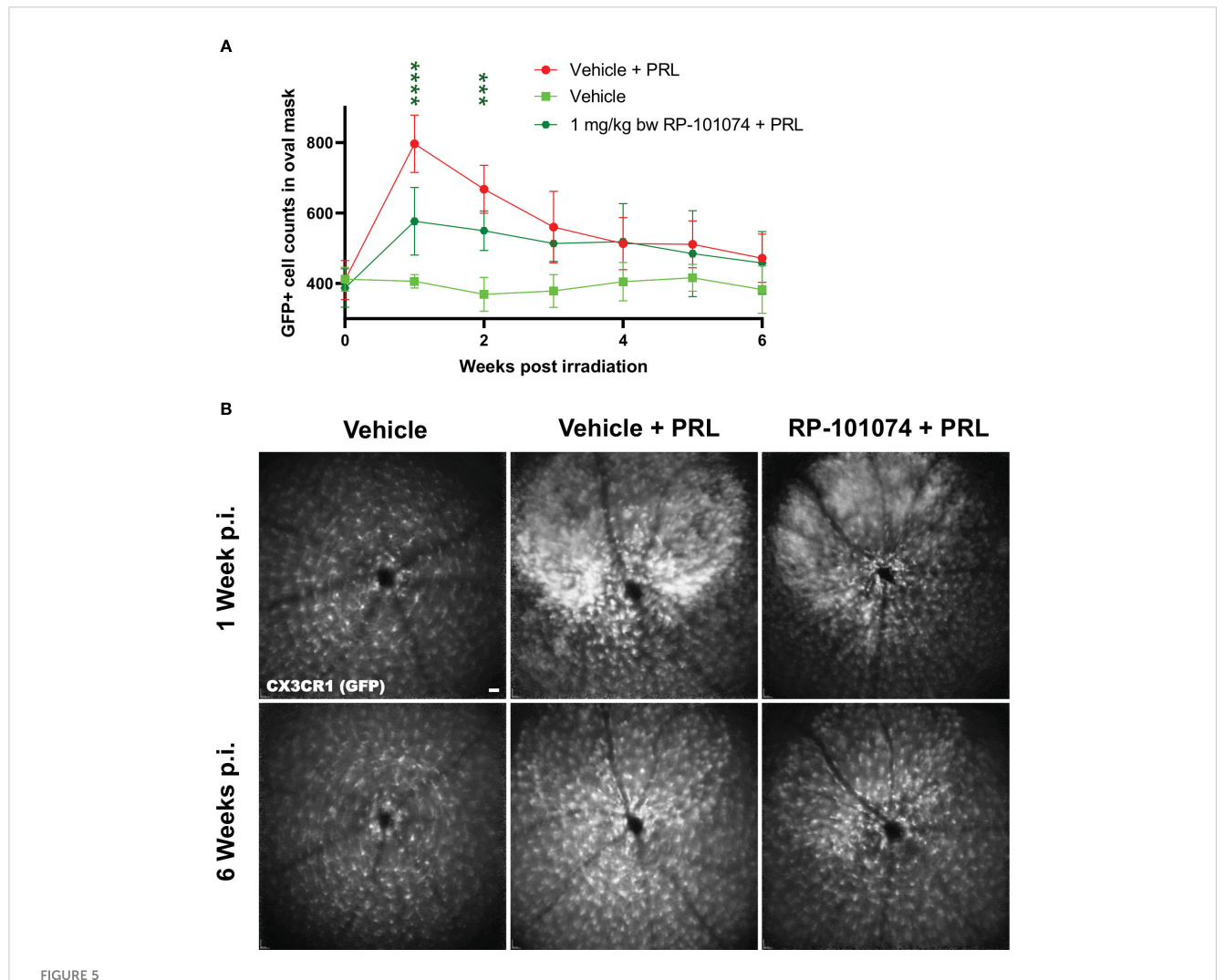
Collectively, these findings suggest that RP-101074 treatment leads to a significant upregulation of OPC markers, NG2 and PDGFR $\alpha$ , pointing towards a beneficial effect in enhancing oligodendrocyte progenitor populations following PRL.

# 4 Discussion

In this study, the protective capacity of the S1PR-1/-5 modulator RP-101074 was assessed in a primary degenerative model of photoreceptor degeneration induced by light overstimulation. Initially, we established a standardized protocol wherein all mice were subjected to identical conditions during LI-PRL treatment, maintaining consistent parameters such as the angle of the light source to the eye, light intensity, light temperature, and light exposure duration. Given that the in vivo OCT and cSLO measurements were performed around the optic disc in a specified area, the eye/head position of the mice during LI-PRL treatment was standardized to ensure that the primary focus of the light beam targeted the same retinal area in all mice. One of the major factors influencing the degree of degeneration in photoreceptors and the retina following LI-PRL is the distance between the light source and the eye. In our dose-finding study, we initially applied low-intensity (LWI) LI-PRL to induce mild retinal degeneration in the animals' retinae. However, while OMR revealed reduced visual acuity, no significant degeneration

was observed in the retinal layer's structural analysis using OCT among all groups. An intermediate RP-101074 concentration (1 mg/kg BW) provided more pronounced protection from visual function loss after LWI-LI-PRL than a higher concentration of 5 mg/kg BW, resembling a bell-shaped dose-response curve. This finding was consistent with our previous studies using the S1PR 1-/-5 modulator siponimod, wherein the lower dose was more effective than the higher dose in preventing retinal neurodegeneration during experimental optic neuritis (15). Recent studies conducted by peers researching S1PR modulators also exhibit bell-curve dose-dependent results (18, 19). A plausible explanation is that a high dose of RP-101074 (5 mg/kg BW) leads to a more potent internalization and degradation of S1P receptors (compared to 1 mg/kg BW), resulting not only in immunemodulating effects primarily attributed to the modulation of S1PR-1 but also in cascades that influence the function of oligodendrocytes and other cells in the CNS expressing S1PR-5 (20). The observed bellshaped dose-response curve corresponds with earlier studies on FTY720, another S1P receptor modulator, further highlighting the intricate and often counterintuitive pharmacodynamics of these compounds (21).

After observing limited discernible outcomes after mild irradiating conditions (LWI), we decided to explore more potent conditions to induce degeneration to the retinal tissue. We here only employed the most efficacious dose of 1 mg/kg in the (HHI) setting due to our observation, that doses lower or higher doses failed to elicit significant

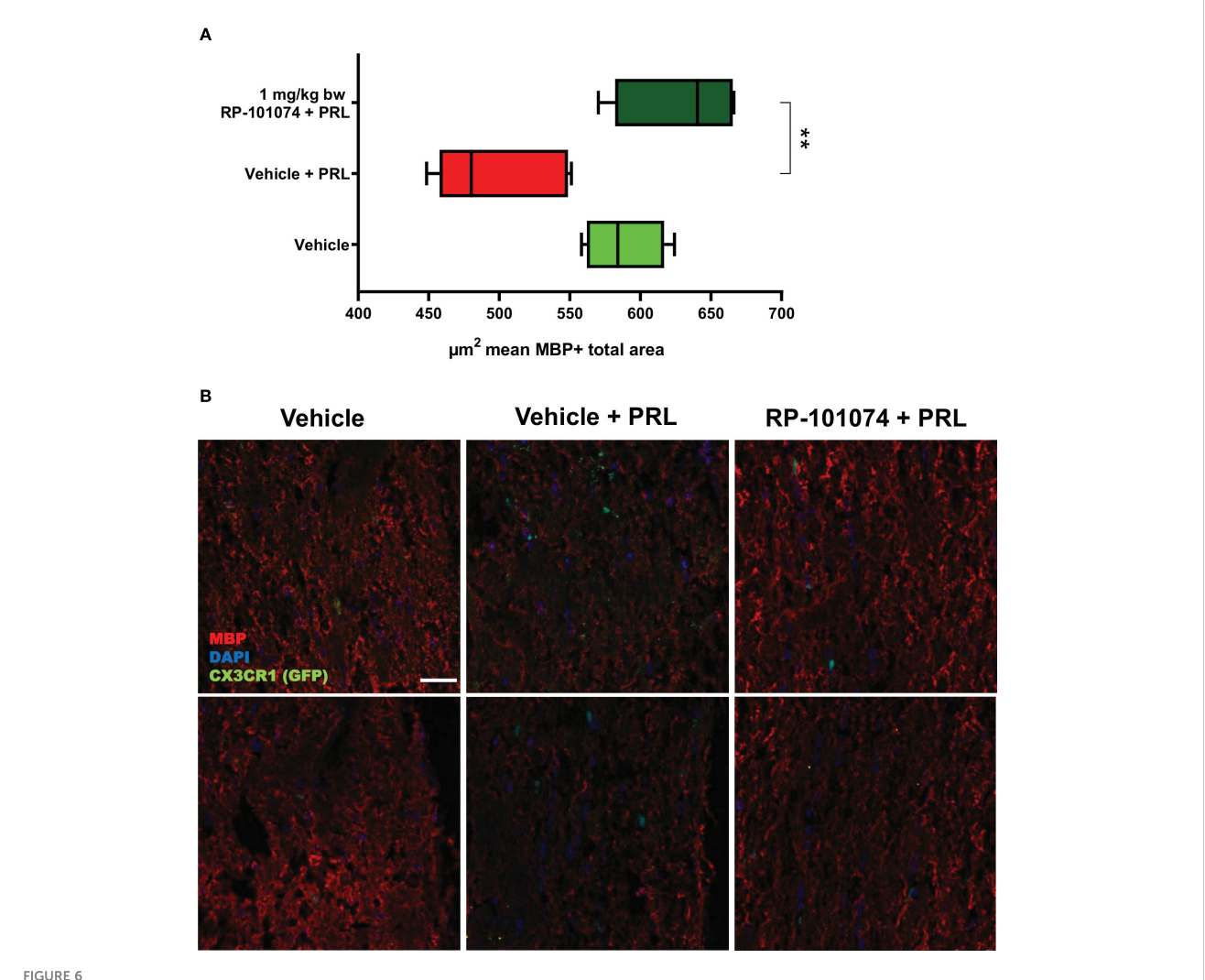


GFP+ cell counts in the retina of CX3CR1<sup>GFP</sup> mice after HHI-LI-PRL treatment. Figure 5 demonstrates automated GFP+ cell counts in the retina of CX3CR1GFP mice after HHI-LI-PRL treatment as shown in Figure 2. The results of the cell count are presented in (A), with the process repeated for all captures over a period of 6 weeks post-irradiation (p.i.). (B) shows example images one week p.i. and 6 weeks p.i. Scale-bar: 200 µm. All graphs show the pooled mean ± SEM (n=6 animals (12 eyes) per group in total, in two independent experiments), with \*\*\*p<0.001, \*\*\*\*p<0.0001 when compared to the vehicle + PRL group (if not otherwise mentioned) using GEE analysis. Multiple comparison: Dark green asterisk=1 mg/kg BW RP-101074 group vs. Vehicle + PRL group.

effects under LWI. We concluded, that other doses would likely not yield substantial effects under the stronger HHI conditions, as they did not exhibit any noticeable impact even under the comparatively milder LWI setting. Although the protective effects of 5 mg/kg BW RP-101074 were also significant, we opted to use the most effective dose of 1 mg/kg BW RP-101074 in our subsequent HHI LI-PRL studies. A recent study showed, that ozanimod showed efficacy at doses of 0.2 mg/kg in a mouse model of experimental autoimmune encephalomyelitis. This dose is 5 times lower than the dose of 1mg/kg RP-101074, which was proved most effective in our study. Due to their calculations, the predicted human equivalent dose would be 0.96 mg, very similar to the 0.92 mg label dose of ozanimod (22). However, it is important to note that the model used in the cited work differs from our model, particularly regarding intensity of retinal inflammation. Doses of 0.1 and 0.3 mg per day used in our study did not yield in any beneficial effects in the LWI setting. We, therefore, hypothesize that the 0.2 mg dose would also not yield significant effects under HHI radiation.

However, we acknowledge that it cannot completely excluded that doses lower that 1 mg could have beneficial effects under the HHI conditions. It is important to highlight that the substance utilized in our study was not ozanimod but rather RP-101074 and that no comparable dose finding data are available.

As illustrated in Figure 4, prophylactic RP-101074 treatment resulted in significant protection from retinal degeneration in both inner and outer layers. As depicted in Figure 4A, one week after HHI-LI-PRL, the degeneration of the outer retinal layers, including the photoreceptor layer, was similar in both irradiated groups (vehicle + PRL and RP-101074 + PRL). This observation suggests that the photoreceptor layer predominantly degenerates in the context of HHI-LI-PRL. Interestingly, the degeneration of the inner retinal layers, which encompass the retinal nerve fiber layer, ganglion cell layer, and their dendrites in the inner plexiform layer, was only significantly induced after HHI-LI-PRL in the group without RP-101074 treatment. This finding indicates that RP-101074 appears to



MBP+ total area measurements in optic nerves of CX3CR1<sup>GFP</sup> mice: Figure 6 illustrates the automated total area measurement for MBP staining in longitudinal optic nerve sections of CX3CR1-GFP mice as shown in Figure 2. The results are shown in (A). Representative images (B) portray the longitudinal optic nerve sections with MBP staining (red). The indicated  $\mu$ m² mean of MBP+ total area has been calculated out of a total 8.100  $\mu$ m² captured area. All graphs depict the pooled mean  $\pm$  SEM (n=6 animals (12 eyes) per group in total, in two independent experiments), with \*\*p<0.01, as determined by one-way ANOVA with Dunnett's *post hoc* test.

exhibit protective effects on both directly affected photoreceptor cells and indirectly on ganglion cells and their axons. These protective effects were observed in both short-term (Figure 4A, two weeks after HHI-LI-PRL treatment) and long-term follow-ups (Figure 4A, six weeks after HHI-LI-PRL treatment). The increased abundance of Sox2-positive neural stem cells upon RP-101074 treatment, as shown in Figure 8, suggests that the protective action of this treatment may involve the activation and/or recruitment of neural progenitors and/or the release of neuroprotective factors, in addition to the modulation of inflammatory responses. The activation and recruitment of neural progenitors as a response to RP-101074 treatment aligns with findings from 23, where modulation of S1P receptors was found to enhance the regenerative capacity of neural cells in a murine stroke model, further hinting at the multi-faceted therapeutic potential of such modulators.

As described above, the change in inner retinal thickness (indirectly affected cells) seems to occur at an earlier time point, specifically, one week after HHI-LI-PRL, than the changes in the

outer retinal layers (directly affected cells), where the most pronounced degeneration was observed two weeks after HHI-LI-PRL (Figure 4). This finding might be attributable to swelling of the outer retinal layers following inflammatory processes, where microglial migration from the inner retinal layers to the outer retinal layers, as well as an amoeba-like shift of microglial cells, occurs during inflammation (24).

Microglial activation has been linked to retinal degeneration in CNS disorders (25) and others like Alzheimer's, Parkinson's, and Huntington's diseases (26); therefore, the number of CX3CR1-positive microglia was evaluated *in vivo* using cSLO over a period of six weeks following HHI-LI-PRL. As depicted in Figure 5, RP-101074 treatment resulted in significantly reduced numbers of CX3CR1-positive cells around the optic disc in the retina one week after HHI-LI-PRL, suggesting a diminished activation of the innate immune response in the retina. This effect can likely be attributed to the immunomodulatory mode of action of S1PR-1/-5 modulators

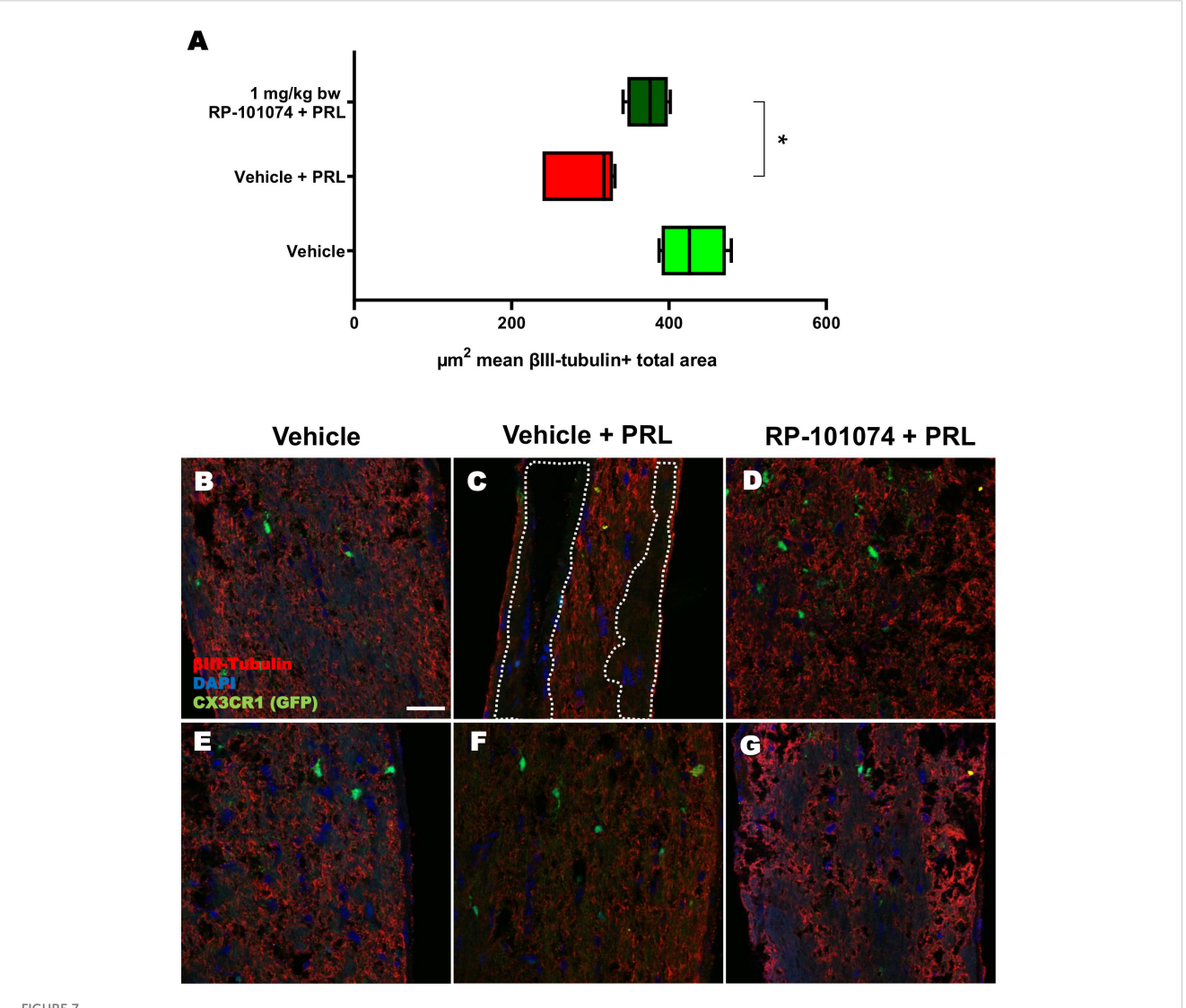


FIGURE 7

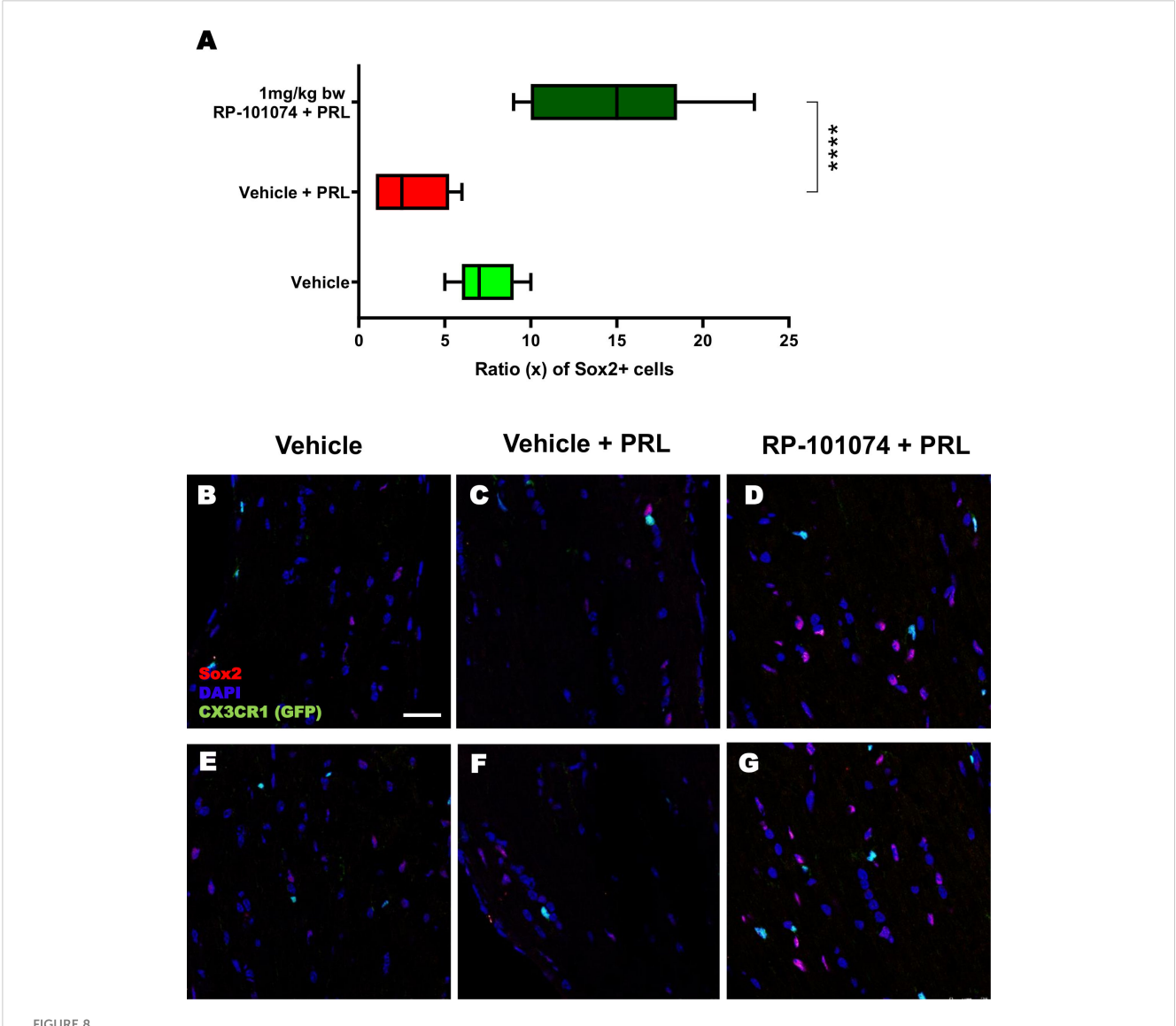
βIII-Tubulin+ total area measurements in optic nerves of CX3CR1<sup>GFP</sup> mice. Figure 7 presents the outcomes of an automated total area measurement for βIII-Tubulin staining in longitudinal optic nerve sections of CX3CR1GFP mice as shown in Figure 2. The results are illustrated in Chart (A), while Figures (B–G) displays representative images. The marked area within the example image (C) denotes regions with axonal damage. The indicated  $\mu$ m² mean of βIII-Tubulin+ total area has been calculated out of a total 8.100  $\mu$ m² captured area. All graphs represent the pooled mean  $\pm$  SEM (n=6 animals (12 eyes) per group in total, in two independent experiments) with \*p<0.05, determined by 1-way ANOVA with the Dunnett post hoc test.

(15, 20). This effect was most prominent one week after irradiation and was followed by a convergence of microglial cell counts between RP-101074- and vehicle-treated groups within the subsequent five weeks. Our own and other studies have even suggested a shift of microglial cells under S1PR-modulator treatment towards a regenerative phenotype (15, 27). Despite observing most significant changes within the first 3 weeks after irradiation, we made the decision to extend the observational period in order to thoroughly evaluate the progression of neurodegeneration and potential regenerative processes following the resolution of inflammation, also focusing on potential regenerative aspects of the treatment (28).

Interestingly, Naruse and colleagues found in 2018, that microglial activation could induce OPC generation following focal demyelination, suggesting a potential role for these cells in regeneration (29). Other recent studies show that S1PR

modulators shows growing evidence that targeting S1PR modulates mechanisms beyond immunomodulation, such as remyelination (15, 30, 31). Furthermore, S1PRs could also play a direct role in the regulation of stem cell migration, proliferation, and differentiation (32). Understanding the details between S1PRs and its pathway contributing to shifting myeloid activity or even direct stem cell interaction will be crucial in developing novel therapeutic strategies to modulate the behavior of these versatile cells in neurodegenerative diseases.

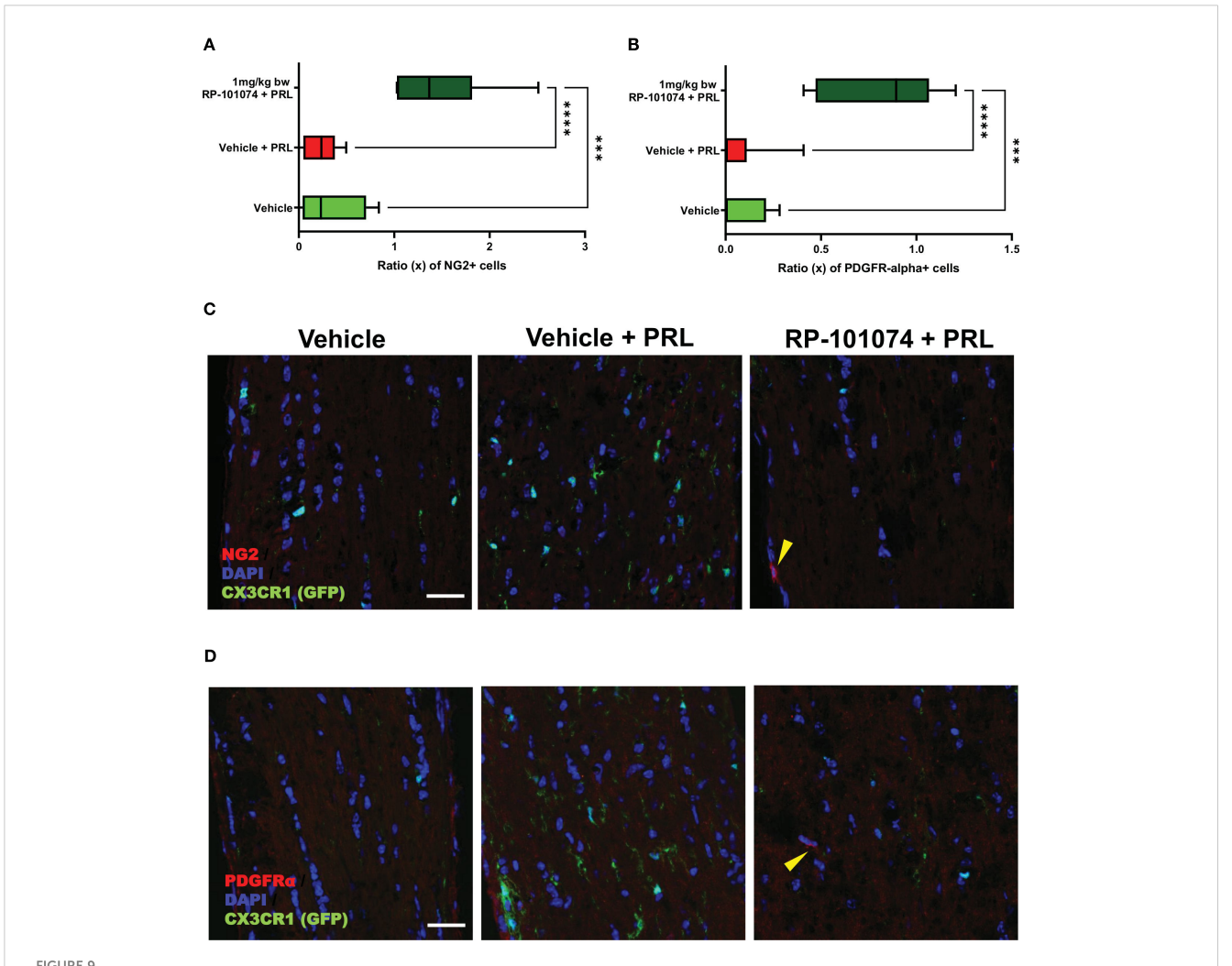
Axonal damage and demyelination resulting from autoimmune inflammation are among the main reasons for clinical disability in MS patients and their animal models. Consequently, we further investigated whether RP-101074 affected the myelin status and axonal integrity of the optic nerve in our model. We analyzed longitudinal sections of the optic nerves, staining for MBP, a marker



Sox2+ cell counts in optic nerves of CX3CR1<sup>GFP</sup> mice. Cell counting of Sox2+ cells in relation to the total cell number (DAPI) was performed in longitudinal optic nerve sections of CX3CR1-GFP mice. Figures (**B**–**G**) exhibit example images, while the results are presented in Figure (**A**). X-axis of (**A**) indicates the ratio (x) of Sox2+ cells to total cells (DAPI) in % (x/100). All graphs represent the pooled mean  $\pm$  SEM (n=6 animals (12 eyes) per group in total, in two independent experiments), with \*\*\*\*p<0.0001 determined by 1-way ANOVA with the Dunnett *post hoc* test.

for myelin, and Sox2, a marker for neural stem cells and for newly differentiated myelinating oligodendrocytes (mOLs) in the adult brain and spinal cord. MBP is a sensitive marker of myelination (33), indicating the involvement of differentiated, myelinating oligodendrocytes. Sox2, on the other hand, is one of various transcription factors critical for oligodendrocyte (OL) development, OL regeneration, and OPC (oligodendrocyte progenitor cell) differentiation (34). Recent studies suggest that Sox2 may act as a transcriptional master regulator at the epigenetic level, affecting the expression of crucial downstream factors involved in oligodendrocyte development (35).

Histological analyses of longitudinal sections of the optic nerve demonstrated significantly decreased myelination and reduced neural stem cell numbers following HHI-LI-PRL. Prophylactic treatment with RP-101074 resulted in significantly increased numbers of Sox2+ cells compared to the vehicle control group and a higher amount of myelin compared to the vehicle + PRL group. Furthermore, elevated expression levels of NG2 and PDGFR $\alpha$  in the RP-101074 treated group not only align with the observed increase in myelination and progenitor cell numbers but also hint towards a possible role in fostering OPC populations. We, therefore, conclude that RP-101074 treatment might lead to the recruitment of OPCs and/or regeneration of OLs, resulting in increased remyelination. To further assess whether the reduced amounts of myelin after HHI-LI-PRL were due to axonal damage,  $\beta$ III-Tubulin staining of longitudinal optic nerve sections was performed. The analysis revealed prominent axonal damage in the context of HHI-LI-PRL, while animals prophylactically treated with RP-101074 displayed higher amounts of  $\beta$ III-Tubulin, indicating protective effects. These effects may, at least in



NG2 and PDGFR $\alpha$  expression in optic nerves following photoreceptor loss. Expression levels of OPC markers, NG2 and PDGFR $\alpha$ , were assessed in longitudinal optic nerve sections. Figures (**C**, **D**) provide representative images for NG2 and PDGFR $\alpha$  respectively, while the quantitative results are portrayed in Figures (**A**, **B**). Quantification was accomplished using ImageJ by blinded raters. X-axis of Figures (**A**, **B**) represent the relative expression levels (% of DAPI cells) of NG2 and PDGFR $\alpha$ , respectively. Yellow arrows indicates positive counted cells. All graphs represent the pooled mean  $\pm$  SEM (n=6 animals (12 eyes) per group in total, in two independent experiments), with \*\*\*p<0.001, \*\*\*\*p<0.0001 determined by 1-way ANOVA with the Dunnett *post hoc* test.

part, explain the increased myelin abundance in the optic nerve upon RP-101074 treatment during HHI-LI-PRL.

The reduction of retinal degeneration observed by OCT in the RP-101074 group is certainly at least in part resulting from immunomodulation, including decreased microglial activation or recruitment. Nevertheless, our histological evaluations of myelination (MBP), progenitor cells (Sox2) and OPC's (NG2, PDGFRα) demonstrate an increased expression in the RP-101074 treated animals even when compared to the untreated control group. These observations suggest an impact of RP-101074 that is not solely due to its immunomodulatory function. While it is possible that our data predominantly exhibits an anti-inflammatory effect, the increased myelination and number of progenitor cells and OPC's in the RP-101074 group could suggest an additional protective or regenerative mode of action.

Nevertheless, our research is not without limitations. While the presented light-induced photoreceptor loss is a model for mimicking

neurodegeneration without a T- and B-cell driven component, it still includes inherent inflammatory effects. As such, it remains unclear if the observed effects of RP-101074 are primarily due to its effects on OPCs and myelin or the result of reduced microglial response leading to less neuronal damage. Additionally, our LI-PRL model, although successful in representing certain elements of neurodegeneration, might not fully grasp the multifaceted pathophysiology of human diseases involving neurodegeneration. Hence, validating the applicability of our findings to additional preclinical models and of course human pathology is essential. It would be beneficial to further examine the RP-101074's anti-inflammatory and neuroprotective properties in detailed mechanistic studies involving a variety of preclinical models to better understand its therapeutic potential.To summarize, our preliminary research suggests that RP-101074, an S1PR-1/-5 modulator, might have beneficial effects that extend beyond its known immunomodulatory action. This was demonstrated using the LI-PRL primary degenerative model. The

protective effects could be potentially linked to the enhanced recruitment of Sox2+ cells and oligodendroglial cells, along with the regulation of microglial cell activity via S1PR-1.

# Data availability statement

The original contributions presented in the study are included in the article/supplementary material. Further inquiries can be directed to the corresponding author.

## **Ethics statement**

The animal study was reviewed and approved by State Agency for Nature, Environment and Consumer Protection; AZ 81-02.04.2019.A063.

## **Author contributions**

MS, CH, AI and MD performed the experiments and analyzed the data. MS, MD and PA wrote the manuscript. SM, TR, PA and MD were involved in revising the manuscript critically for important intellectual content and made substantial contributions to interpretation of data. PA and MD conceived the study and supervised experiments. All authors contributed to the article and approved the submitted version.

# **Funding**

The authors declare that this study received funding and substance (RP-101074) from Bristol-Myers Squibb. The funder was not involved in the study design, collection, analysis, interpretation of data, the writing of this article, or the decision to submit it for publication.

# Conflict of interest

Author PA is employed by Maria Hilf Clinics GmbH, Mönchengladbach. The following financial disclosures are

unrelated to the work: SM received honoraria for lecturing and travel expenses for attending meetings from Almirall, Amicus Therapeutics Germany, Bayer Health Care, Biogen, Celgene, Diamed, Genzyme, MedDay Pharmaceuticals, Merck Serono, Novartis, Novo Nordisk, ONO Pharma, Roche, Sanofi-Aventis, Chugai Pharma, QuintilesIMS, and Teva. His research is funded by the German Ministry for Education and Research (BMBF), Deutsche Forschungsgemeinschaft (DFG), Else Kröner Fresenius Foundation, German Academic Exchange Service, Hertie Foundation, Interdisciplinary Center for Clinical Studies (IZKF) Muenster, German Foundation Neurology, and by Almirall, Amicus Therapeutics Germany, Biogen, Diamed, Fresenius Medical Care, Genzyme, Merck Serono, Novartis, ONO Pharma, Roche, and Teva. MD received speaker honoraria from Merck and Novartis. PA is employed by Maria Hilf Clinics GmbH, Mönchengladbach. He received compensation for serving on Scientific Advisory Boards for Ipsen, Novartis, Biogen; he received speaker honoraria and travel support from Novartis, Teva, Biogen, Merz Pharmaceuticals, Ipsen, Allergan, Bayer Healthcare, Esai, UCB and Glaxo Smith Kline; he received research support from Novartis, Biogen, Teva, Merz Pharmaceuticals, Ipsen, Bristol-Myers Squibb and Roche. TR reports grants from German Ministry of Education, Science, Research and Technology, during the conduct of the study; grants and personal fees from Sanofi-Genzyme; personal fees from Biogen; personal fees and non-financial support from Merck Serono; personal fees from Roche, Teva, Alexion, Argenx, UCB, and BMS outside the submitted work.

The remaining authors declare that the research was conducted in the absence of any commercial or financial relationships that could be construed as a potential conflict of interest. The work was funded by a research grant from Celgene / Bristol Myers Squibb to PA.

# Publisher's note

All claims expressed in this article are solely those of the authors and do not necessarily represent those of their affiliated organizations, or those of the publisher, the editors and the reviewers. Any product that may be evaluated in this article, or claim that may be made by its manufacturer, is not guaranteed or endorsed by the publisher.

# References

- 1. Reich DS, Lucchinetti CF, Calabresi PA. Multiple sclerosis. N Engl J Med (2018) 378(2):169–80. doi: 10.1056/NEIMra1401483
- 2. Fischer MT, Sharma R, Lim JL, Haider L, Frischer JM, Drexhage J, et al. NADPH oxidase expression in active multiple sclerosis lesions in relation to oxidative tissue damage and mitochondrial injury. *Brain: A J Neurol* (2012) 135(Pt 3):886–99. doi: 10.1093/brain/aws012
- 3. Cohen JA, Arnold DL, Comi G, Bar-Or A, Gujrathi S, Hartung JP, et al. Safety and efficacy of the selective sphingosine 1-phosphate receptor modulator ozanimod in relapsing multiple sclerosis (RADIANCE): A randomised, placebo-controlled, phase 2 trial. *Lancet Neurol* (2016) 15(4):373–81. doi: 10.1016/S1474-4422(16)00018-1
- 4. Scott FL, Clemons B, Brooks J, Brahmachary E, Powell R, Dedman H, et al. Ozanimod (RPC1063) is a potent sphingosine-1-phosphate receptor-1 (S1P1 ) and

receptor-5 (S1P5 ) agonist with autoimmune disease-modifying activity. Br J Pharmacol (2016) 173(11):1778–92. doi: 10.1111/bph.13476

- 5. Kappos L, Bar-Or A, Cree BAC, Fox RJ, Giovannoni G, Gold R, et al. Siponimod versus placebo in secondary progressive multiple sclerosis (EXPAND): A double-blind, randomised, phase 3 study. *Lancet (London England)* (2018) 391(10127):1263–73. doi: 10.1016/S0140-6736(18)30475-6
- 6. Furman MJ, Meuth SG, Albrecht P, Dietrich M, Blum H, Mares J, et al. B cell targeted therapies in inflammatory autoimmune disease of the central nervous system. Front Immunol (2023) 14:1129906. doi: 10.3389/fimmu.2023.1129906
- 7. Albrecht P, Fröhlich R, Hartung H-P, Kieseier BC, Methner A. Optical coherence tomography measures axonal loss in multiple sclerosis independently of optic neuritis. *J Neurol* (2007) 254(11):1595–6. doi: 10.1007/s00415-007-0538-3

- 8. Saidha S, Syc SB, Ibrahim MA, Eckstein C, Warner CV, Farrell SK, et al. Primary retinal pathology in multiple sclerosis as detected by optical coherence tomography. *Brain: A J Neurol* (2011) 134(Pt 2):518–33. doi: 10.1093/brain/awq346
- 9. Albrecht P, Ringelstein M, Müller AK, Keser N, Dietlein T, Lappas A, et al. Degeneration of retinal layers in multiple sclerosis subtypes quantified by optical coherence tomography. *Multiple Sclerosis (Houndmills Basingstoke England)* (2012) 18 (10):1422–9. doi: 10.1177/1352458512439237
- 10. Galetta KM, Calabresi PA, Frohman EM, Balcer LJ. Optical coherence tomography (OCT): Imaging the visual pathway as a model for neurodegeneration. Neurother: J Am Soc Exp Neurother (2011) 8(1):117-32. doi: 10.1007/s13311-010-0005-1
- 11. Dörr J, Wernecke KD, Bock M, Gaede G, Wuerfel JT, Pfueller CF, et al. Association of retinal and macular damage with brain atrophy in multiple sclerosis. *PloS One* (2011) 6(4):e18132. doi: 10.1371/journal.pone.0018132
- 12. Saidha S, Al-Louzi O, Ratchford JN, Bhargava P, Oh J, Newsome SD, et al. Optical coherence tomography reflects brain atrophy in multiple sclerosis: A four-year study. *Ann Neurol* (2015) 78(5):801–13. doi: 10.1002/ana.24487
- 13. Dietrich M, Hecker C, Nasiri M, Samsam S, Issberner A, Kohne Z, et al. Neuroprotective properties of dimethyl fumarate measured by optical coherence tomography in non-inflammatory animal models. *Front Neurol* (2020) 11:601628. doi: 10.3389/fneur.2020.601628
- 14. Dietrich M, Cruz-Herranz A, Yiu H, Aktas O, Brandt AU, Hartung H-P, et al. Whole-body positional manipulators for ocular imaging of anaesthetised mice and rats: A do-it-yourself guide. *BMJ Open Ophthalmol* (2017) 1(1):e000008. doi: 10.1136/bmjophth-2016-000008
- 15. Dietrich M, Hecker C, Martin E, Langui D, Gliem M, Stankoff B, et al. Increased remyelination and proregenerative microglia under siponimod therapy in mechanistic models. *Neurol (R) Neuroimmunol Neuroinflamm* (2022) 9(3):e1161. doi: 10.1212/NXI.0000000000001161
- 16. Frenger MJ, Hecker C, Sindi M, Issberner A, Hartung H-P, Meuth SG, et al. Semi-automated live tracking of microglial activation in CX3CR1GFP mice during experimental autoimmune encephalomyelitis by confocal scanning laser ophthalmoscopy. Front Immunol (2021) 12:761776. doi: 10.3389/fimmu.2021.761776
- 17. Hecker C, Dietrich M, Issberner A, Hartung H-P, Albrecht P. Comparison of different optomotor response readouts for visual testing in experimental autoimmune encephalomyelitis-optic neuritis. *J Neuroinflamm* (2020) 17(1):216. doi: 10.1186/s12974-020-01889-z
- 18. Messias CV, Santana-Van-Vliet E, Lemos JP, Moreira OC, Cotta-de-Almeida V, Savino W, et al. Sphingosine-1-Phosphate induces dose-dependent chemotaxis or fugetaxis of T-ALL blasts through S1P1 activation. *PloS One* (2016) 11(1):e0148137. doi: 10.1371/journal.pone.0148137
- 19. Schlicher L, Kulig P, von Münchow A, Murphy MJ, Keller MP. *In vitro* characterization of Sphingosine 1-Phosphate receptor 1 (S1P1) expression and mediated migration of primary human T and B cells in the context of cenerimod, a novel, selective S1P1 receptor modulator. *Int J Mol Sci* (2022) 23(3):1191. doi: 10.3390/ijms23031191
- 20. Subei AM, Cohen JA. Sphingosine 1-Phosphate receptor modulators in multiple sclerosis. CNS Drugs (2015) 29(7):565–75. doi: 10.1007/s40263-015-0261-z

- 21. Brinkmann V, Billich A, Baumruker T, Heining P, Schmouder R, Francis G, et al. Fingolimod (FTY720): Discovery and development of an oral drug to treat multiple sclerosis. *Nat Rev Drug Discovery* (2010) 9(11):883–97. doi: 10.1038/nrd3248
- 22. Liu W, Yu Z, Wang Z, Waubant EL, Zhai S, Benet LZ. Using an animal model to predict the effective human dose for oral multiple sclerosis drugs.  $Clin\ Trans\ Sci\ (2023)\ 16(3):467–77.$  doi: 10.1111/cts.13458
- 23. Huang H, Shi M, Qi C, Tian Q, Li H, Liu M, et al. Sphingosine-1-phosphate receptor modulation improves neurogenesis and functional recovery after stroke. *FASEB J* (2022) 36(12):e22616. doi: 10.1096/fj.202200533RR
- 24. Beck SC, Karlstetter M, Garcia Garrido M, Feng Y, Dannhausen K, Mühlfriedel R, et al. Cystoid edema, neovascularization and inflammatory processes in the murine Norrin-deficient retina. *Sci Rep* (2018) 8(1):5970. doi: 10.1038/s41598-018-24476-y
- 25. Chu F, Shi M, Zheng C, Shen D, Zhu J, Zheng X, et al. The roles of macrophages and microglia in multiple sclerosis and experimental autoimmune encephalomyelitis. *J Neuroimmunol* (2018) 318:1–7. doi: 10.1016/j.jneuroim.2018.02.015
- 26. Hickman S, Izzy S, Sen P, Morsett L, El Khoury J. Microglia in neurodegeneration. Nat Neurosci (2018) 21(10):1359–69. doi: 10.1038/s41593-018-0242-x
- 27. Behrangi N, Fischbach F, Kipp M. Mechanism of siponimod: anti-inflammatory and neuroprotective mode of action. *Cells* (2019) 8(1):24. doi: 10.3390/cells8010024
- 28. Baydyuk M, Cha DS, Hu J, Yamazaki R, Miller EM, Smith VN, et al. Tracking the evolution of CNS remyelinating lesion in mice with neutral red dye. *Proc Natl Acad Sci USA* (2019) 116(28):14290–9. doi: 10.1073/pnas.1819343116
- 29. Naruse M, Shibasaki K, Shimauchi-Ohtaki H, Ishizaki Y. Microglial activation induces generation of oligodendrocyte progenitor cells from the subventricular zone after focal demyelination in the Corpus callosum. *Dev Neurosci* (2018) 40(1):54–63. doi: 10.1159/000486332
- 30. Roggeri A, Schepers M, Tiane A, Rombaut B, van Veggel L, Hellings N, et al. Sphingosine-1-Phosphate receptor modulators and oligodendroglial cells: beyond immunomodulation. *Int J Mol Sci* (2020) 21(20):7537. doi: 10.3390/ijms21207537
- 31. Song H, McEwen HP, Duncan T, Lee JY, Teo JD, Don AS. Sphingosine kinase 2 is essential for remyelination following cuprizone intoxication. Glia (2021) 69 (12):2863–81. doi: 10.1002/glia.24074
- 32. Price ST, Beckham TH, Cheng JC, Lu P, Liu X, Norris JS. Sphingosine 1-Phosphate receptor 2 regulates the migration, proliferation, and differentiation of mesenchymal stem cells. *Int J Stem Cell Res Ther* (2015) 2(2):14. doi: 10.23937/2469-570x/1410014
- 33. Bodhireddy SR, Lyman WD, Rashbaum WK, Weidenheim KM. Immunohistochemical detection of myelin basic protein is a sensitive marker of myelination in second trimester human fetal spinal cord. *J Neuropathol Exp Neurol* (1994) 53(2):144–9. doi: 10.1097/00005072-199403000-00005
- 34. Zhang S, Zhu X, Gui X, Croteau C, Song L, Xu J, et al. Sox2 is essential for oligodendroglial proliferation and differentiation during postnatal brain myelination and CNS remyelination. *J Neurosci* (2018) 38(7):1802–20. doi: 10.1523/JNEUROSCI.1291-17.2018
- 35. Kuhbandner K. Uncovering the role of Sox2 in oligodendroglia. *J Neurosci* (2018) 38(19):4460–1. doi: 10.1523/JNEUROSCI.0556-18.2018



### **OPEN ACCESS**

EDITED BY

Rune Alexander Aamodt Høglund, Akershus University Hospital, Norway

REVIEWED BY

Oliver W Gramlich, The University of Iowa, United States Shamundeeswari Anandan, University of Bergen, Norway

\*CORRESPONDENCE

Philipp Albrecht

phil.albrecht@gmail.com

RECEIVED 22 November 2024 ACCEPTED 14 February 2025 PUBLISHED 05 March 2025

### CITATION

Sindi M, Dietrich M, Klees D, Gruchot J, Hecker C, Silbereis J, Issberner A, Hartung H-P, Ruck T, Stark H, Kurz T, Küry P, Meuth SG and Albrecht P (2025) Positive allosteric modulation of AMPA receptors via PF4778574 leads to reduced demyelination and clinical disability in experimental models of multiple sclerosis. *Front. Immunol.* 16:1532877.

### COPYRIGHT

© 2025 Sindi, Dietrich, Klees, Gruchot, Hecker, Silbereis, Issberner, Hartung, Ruck, Stark, Kurz, Küry, Meuth and Albrecht. This is an openaccess article distributed under the terms of the Creative Commons Attribution License (CC BY). The use, distribution or reproduction in other forums is permitted, provided the original author(s) and the copyright owner(s) are credited and that the original publication in this journal is cited, in accordance with accepted academic practice. No use, distribution or reproduction is permitted which does not comply with these terms.

# Positive allosteric modulation of AMPA receptors via PF4778574 leads to reduced demyelination and clinical disability in experimental models of multiple sclerosis

Mustafa Sindi<sup>1</sup>, Michael Dietrich<sup>1</sup>, Diana Klees<sup>1</sup>, Joel Gruchot<sup>1</sup>, Christina Hecker<sup>1</sup>, John Silbereis<sup>2</sup>, Andrea Issberner<sup>1</sup>, Hans-Peter Hartung<sup>1,3,4</sup>, Tobias Ruck<sup>1</sup>, Holger Stark<sup>5</sup>, Thomas Kurz<sup>5</sup>, Patrick Küry<sup>1</sup>, Sven G. Meuth<sup>1</sup> and Philipp Albrecht<sup>1,6\*</sup>

<sup>1</sup>Medical Faculty and University Hospital Düsseldorf, Department of Neurology, Heinrich Heine University, Düsseldorf, Germany, <sup>2</sup>Department of Medical Research, Multiple Sclerosis Unit, Biogen, Cambridge, MA, United States, <sup>3</sup>Brain and Mind Center, University of Sydney, Sydney, NSW, Australia, <sup>4</sup>Department of Neurology, Palacky University Olomouc, Olomouc, Czechia, <sup>5</sup>Faculty of Mathematics and Natural Sciences, Institute of Pharmaceutical and Medicinal Chemistry, Heinrich Heine University, Düsseldorf, Germany, <sup>6</sup>Department of Neurology, Maria Hilf Clinics, Mönchengladbach, Germany

**Introduction:** Multiple Sclerosis (MS), a debilitating central nervous system (CNS) disorder, is characterized by inflammation, demyelination, and neuronal degeneration. Despite advancements in immunomodulatory treatments, neuroprotective or restorative strategies remain inadequate. Our research is focusing on the potential of the positive allosteric modulator of AMPA receptors (AMPA-PAM), PF4778574, in addressing MS symptoms.

**Methods:** We utilized the MOG35-55 induced experimental autoimmune encephalomyelitis (EAE) model in C57BL6J mice to examine PF4778574's therapeutic and prophylactic efficacy. Our comprehensive approach included clinical scoring, optical coherence tomography (OCT), optomotor response (OMR) and histological assessments. Additionally, we explored the effects of PF4778574 in comparison and in combination with the immunomodulatory agent fingolimod, and investigated the impact on Cuprizone induced toxic demyelination.

**Results:** Prophylactic administration of PF4778574 showed notable improvement in clinical EAE indices and reduction in neuronal loss. While it did not diminish microglial activity, it reduced demyelinated areas in optic nerves and in the corpus callosum. Both PF4778574 and fingolimod significantly enhanced clinical EAE scores and decreased demyelination. However, their combination did not yield additional benefits. In the cuprizone model, PF4778574 increased oligodendrocyte precursor and mature myelin-forming cells, suggesting a pro-remyelinating effect.

**Discussion:** PF4778574 demonstrates promise in mitigating EAE effects, especially in terms of clinical disability and demyelination. These results suggest AMPA-PAMs as potential targets of interest for MS treatment beyond immunomodulatory approaches.

KEYWORDS

AMPA-PAM, AMPA, EAE, excitotoxicity, neuroprotection, multiple sclerosis, optical coherence tomography

# 1 Introduction

Multiple Sclerosis (MS) is an autoimmune disorder of the central nervous system marked by inflammation and demyelination, leading to the dysfunction of oligodendrocytes, subsequent harm to axons, and neuronal degeneration in the central nervous system (1). The chronic neurodegeneration is the main reason for the sustained clinical impairment in patients with MS and is not addressable to traditional immunosuppressants and immunomodulatory treatments. Hallmarks of MS include pathological changes marked by lymphocytes and macrophages penetrating the CNS tissue, leading to the accumulation of adhesion molecules and the promotion of immune cell engagement through pro-inflammatory cytokines. These series of events results in glial damage and neuronal injury. Although the precise underlying process is yet to be completely understood, recent studies have suggested that enhancing axonal and synaptic function in MS can reduce symptoms and potentially even have protective capacities (2, 3).

AMPA-type ionotropic glutamate receptor positive allosteric modulators (AMPA-PAMs) are considered as synaptic enhancers and have been recognized for their potential in the therapeutic management of cognitive and mood disorders (4-6). These agents modulate the function of AMPA receptors, which are central to fast synaptic transmission in the nervous system. By enhancing the activity of these receptors, AMPA-PAMs facilitate various cognitive processes and could have considerable therapeutic implications (7). AMPA-PAMs bind to the AMPA receptor (AMPAR) complex's allosteric sites, boosting the receptor. However, unlike AMPAR agonists, PAMs only enhance signals when glutamate is present, but do not directly trigger the receptor. They can also selectively target specific AMPAR subgroups (8, 9). AMPA-PAMs are divided into two types; low-impact PAMs, which minimally affect the field excitatory postsynaptic potential (fEPSP), and high-impact PAMs, which noticeably alter the fEPSP. Only high-impact PAMs, such as the compound PF4778574 tested in this study bind to the cyclothiazide site and trigger BDNF expression. Low-impact PAMs boost synaptic currents by reducing AMPAR deactivation, while high-impact PAMs enhance and extend synaptic currents by decreasing both deactivation and desensitization (10).

MS, particularly in its chronic phases, can be considered a neurodegenerative disease due to the irreversible loss of neurons

and associated cognitive decline (11). At the cellular level, glutamate-induced excitotoxicity is known to contribute significantly to the neuronal damage observed in MS (12). AMPA receptors, being the primary mediators of fast excitatory synaptic transmission, are thought to play a substantial role in this process. Over-activation of AMPA receptors leads to an excessive influx of calcium ions, triggering a cascade of harmful intracellular processes that culminate in neuronal death. AMPA-PAMs, however, modulate the receptor's function to enhance synaptic transmission without causing receptor over-activation and the ensuing excitotoxicity (6). This modulation, in essence, could aid in maintaining neuronal communication while preventing harmful consequences to the neurons. In addition, beyond their role in neurotransmission, AMPA receptors have also been implicated in inflammatory processes. Studies suggest that AMPA receptor antagonists can reduce the release of pro-inflammatory cytokines (13-15), implying that modulating AMPA receptor function might have potential anti-inflammatory effects. While the therapeutic effects of AMPA-PAMs have neither been evaluated in MS nor in experimental autoimmune encephalomyelitis (EAE), these mechanistic insights provide a rationale for further investigation. Moreover, the possibility of modulating neuroinflammation and excitotoxicity, two central processes in MS, suggests that AMPA-PAMs could also influence disease progression.

In this study, we investigated whether AMPA-PAM can help protect against neurodegeneration and demyelination—two major pathologies of MS alongside neuroinflammation. We employed the MOG35-55-induced EAE model to assess both prophylactic and therapeutic administration of AMPA-PAM alone or in combination with fingolimod, a well-established immunomodulatory drug. By integrating clinical scoring, optical coherence tomography (OCT), optomotor response (OMR), and comprehensive histological analyses, we aimed to determine if AMPA-PAM could preserve neuronal structures and myelin integrity in the setting of autoimmune inflammation. We further extended our approach to the cuprizone model to explore whether AMPA-PAM might promote remyelination under toxic demyelinating conditions. We hypothesized that AMPA-PAM would provide neuroprotection and could potentially synergize with classical immunomodulatory strategies. Although existing MS therapies effectively target inflammation, they often fail to prevent ongoing neurodegeneration. By focusing on the positive modulation of

AMPA receptors, our study addresses a critical gap in current MS research investigating whether synaptic enhancement can confer neuroprotective and pro-remyelinating benefits. Ultimately, our findings may offer novel insights that help expand future therapeutic approaches beyond immunosuppression, with the aim of preserving and restoring neural function in MS.

Given these considerations, the role of AMPA-PAMs in MS warrants further investigation. This could potentially lead to therapeutic strategies not only for MS but also for a broader range of inflammatory and neurodegenerative diseases where excitotoxicity and axonal loss are involved. As such, this line of research holds promise in contributing to our understanding and treatment of neuroinflammatory and neurodegenerative diseases.

# 2 Materials and methods

# 2.1 Subject animals, models and treatment protocols

EAE induction: Six-week-old female C57BL/6J mice, sourced from Janvier Labs (Le Genest-Saint-Isle, France), were utilized for the experiment. The EAE mouse model involved immunization of mice with 200  $\mu$ g of myelin oligodendrocyte glycoprotein fragment 35–55 (MOG35–55), which was acquired from BIOTREND. The immunization was emulsified in 200  $\mu$ l of complete Freund's adjuvant (CFA) and augmented with 800  $\mu$ g of thermally inactivated Mt., H37Ra. Both of these components were procured from BD Difco. The immunization process included subcutaneous injection distributed over four points on the front and hind flank. Additionally, intraperitoneal injections of 200 ng of pertussis toxin (PTX), obtained from Sigma-Aldrich, were administered on days 0 and 2 post-immunization. The sham control group was treated with PTX and CFA, excluding the MOG35–55 peptide.

Cuprizone treatment protocol for remyelination study according to the protocol of 16, shortly: Eight-week-old C57BL/6J mice were used in the experiment and divided into three dietary groups. The first group was fed control pellets, while the second and third groups were fed 0.2% cuprizone-containing food pellets (Both SNIFF, Soest, Germany). Starting in the third week of treatment, mice in the AMPA-PAM group received daily doses of PF-4778574, while those in the vehicle group received an equivalent volume of vehicle. After six weeks of cuprizone treatment, all animals were switched to a control diet for one week to promote remyelination (Figure 1C).

We carried out a dose-finding study and a subsequent comparative/combination experiment to evaluate prophylactic and therapeutic administration of PF4778574 in both the EAE and cuprizone models. Based on a power calculation (G\*Power version 3.1.9.7) aiming at a power (1-ß) of 0.8 and an alpha of 0.05 at an effect size of 1.5 and 1.4six animals per group were used in the EAE experiments and eight animals per group in the cuprizone model, respectively. The dose-finding study compared 0.1 mg/kg and 0.8 mg/kg PF4778574 (administered once daily) versus vehicle, incorporating regular OCT measurements on days 0 (baseline), 7, 14, 21, 35, 41, 56, 70, 84, and 112, with optomotor response (OMR)

testing one day prior to each OCT session. In the subsequent comparative and combination study, OCT was performed on days 0, 42, and 85, while OMR assessments occurred on days 0, 7, 14, 21, 28, 42, 56, and 85. In both experiments, animals were assessed clinically on a daily basis. PF4778574 and fingolimod were administered orally each day at the doses described in Table 1.

# 2.2 Euthanization and anesthesia protocol

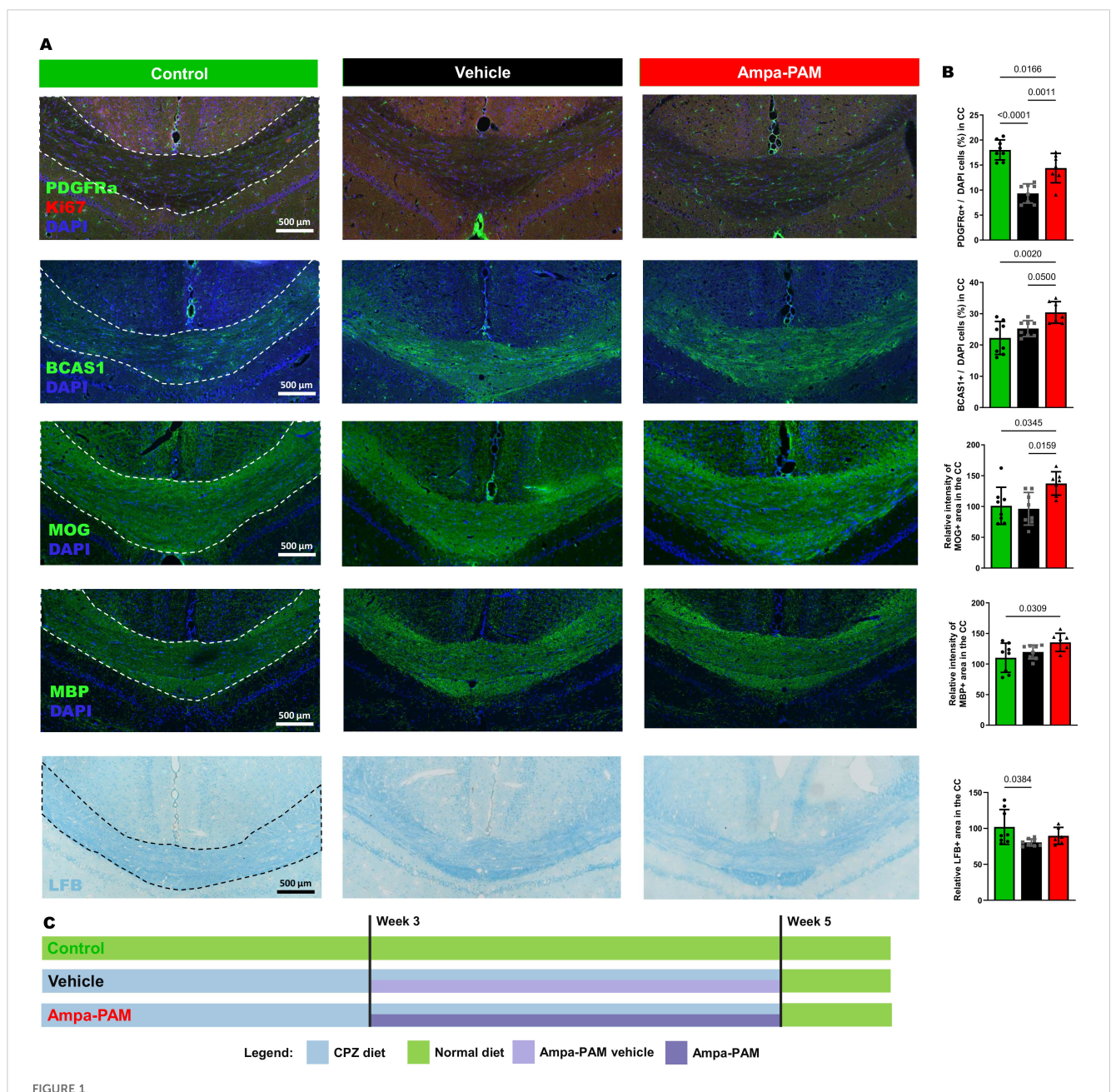
For the OCT measurements, the animals were anesthetized using isoflurane, a widely used inhalational anesthetic known for its rapid induction and recovery properties. The anesthesia setup included a vaporizer provided by Harvard Apparatus Anesthetic Vaporizors, while the isoflurane itself was sourced from Piramal Critical Care. The induction phase was conducted at a concentration of 3.5% isoflurane to ensure a quick and effective loss of consciousness in the animals, followed by maintenance at a reduced concentration of 2% isoflurane to keep the animals in a stable anesthetized state throughout the procedure. A controlled oxygen flow rate of 0.6 liters per minute was employed to ensure adequate oxygenation during anesthesia. The anesthetic gas mixture was delivered directly to the mice through custom-designed nose cones, which allowed precise administration and minimized waste of the anesthetic agent.

Following the experimental procedures, the animals were humanely euthanized to ensure minimal suffering. This was achieved through intraperitoneal injection of a prepared solution containing 100 mg/kg of Ketamine and 20 mg/kg of Xylazine, dissolved in 250  $\mu$ l of 0.9% NaCl saline solution. This combination is widely recognized for its effectiveness in humane animal euthanasia. Cardiac perfusion was subsequently performed. This involved flushing the circulatory system with phosphate-buffered saline (PBS) obtained from Gibco (Carlsbad, USA) to remove blood and prepare tissues for downstream analyses. These steps were carried out in strict adherence to ethical guidelines and protocols for animal experimentation to ensure the welfare of the animals and the reliability of the experimental results as mentioned in point 11.

# 2.3 OCT, OMR and other outcome measures

OCT assessments were performed as previously described and are reported in line with the APOSTEL reporting guidelines (17, 18). The OCT-based primary outcome parameters included the thickness of the inner retinal layers, total retinal thickness, and outer retinal layers as evaluated in volume scans around the optic disc. During OCT measurements, the animals were anesthetized as described in point 2.2.

We carried out regular OCT measurements using the Spectralis<sup>®</sup> HRA + OCT instrument (Heidelberg Engineering, Germany), which was modified for rodent use as previously explained (19). The Heidelberg Eye Explorer software was utilized to segment retinal volume scans, with manual correction for any



Remyelination marker in corpus callosum region post-Cuprizone treatment. Histological sections and quantitative analysis of remyelination in the corpus callosum are depicted, comparing vehicle and PF-4778574 treated animals. Expression levels of markers relevant for remyelination: PDGFR $\alpha$ / Ki-67, BCAS1, MOG, MBP and LFB was assessed in mice coronal brain sections. (A) provides representative images of these staining while the quantitative results are portrayed in (B). (C) illustrates the demyelination and remyelination protocol using eight-week-old C57BL/6J mice divided into three groups: One fed control pellets (green, Control), and two fed 0.2% cuprizone pellets (black, Vehicle; red, AMPA-PAM). From week three, the AMPA-PAM group received daily PF-4778574 doses, while the Vehicle group received a vehicle. After six weeks of cuprizone, all mice switched to a control diet for one week to promote remyelination. Quantification was accomplished as described in section 2.2. All graphs represent the pooled mean  $\pm$  SD (n=8 animals per group in total). The bar graph presents statistical significance, with p-values displayed over the bars, determined using ANOVA with Tukey's *post hoc* test.

segmentation errors. The volume of the area around the optic disc was evaluated using the ETDRS grid, avoiding the center with the disc, as previously documented (20). Periodic examinations were made of the inner retinal layer (IRL), outer retinal layer (ORL), and total retinal thickness (TRT), and were compared with baseline measurements. The IRL layer includes: NFL, GCL and IPL whereas the ORL layer contains: INL, OPL, ONL, ELM, IS/OS, RPE and Choroid. The TRT consists of both: IRL + ORL.

The spatial frequency measurement via OMR was taken as a primary functional output (21). We carried out OMR measurements at periodic intervals using the OptoMotry<sup>®</sup> system from Cerebral Mechanics, simultaneously with OCT and cSLO measurements. The parameter for visual function was the spatial frequency, which was identified by varying the spatial frequency randomly to determine the threshold where the mouse could track, as reported earlier (20, 21).

TABLE 1 Treatment groups, therapy and treatment start.

Group name	Therapy and start of treatment (days post-immunization)
Sham+vehicle	DMSO: Cremophor:ddH2O (5:5:90), day 0
MOG+vehicle	DMSO: Cremophor:ddH2O (5:5:90), day 0
MOG+AMPA-PAM (d0)	0.1 mg/kg PF4778574, day 0
MOG+fingo (d0)	3 mg/kg fingolimod, day 0
MOG+AMPA-PAM (d14)	0.1 mg/kg PF4778574, day 14
MOG+AMPA-PAM(d0) +fingo (d0)	0.1 mg/kg PF4778574, day 0 + 3 mg/kg fingolimod, day 0

Other histology-based parameters were assessed as secondary outcome criteria. A standardized scoring system was employed to evaluate the severity of EAE symptoms. In the EAE model, disease severity is monitored using a clinical scoring system from 0.5 to 5, where 0.5 indicates general weakness and fatigue, 1 indicates complete tail paralysis without other neurological deficits, 1.5 adds a restricted righting reflex, 2 (weak) and 2.5 (severe) further introduces partial hind limb paralysis, 3 indicates reversible complete hind limb paralysis, 3.5 includes a  $\geq$ 20% reduction in body weight, 4 adds partial forelimb paralysis, and 5 denotes a moribund animal or death due to EAE.

# 2.4 Histological analysis

After euthanization of the mice as described in point 2.2, the optic nerves were then isolated, fixed overnight in 4% paraformaldehyde (Carl Roth, Karlsruhe, Germany), and later treated with a sucrose gradient for dehydration and embedded in O.C.T. compound (Sakura<sup>TM</sup> Finetek, Alphen aan den Rijn, Netherlands).

Optic nerve: Longitudinal optic nerve slices of five micrometers were obtained for fluorescence staining. Cross-sectional slices of the optic nerves were utilized to quantify and evaluate the condition of myelination using antibodies against myelin basic protein (MBP) (Millipore, #MAB386, 1:500). Microglial activation was assessed using antibodies against Iba1 (Wako, #019-19741, 1:500) under a Leica DMi8 confocal microscope equipped with a Leica HyD detector (63x objective lens magnification). The secondary antibodies used were goat anti-mouse Cy 2, goat anti-rabbit Cy 3, goat ant-rat Cy3 (Millipore, 1:500) and Alexa Fluor TM 488 rabbit anti-mouse (Invitrogen, 1:500). ImageJ software was utilized to analyze the numbers of cells stained with Iba1, expressed as a ratio to DAPI staining, and the overall signal for MBP (positive total area in the red channel).

Retinal whole mount: To further examine the retina, a semiautomated count of Brn3a+ cells on retinal flatmounts was performed. The retinae were stained with Brn3a (Santa Cruz Biotechnology, #sc-8429, 1:200) antibody and subsequently flatmounted on glass slides. The secondary antibodies used was Alexa Fluor 488 rabbit anti-mouse (Invitrogen, 1:500). Each retina was partitioned into four quadrants, each with three areas: central, midperiphery, and far-periphery. For each eye, the total count of Brn3a + cells were calculated by aggregating the counts from all 12 imaged areas.

Brain: Brain cross sections were obtained for fluorescence staining to quantify myelination status and OPC's activation. OPC's were detected using antibodies against PDGFRa (ThermoFisher Scientific, #A21207, 1:250). Cell proliferation was detected using antibodies against Ki-67 (AbCam, #16667, 1:250). MOG was detected using antibodies at 1:500 dilution (Millipore, #8-81805). MBP was detected using antibodies at 1:250 dilution (Bio-Rad, #MCA409S). BCAS1 was detected using antibodies at 1:250 dilution (Santa Cruz, #10839529). The secondary antibodies used were goat anti-rat Cy3 (Millipore, 1:500) and Alexa Fluor TM 488 goat anti-mouse (Invitrogen, 1:250). Further, slides containing 12-µm coronal section were incubated overnight in LFB (Sigma-Aldrich) solution (0.1% LFB, 4% glacial acetic acid in 96% ethanol) at 56°C. Afterward, redundant LFB staining was washed out using 0.05% lithium carbonate solution (in ddH2O), tissue was dehydrated and embedded in ROTI-Histokit II (Carl Roth, Karlsruhe, Germany). Quantification was performed as follows: For PDGFRα and BCAS1, the number of positive cells was counted and expressed as a ratio relative to DAPI-positive cells within the marked corpus callosum area. For MOG and MBP, the relative intensity of the MOG and/or MBP-positive regions was measured within the marked corpus callosum area after normalization. Similarly, for LFB, the relative area of LFB positivity within the marked corpus callosum region was determined following normalization.

# 2.5 Data analysis

Prism (version 9, Graphpad Software, Inc.) and IBM SPSS Statistics (version 20, IBM Corporation, USA) were used for statistical analysis. The data of retinal parameters were analyzed using generalized estimation equation (GEE) models. The Dunnett's *post hoc* test, in conjunction with a one-way ANOVA, was used for group means analysis, except for the corpus callosum analyses, which were evaluated using Tukey's test.

For OCT data analysis, we followed our previously published approaches for evaluating EAE outcomes, which provide detailed guidance on handling measurements from both eyes in a statistically appropriate manner (17, 22). Briefly, we first applied the OCT device software's automated segmentation to derive thickness values for relevant retinal layers; afterward, we performed manual correction of any segmentation errors while ensuring the investigator was blinded to experimental groups. We then used the 1, 2, and 3 mm ETDRS grid to calculate mean thickness values, excluding the inner 1 mm region containing the optic disc, which typically covered an angle of approximately 25°. All scans were evaluated based on predefined quality cutoffs (e.g., >20 decibels) to maintain consistency across samples. For statistical analysis, we employed generalized estimating equation models using an exchangeable working correlation matrix accounting for within-subject inter-eye correlations (), to ensure valid inferences from animals in which both eyes were assessed (17, 18, 22).

For OMR data analysis, we also incorporated methodologies outlined in our earlier work (22), with attention to the potential dependence of measurements from both eyes. In this setup, the software randomly changed the direction of the moving grid, and the tracking response (clockwise vs. counterclockwise) was used to determine whether the animal followed the left or right eye stimulus. Step sizes of the stimulus were either adjusted manually or automatically through the software's adaptive feature. To maintain robust engagement throughout the testing session, we stimulated the animals with whistling sounds and sporadic screen blanking. At the end of each trial, the summary data were exported for further processing, and statistical analyses again utilized the GEE models outlined above.

# 3 Results

# 3.1 Dose finding study

In our study aimed at evaluating the efficacy of PF4778574 in preventing acute inflammatory exacerbations and chronic degeneration, we conducted a 110-day longitudinal analysis of retinal neurodegeneration using the MOG33-55 peptide-induced EAE model in C57BL/6J mice. We examined the effects of two different concentrations of PF4778574 (0.1 and 0.8 mg/kg bodyweight, administered subcutaneously), starting the treatment at the same time as the immunization (prophylactic treatment), comparing treated animals with untreated EAE mice (MOG+vehicle) and sham non-EAE mice (sham+vehicle).

The prophylactic administration of 0.1 mg/kg PF4778574 had a significant positive impact on the clinical EAE scores (Mean Difference [MD]: 0.5487, p<0.05), whereas the higher dose of 0.8 mg/kg did not result in a statistically significant effect (MD: 0.3303, not significant [ns]), as shown in Figure 2A.

When examining structural changes in the retina via OCT measurements, untreated sham control mice maintained a stable inner retinal layer (IRL) thickness throughout the study period. In contrast, mice immunized with the MOG peptide exhibited a significant reduction in IRL thickness (MD: 3.740, p<0.001), which persisted up to day 110. The 0.1 mg/kg PF4778574 treatment significantly slowed the degeneration of the IRL (MD: 0.8487, p<0.05) compared to vehicle-treated MOG EAE mice (Figure 2B). However, the 0.8 mg/kg dose did not significantly affect IRL degeneration (MD: 0.4244, ns).

Furthermore, PF4778574 did not show a significant benefit in preserving visual acuity, as both the 0.1 mg/kg (MD: 0.009406) and 0.8 mg/kg (MD: 0.004781) doses failed to produce statistically significant improvements compared to vehicle-treated MOG EAE mice (Figure 2C).

Immunohistological staining of retinal wholemounts revealed that untreated EAE mice experienced substantial retinal ganglion cell (RGC) loss, as shown in Figures 2D, E. The 0.1 mg/kg dose of PF4778574 modestly reduced this loss (MD: 252.8, p<0.05), whereas the 0.8 mg/kg dose did not yield a significant effect (MD: 173.0, ns). These findings align with the EAE clinical scores. Figure 6F shows the treatment and readout intervals.

To assess the impact of PF4778574 on immune cell infiltration into the CNS during EAE, we performed histological analysis of Iba1+ microglia in longitudinal sections of the optic nerve (Figure 3A). Neither the 0.1 mg/kg (MD: 9.894, ns) nor the 0.8 mg/kg (MD: 10.27, ns) prophylactic treatments resulted in a significant reduction in microglial activity in the optic nerves compared to untreated EAE mice (Figure 3B).

We also evaluated the myelin integrity of the optic nerve by performing immunohistological staining for Myelin Basic Protein (MBP). MOG-immunized mice showed extensive demyelination in the optic nerve, whereas untreated sham mice exhibited uniform myelin structure (MD: 1.278, p<0.001). Treatment with PF4778574 led to a significant reduction in the extent of lesions in the MBP-stained optic nerves at both the 0.1 mg/kg (MD: 0.8333, p<0.01) and 0.8 mg/kg (MD: 0.5833, p<0.05) doses (Figures 3C, D).

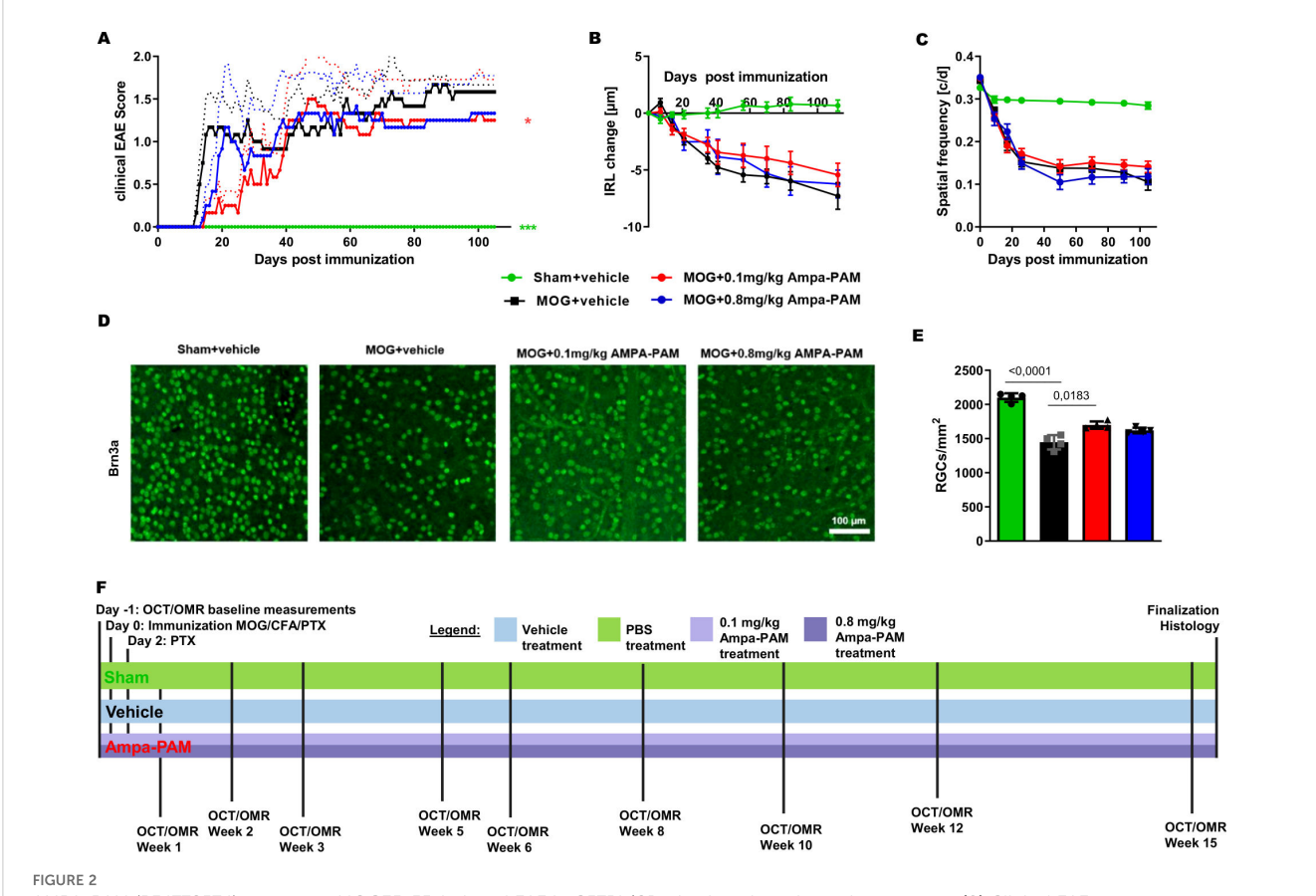
# 3.2 Comparative and combinatory study

In the subsequent phase of our study, we combined the dose of PF4778574 that demonstrated the highest efficacy in the earlier dose-response experiment (0.1 mg/kg) with the well-established immunomodulatory agent, fingolimod, at 3 mg/kg (administered orally) in the EAE model. The treatment protocols used are outlined in Table 1.

Both prophylactic treatment with fingolimod (MD: 0.8279, p<0.001) and PF4778574 (MD: 0.6605, p<0.01) significantly reduced the clinical EAE scores. Even when PF4778574 treatment was delayed and initiated therapeutically 14 days postimmunization, we observed a notable improvement in clinical disability in EAE mice (MD: 0.3488, p<0.05) compared to the untreated MOG group. However, combining PF4778574 with fingolimod did not result in any synergistic effects beyond what was achieved with fingolimod (fingo) alone (MD: 0.7337, p<0.001). These findings from the EAE clinical scores were supported by OCT evaluations of the inner retinal layer (IRL) thickness (MD: Fingo D0 = 2.493, p<0.01; AMPA-PAM D0 = 1.750, p<0.05; Fingo D0 & AMPA-PAM D0 = 1.963, p<0.05), except in the case of delayed PF4778574 monotherapy, which did not show a significant difference compared to the vehicle treated MOG control (Figures 4A, B).

Functionally, only fingolimod monotherapy significantly improved visual acuity (MD: 0.04798, p<0.001), while PF4778574 (MD: 0.01261, ns) and all combination therapies did not significantly alter visual function in EAE mice (Figure 4C). Histologically, retinal ganglion cell (RGC) loss after 90 days of EAE was reduced by both prophylactic PF4778574 (MD: 609.5, p<0.01) and prophylactic fingolimod (MD: 813.0, p<0.001), as well as by the combination therapy (MD: 565.1, p<0.05) (Figures 4D, E).

Further histological analysis of the spinal cord 90 days post-MOG35-55 immunization revealed that neither prophylactic nor therapeutic PF4778574 monotherapy reduced the number of Iba1+ microglia. However, both fingolimod monotherapy (MD: 37.60, p<0.001) and the combination therapy (MD: 38.67, p<0.001) significantly decreased the number of these microglial infiltrates compared to untreated EAE mice (Figures 5A, B).



AMPA-PAM (PF4778574) attenuates MOG35-55-induced EAE in C57BL/6J mice in a dose dependent manner. (A) Clinical EAE score, (B) degeneration of the inner retinal layers and (C) visual function by spatial frequency in cycles per degree (c/d) of female C57BL/6J EAE mice over 110 days of EAE. (D) Brn3a stained RGCs after 110 days of EAE of Sham, MOG EAE and AMPA-PAM treated mice. (E) The bar graph shows the RGC density 110 days after immunization. AMPA-PAM was administered on the day of immunization. (F) Illustrates the treatment and evaluation regimen of the EAE experiment. Graphs A-C represent the pooled mean ± SEM (out of two independent experiments each with n = 6 animals per group), with \*p<0.05, AUC compared by ANOVA with LSD post hoc test for time course compared to untreated MOG EAE. The bar graph E presents statistical significance, with p-values displayed over the bars, determined using ANOVA with Dunnett's post hoc test, compared to MOG EAE untreated mice.

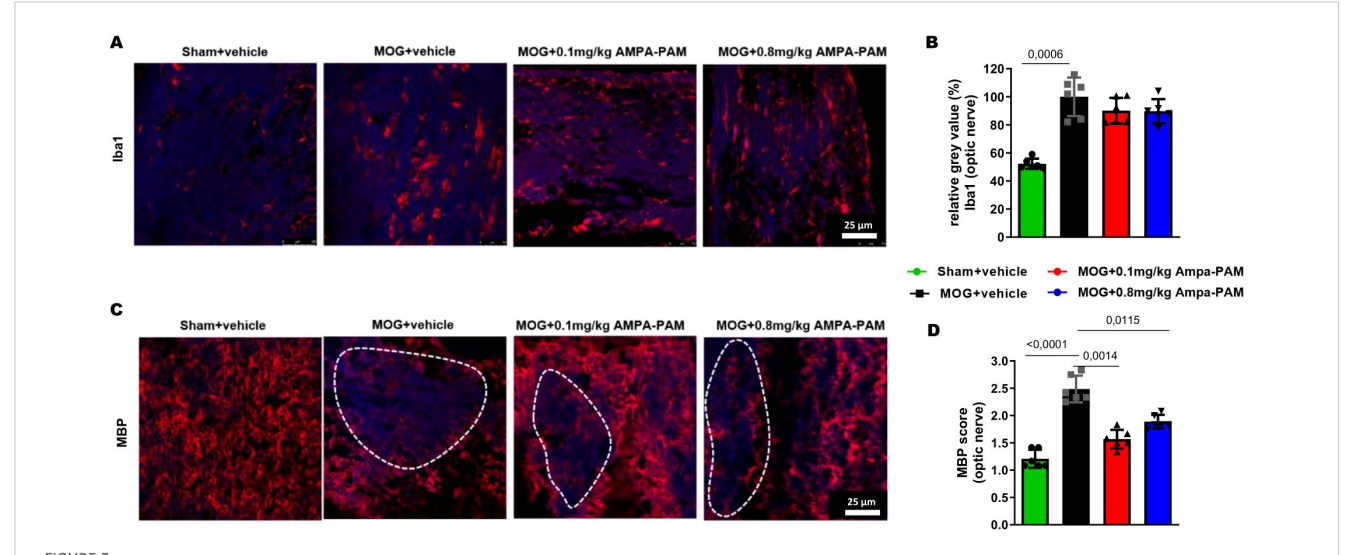
To assess the protective effects against demyelination in the spinal cord, MBP staining was performed. It showed that both prophylactic PF4778574 (MD: 0.7333, p<0.01) and fingolimod (MD: 1.067, p<0.001) monotherapy, as well as the combination therapy (MD: 1.100, p<0.01), significantly reduced the extent of demyelination in the EAE model compared to the untreated MOG cohort 90 days post-immunization. However, therapeutic PF4778574 intervention did not significantly reduce lesion areas in the spinal cord (MD: 0.6333, ns) (Figures 6A, B).

To further assess the remyelinating potential of PF4778574, we used the Cuprizone model as described in point 2.1., focusing on histological sections of the corpus callosum (Figure 1A). PF4778574 treatment led to a significant increase in PDGFRα-positive cells (MD: 5.064, p<0.01) compared to vehicle-treated animals, indicating an enhanced presence of oligodendrocyte precursor cells (OPCs) crucial for myelin development and regeneration. BCAS1 staining revealed a significant rise in late-stage oligodendrocyte lineage cells involved in active myelination processes in the PF4778574-treated group (MD: 5.179, p<0.05). Additionally, PF4778574 treatment resulted in a higher relative intensity of the MOG-positive area (MD: 41.14, p<0.05), suggesting improved myelin integrity. While MBP staining (MD:

15.73, ns) and LFB staining (MD: 9.229, ns) did not show statistically significant differences, both exhibited trends toward higher expression in the treated group (Figure 1B). Figure 1C illustrates the diet and treatment regimen. MBP is an essential protein reflecting the extent of myelination, and LFB is a staining technique that highlights overall myelin content. These observations suggest that PF4778574 may enhance remyelination, even if some marker-quantification did not reach statistical significance.

# 4 Discussion

In the present study, we aimed to systematically investigate the therapeutic and preventive effects of the type-II AMPA-PAM PF4778574 as well as a combination therapy of PF4778574 and fingolimod, - as an example for an approved immunomodulatory treatment for MS - on EAEON, an established experimental rodent model of MS optic neuritis. To conduct a comprehensive assessment, we utilized a multifaceted approach, incorporating both clinical and experimental measures. Our evaluation included clinical EAE scoring, which served to assess the severity of clinical manifestations in the



Prophylactic AMPA-PAM (PF4778574) therapy attenuates optic nerve demyelination. Longitudinal sections of optic nerves of C57Bl/6J mice were stained for (A) Iba1 and (C) MBP 110 days after MOG35-55 immunization; dotted lines indicate areas of demyelination. Quantitative analyses of microglial activation (Iba1+ cells) (B) by fluorescence intensity measurement and myelin status (MBP intensity score) (D). One optic nerve per mouse was included. All graphs represent the pooled mean  $\pm$  SEM (n = 6 animals per group out of two independent experiments). The bar graph presents statistical significance, with p-values displayed over the bars, determined using ANOVA with Dunnett's *post hoc* test, compared to MOG EAE untreated mice.

disease model. Further, we incorporated OCT and OMR evaluations, established *in-vivo* readout methodologies in the examination of visual function and structural integrity in the context of optic neuritis. Finally, we performed histological evaluations, which provided insights into the cellular and structural changes within the CNS, thereby complementing our clinical observations with a deeper understanding of the underlying pathological alterations.

The role of excitotoxicity, where overactive glutamate receptors lead to neuronal damage, is documented in MS (12). This study's focus is on AMPA-PAMs, which modulate AMPA receptors to prevent over-activation and excitotoxicity, therefore providing a promising aspect of investigation in the context of MS pathology. Additionally, the mode of action of AMPA-PAMs could also involve enhancing synaptic transmission in cases of neuronal

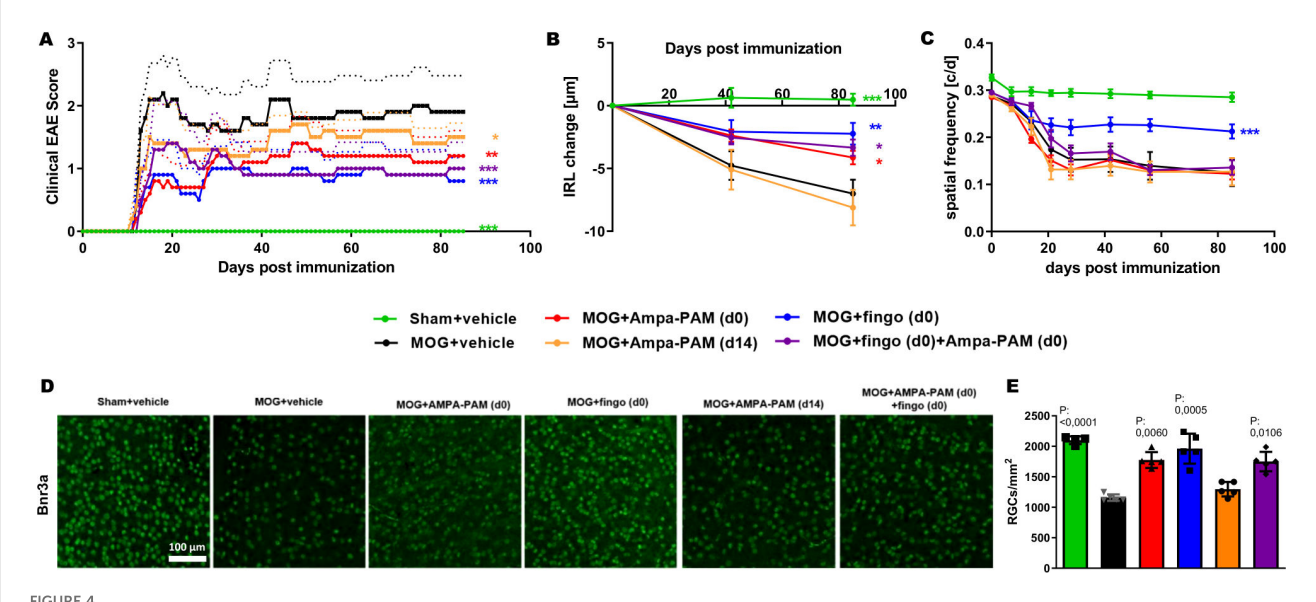
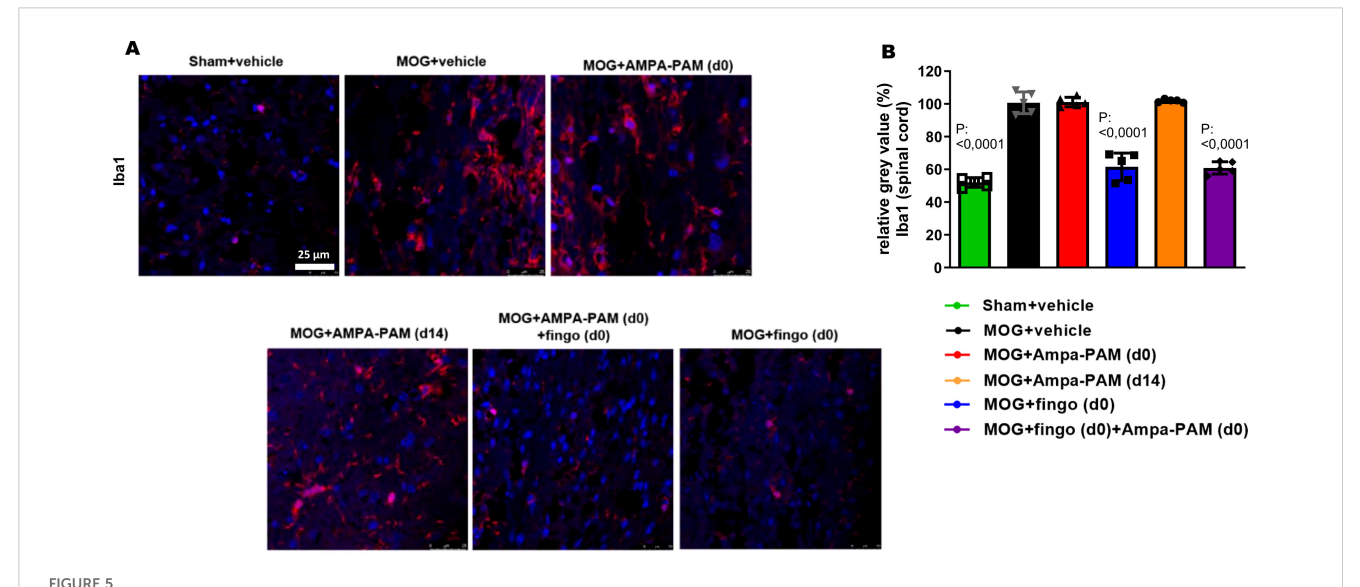


FIGURE 4
PF4778574 and fingolimod therapy attenuate MOG35-55-induced EAE in C57BL/6J mice. (A) Clinical EAE score, (B) degeneration of the inner retinal layers and (C) visual function by spatial frequency in cycles per degree (c/d) of female C57BL/6J EAE mice over 90 days of EAE. (D) Brn3a stained RGCs after 90 days of EAE of Sham, MOG EAE and AMPA-PAM treated mice. (E) The bar graph shows the RGC density 90 days after immunization. AMPA-PAM was administered on the day of immunization. All graphs represent the pooled mean ± SEM (n = 6 animals per group), with \*p<0.05, \*\*p<0.01, \*\*\*p<0.01, \*\*\*p<0.001, area under the curve compared by ANOVA with Dunnett's post hoc test for time course compared to untreated MOG EAE. The graphs present statistical significance, with p-values displayed over the bars, determined using ANOVA with Dunnett's post hoc test, compared to MOG EAE untreated mice.

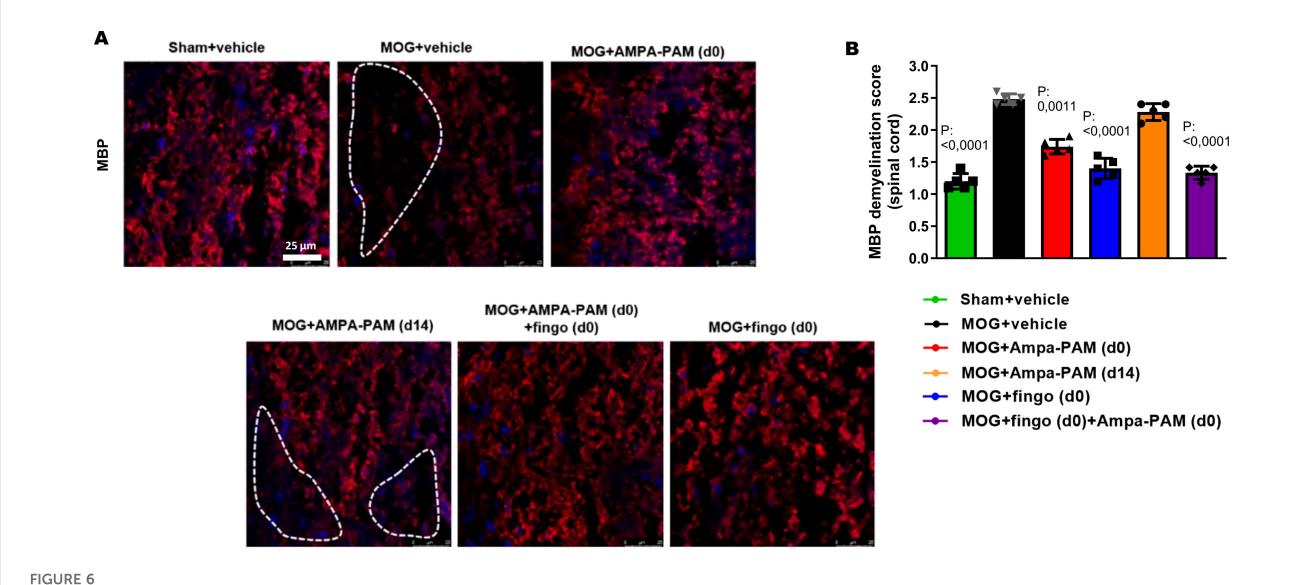


PF4778574 does not reduce the number of lba1+ infiltrates into the spinal cord of EAE mice. (A) Longitudinal sections of spinal cord of C57Bl/6J mice were stained for lba1 90 days after MOG35-55 immunization; dotted lines indicate areas of demyelination. (B) Quantitative analyses of microglial activation (lba1) by fluorescence intensity measurement. All graphs represent the pooled mean  $\pm$  SEM (n = 6 animals per group). The bar graph presents statistical significance, with p-values displayed over the bars, determined using ANOVA with Dunnett's *post hoc* test, compared to MOG EAE untreated mice.

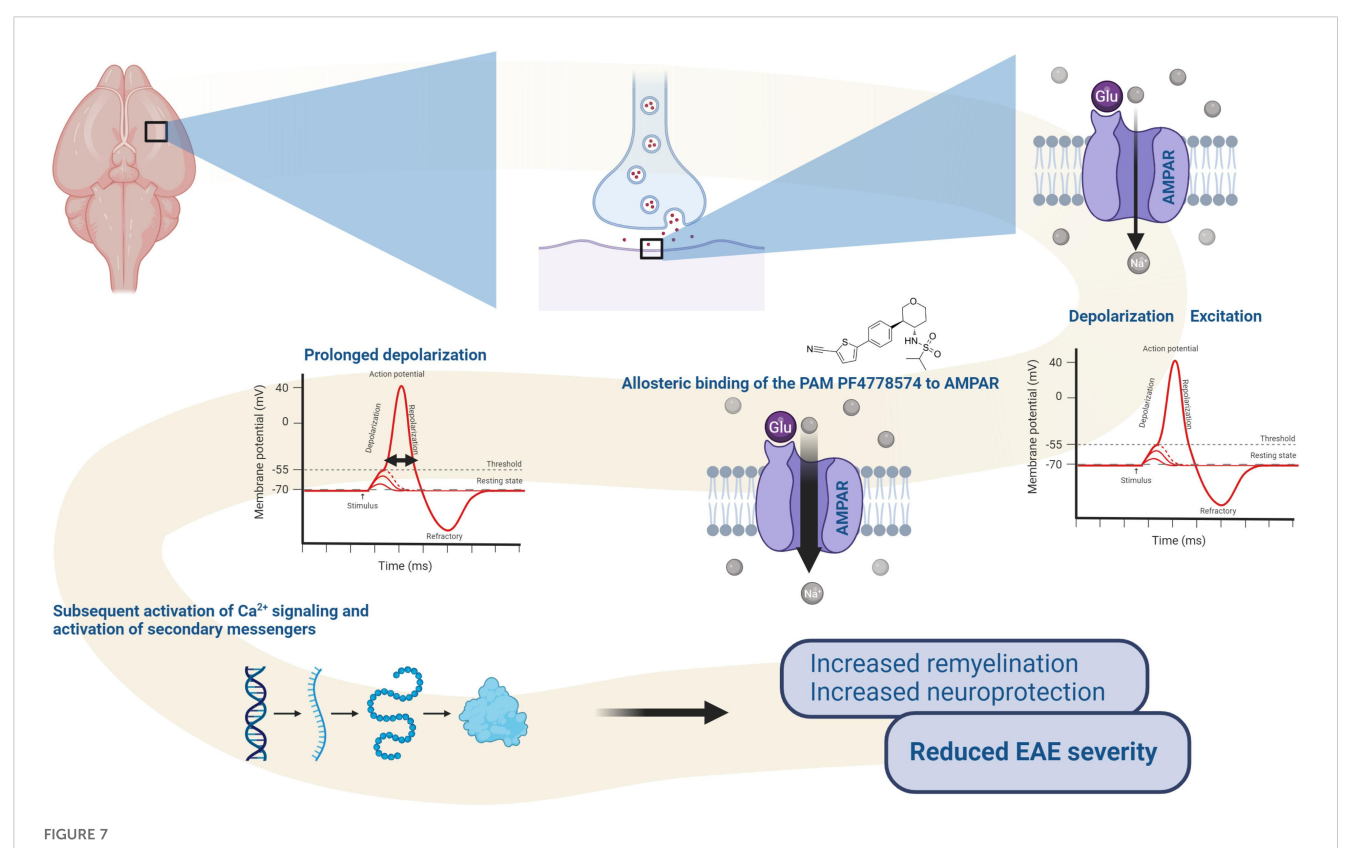
dysfunction, which results from demyelination and degeneration in the CNS. This dual potential—preventing excitotoxic damage while supporting synaptic function—underscores the therapeutic promise of AMPA-PAMs in managing MS.

A central observation from this study is the successful mitigation of clinical disability in the EAE model following both prophylactic and therapeutic administration of the AMPA-PAM PF4778574. However, the lack of impact on Iba1+ microglia

contrasts with prior findings that AMPA receptor modulation might also have potential anti-inflammatory effects (13–15). Of note, these previous studies investigated the effect of AMPA-antagonists, rather than AMPA-PAMs, which act in a different pattern on the AMPA receptors than PAMs. This disparity suggests that while AMPA-PAMs like PF4778574 may influence synaptic and neuronal function and/or excitotoxicity, they may not significantly impact neuroinflammation, the essential primary



Prophylactic PF4778574 and fingolimod treatment reduce demyelination of the spinal cord in EAE mice. (A) Longitudinal sections of spinal cord of C57BI/6J mice were stained for MBP 90 days after MOG35-55 immunization; dotted lines indicate areas of demyelination. (B) Quantitative analyses of the myelin status (MBP demyelination score). All graphs represent the pooled mean  $\pm$  SEM (n = 6 animals per group). The bar graph presents statistical significance, with p-values displayed over the bars, determined using ANOVA with Dunnett's *post hoc* test, compared to MOG EAE untreated mice.



Proposed mode of action of PF-4778574: Upon allosteric binding to AMPA receptors, the PAM enhances glutamate-induced sodium ( $Na^+$ ) influx, leading to prolonged depolarization. This sustained depolarization increases the likelihood of activating voltage-gated calcium channels, which in turn triggers calcium ( $Ca^{2^+}$ ) signaling and the activation of secondary messenger pathways. These processes promote the activation of oligodendrocyte precursor cells (OPCs), facilitating remyelination and contributing to the reduced severity of EAE symptoms. The diagram highlights the impact of AMPA-PAM on synaptic activity, neural signaling, and therapeutic outcomes in demyelinating conditions.

process in MS which can very effectively be targeted by approved therapeutics like the fingolimod used in our study.

We observed an enhanced myelin integrity in the optic nerve, corpus callosum and spinal cord following prophylactic AMPA-PAM treatment. Furthermore, AMPA-PAM treatment significantly reduced the loss of retinal ganglion during optic neuritis. This finding aligns with recent studies which highlight the potential neuroprotective roles of AMPA-PAMs beyond merely neurotransmission (23). Such effects could have significant therapeutic implications in neuroinflammatory or degenerative conditions where myelin loss is prominent.

The lack of additive benefits and diminished efficacy in combined treatment regimens involving PF4778574 and fingolimod was disappointing. Potential reason may have been drug interactions as both substances undergo metabolism by cytochrome P450 (CYP) (24). Further investigations to understand this interaction could offer insights into optimizing combination treatments involving AMPA-PAMs and existing MS therapies.

Interestingly, the lower dose of PF4778574 in our study contributed to a better outcome compared to the higher dose. Such a bell shaped dose response curve is characteristic for hormesis, which is classically observed when doses above a certain threshold lead to harmful or toxic effects (25) and has been observed in the context of other remyelinating therapeutics (20). The typical bell-shaped dose-

response curve is thought to arise from the balance between beneficial adaptive responses and potential toxicity at higher doses (26). However, regarding PF4778574 specifically, the typical adverse effects are seizures. We carefully adjusted the treatment dose below the seizure threshold and observed no seizures during our experiments. Thus, harmful effects resulting from the high PF4778574 dose in our experiments might result from a sub-seizure threshold overstimulation of AMPA receptors, potentially leading to a mild form of excitotoxicity (27). This might explain why the lower dose was more beneficial in the EAE model.

While we did not directly measure the electrical activity of retinal ganglion cells or optic nerve conduction speed (e.g., via pattern electroretinography [pERG] or visual evoked potentials [VEP]), these techniques could provide valuable insights into whether PF4778574 influences neuronal excitability *in vivo*. Future studies incorporating pERG or VEP could help clarify any dose-dependent effects on RGC function and optic nerve signal transmission, thereby offering a more complete understanding of how AMPA-PAM treatment modulates neuronal activity in the context of MS.

PF4778574 did not impact microglial activity. Thus, it is plausible to assume that the treatments benefits mainly result from functional and structural protection of the neuronal structures rather than inhibiting neuroinflammation. This is

Sindi et al. 10.3389/fimmu.2025.1532877

consistent with the role of AMPA receptors in neurotransmission and synaptic plasticity (28).

Reduced myelin damage observed with both doses of PF4778574 at the endpoint suggests possible myelin-protective and/or remyelinating effects. These effects might indirectly result from modified neuronal activity, which could affect the local environment and support myelin maintenance and/or remyelination (29, 30). Our results in the cuprizone-induced demyelination model suggest that PF4778574 may indeed enhance remyelination after toxic demyelination, as indicated by increased numbers of oligodendrocyte progenitor cells (OPCs) and increased myelin content within the corpus callosum, as shown by PDGFRα, MOG, and BCAS1 staining, respectively. However, other myelin markers, MBP and LFB, showed only positive trends for remyelinating effects of PF4778574 but did not reach statistical significance. In these short-term cuprizone demyelination experiments, the timing of de- and remyelination is crucial. Further studies with larger sample sizes are needed to evaluate the remyelinating capacity of PF4778574 and its mode of action.

In conclusion, PF4778574 reduces clinical disability in the context of EAE following both prophylactic and therapeutic administration. Improvements in EAE scores were evaluated by structural measurements of the inner retinal layer on OCT and assessments of retinal ganglion cell counts. However, PF4778574 did not affect the number of Iba1+ infiltrates in the optic nerve and spinal cord. Nevertheless, prophylactic AMPA-PAM treatment enhanced myelin integrity. Interestingly, combination treatment with fingolimod did not produce additive benefits and showed diminished efficacy compared to monotherapies. This could potentially be attributed to drug interactions, given that both substances are metabolized by cytochrome P450 enzymes (CYP), and induction of specific CYPs may influence the efficacy of fingolimod. This study adds to the literature exploring the potential of AMPA-PAMs in degenerative and neuroinflammatory diseases such as MS. These observations, as illustrated in the schematic representation in Figure 7, underscore the potential therapeutic benefits of AMPA-PAM. And demonstrates the capacity to regulate neural activity and support the maintenance of myelin integrity. As PF4778574 is well-tolerated and safe, it may be a suitable candidate for further investigation in clinical trials.

#### Data availability statement

The raw data supporting the conclusions of this article will be made available by the authors, without undue reservation.

#### **Ethics statement**

The animal study was approved by State Office for Nature, Environment, and Consumer Protection of North Rhine-Westphalia, Germany ("Landesamt für Natur, Umwelt und Verbraucherschutz Nordrhein-Westfalen, Deutschland"). The study protocol received official approval under reference number Az. 81-02.04.2019.A063. The study was conducted in accordance with the local legislation and institutional requirements.

#### **Author contributions**

MS: Conceptualization, Data curation, Formal Analysis, Investigation, Methodology, Project administration, Resources, Software, Supervision, Validation, Visualization, Writing – original draft, Writing – review & editing. MD: Conceptualization, Data curation, Investigation, Methodology, Resources, Supervision, Validation, Visualization, Writing – review & editing. DK: Investigation, Writing – review & editing. JG: Investigation, Writing – review & editing. JS: Investigation, Writing – review & editing. JS: Investigation, Writing – review & editing. AI: Investigation, Writing – review & editing. HH: Writing – review & editing. TK: Writing – review & editing. HS: Writing – review & editing. SM: Writing – review & editing. PA: Funding acquisition, Writing – review & editing, Conceptualization.

#### **Funding**

The author(s) declare that financial support was received for the research, authorship, and/or publication of this article. This work was supported by grants from Biogen (1009048).

#### **Acknowledgments**

Figure 7 created with BioRender.com.

#### Conflict of interest

Author PA was employed by the company Maria Hilf Clinics GmbH, Mönchengladbach. Author JS was employed the company Biogen. The work was funded by a research grant from Biogen to Author PA. Author TR reports grants from German Ministry of Education, Science, Research and Technology, during the conduct of the study; grants and personal fees from Sanofi-Genzyme; personal fees from Biogen; personal fees and nonfinancial support from Merck Serono; personal fees from Roche, Teva, Alexion, Argenx, UCB, and BMS outside the submitted work.

The remaining authors declare that the research was conducted in the absence of any commercial or financial relationships that could be construed as a potential conflict of interest.

The following financial disclosures are unrelated to the work: SGM received honoraria for lecturing and travel expenses for attending meetings from Almirall, Amicus Therapeutics Germany, Bayer Health Care, Biogen, Celgene, Diamed, Genzyme, MedDay Pharmaceuticals, Merck Serono, Novartis, Novo Nordisk, ONO Pharma, Roche, Sanofi-Aventis, Chugai Pharma, QuintilesIMS, and Teva. His research is funded by the

Sindi et al. 10.3389/fimmu.2025.1532877

German Ministry for Education and Research BMBF, Deutsche Forschungsgemeinschaft DFG, Else Kröner Fresenius Foundation, German Academic Exchange Service, Hertie Foundation, Interdisciplinary Center for Clinical Studies IZKF Muenster, German Foundation Neurology, and by Almirall, Amicus Therapeutics Germany, Biogen, Diamed, Fresenius Medical Care, Genzyme, Merck Serono, Novartis, ONO Pharma, Roche, and Teva. MD received speaker honoraria from Merck and Novartis. PA received compensation for serving on Scientific Advisory Boards for Ipsen, Novartis, Biogen; he received speaker honoraria and travel support from Novartis, Teva, Biogen, Merz Pharmaceuticals, Ipsen, Allergan, Bayer Healthcare, Esai, UCB and Glaxo Smith Kline; he received research support from Novartis, Biogen, Teva, Merz Pharmaceuticals, Ipsen, Bristol-Myers Squibb and Roche.

#### Generative Al statement

The author(s) declare that no Generative AI was used in the creation of this manuscript.

#### Publisher's note

All claims expressed in this article are solely those of the authors and do not necessarily represent those of their affiliated organizations, or those of the publisher, the editors and the reviewers. Any product that may be evaluated in this article, or claim that may be made by its manufacturer, is not guaranteed or endorsed by the publisher.

#### References

- 1. Reich DS, Lucchinetti CF, Calabresi PA. Multiple sclerosis. New Engl J Med. (2018) 378:169–80. doi: 10.1056/NEJMra1401483
- 2. Dietrich M, Koska V, Hecker C, Göttle P, Hilla AM, Heskamp A, et al. Protective effects of 4-aminopyridine in experimental optic neuritis and multiple sclerosis. *Brain: A J Neurol.* (2020) 143:1127–42. doi: 10.1093/brain/awaa062
- 3. Zörner B, Filli L, Reuter K, Kapitza S, Lörincz L, Sutter T, et al. Prolonged-release fampridine in multiple sclerosis: Improved ambulation effected by changes in walking pattern. *Multiple Sclerosis (Houndmills Basingstoke England)*. (2016) 22:1463–75. doi: 10.1177/1352458515622695
- 4. Partin KM. AMPA receptor potentiators: From drug design to cognitive enhancement. Curr Opin Pharmacol. (2015) 20:46–53. doi: 10.1016/j.coph.2014.11.002
- 5. Reuillon T, Ward SE, Beswick P. AMPA receptor positive allosteric modulators: potential for the treatment of neuropsychiatric and neurological disorders. *Curr Topics Medicinal Chem.* (2016) 16:3536–65. doi: 10.2174/1568026616666160627114507
- 6. Ward SE, Harries MH, Aldegheri L, Bradford AM, Ballini E, Dawson L, et al. Pharmacological characterisation of MDI-222, a novel AMPA receptor positive allosteric modulator with an improved safety profile. *J Psychopharmacol (Oxford England)*. (2020) 34:93–102. doi: 10.1177/0269881119872198
- 7. Frydenvang K, Pickering DS, Kastrup JS. Structural basis for positive allosteric modulation of AMPA and kainate receptors. *J Physiol.* (2022) 600:181–200. doi: 10.1113/JP280873
- 8. Black MD. Therapeutic potential of positive AMPA modulators and their relationship to AMPA receptor subunits. A review of preclinical data. *Psychopharmacology.* (2005) 179:154–63. doi: 10.1007/s00213-004-2065-6
- 9. Lee K, Goodman L, Fourie C, Schenk S, Leitch B, Montgomery JM. AMPA receptors as therapeutic targets for neurological disorders. *Adv Protein Chem Struct Biol.* (2016) 103:203–61. doi: 10.1016/bs.apcsb.2015.10.004
- 10. Arai AC, Kessler M. Pharmacology of ampakine modulators: from AMPA receptors to synapses and behavior. *Curr Drug Targets.* (2007) 8(5):583-602. doi: 10.2174/138945007780618490
- 11. Trapp BD, Nave K-A. Multiple sclerosis: An immune or neurodegenerative disorder? *Annu Rev Neurosci.* (2008) 31:247–69. doi: 10.1146/annurev.neuro.30.051606.094313
- 12. Kostic M, Zivkovic N, Stojanovic I. Multiple sclerosis and glutamate excitotoxicity. *Rev Neurosci.* (2013) 24:71–88. doi: 10.1515/revneuro-2012-0062
- 13. Bonnet CS, Williams AS, Gilbert SJ, Harvey AK, Evans BA, Mason DJ. AMPA/kainate glutamate receptors contribute to inflammation, degeneration and pain related behaviour in inflammatory stages of arthritis. *Ann Rheumatic Dis.* (2015) 74:242–51. doi: 10.1136/annrheumdis-2013-203670
- 14. Greene IP, Lee E-Y, Prow N, Ngwang B, Griffin DE. Protection from fatal viral encephalomyelitis: AMPA receptor antagonists have a direct effect on the inflammatory response to infection. *Proc Natl Acad Sci United States America*. (2008) 105:3575–80. doi: 10.1073/pnas.0712390105
- 15. Smith T, Groom A, Zhu B, Turski L. Autoimmune encephalomyelitis ameliorated by AMPA antagonists. *Nat Med.* (2000) 6:62–6. doi: 10.1038/71548
- 16. Göttle P, Groh J, Reiche L, Gruchot J, Rychlik N, Werner L, et al. Teriflunomide as a therapeutic means for myelin repair. *J Neuroinflamm*. (2023) 20:7. doi: 10.1186/s12974-022-02686-6

- 17. Aytulun A, Cruz-Herranz A, Aktas O, Balcer LJ, Balk L, Barboni P, et al. APOSTEL 2.0 recommendations for reporting quantitative optical coherence tomography studies. *Neurology*. (2021) 97:68–79. doi: 10.1212/WNL.0000000000012125
- 18. Cruz-Herranz A, Balk LJ, Oberwahrenbrock T, Saidha S, Martinez-Lapiscina EH, Lagreze WA, et al. The APOSTEL recommendations for reporting quantitative optical coherence tomography studies. *Neurology*. (2016) 86:2303–9. doi: 10.1212/WNL.00000000000002774
- 19. Dietrich M, Cruz-Herranz A, Yiu H, Aktas O, Brandt AU, Hartung H-P, Green A, Albrech P. Whole-body positional manipulators for ocular imaging of anaesthetised mice and rats: a do-it-yourself guide. *BMJ Open Ophthalmol.* (2016) 1:e000008
- 20. Dietrich M, Hecker C, Martin E, Langui D, Gliem M, Stankoff B, et al. Increased remyelination and proregenerative microglia under siponimod therapy in mechanistic models. *Neurology(R) Neuroimmunol Neuroinflamm*. (2022) 9:e1161. doi: 10.1212/NXI.000000000001161
- 21. Hecker C, Dietrich M, Issberner A, Hartung H-P, Albrecht P. Comparison of different optomotor response readouts for visual testing in experimental autoimmune encephalomyelitis-optic neuritis. *J Neuroinflamm*. (2020) 17:216. doi: 10.1186/s12974-020-01889-z
- 22. Dietrich M, Hecker C, Hilla A, Cruz-Herranz A, Hartung H-P, Fischer D, et al. Using optical coherence tomography and optokinetic response as structural and functional visual system readouts in mice and rats. *J Visualized Experiments (JoVE)*. (2019) 143:e58571. doi: 10.3791/58571
- 23. Destot-Wong K-D, Liang K, Gupta SK, Favrais G, Schwendimann L, Pansiot J, et al. The AMPA receptor positive allosteric modulator, S18986, is neuroprotective against neonatal excitotoxic and inflammatory brain damage through BDNF synthesis. *Neuropharmacology.* (2009) 57:277–86. doi: 10.1016/j.neuropharm.2009.05.010
- 24. Jin Y, Zollinger M, Borell H, Zimmerlin A, Patten CJ. CYP4F enzymes are responsible for the elimination of fingolimod (FTY720), a novel treatment of relapsing multiple sclerosis. *Drug Metab Disposition: Biol Fate Chemicals.* (2011) 39:191–8. doi: 10.1124/dmd.110.035378
- 25. Calabrese EJ. Hormesis: Why it is important to toxicology and toxicologists. *Environ Toxicol Chem.* (2008) 27:1451–74. doi: 10.1897/07-541
- 26. Calabrese EJ, Bachmann KA, Bailer AJ, Bolger PM, Borak J, Cai L, et al. Biological stress response terminology: Integrating the concepts of adaptive response and preconditioning stress within a hormetic dose-response framework. *Toxicol Appl Pharmacol.* (2007) 222:122–8. doi: 10.1016/j.taap.2007.02.015
- 27. Lau A, Tymianski M. Glutamate receptors, neurotoxicity and neurodegeneration. *Pflugers Archiv: Eur J Physiol.* (2010) 460:525–42. doi: 10.1007/s00424-010-0809-1
- 28. Song I, Huganir RL. Regulation of AMPA receptors during synaptic plasticity. Trends Neurosci. (2002) 25:578–88. doi: 10.1016/s0166-2236(02)02270-1
- 29. Choi EH, Blasiak A, Lee J, Yang IH. Modulation of neural activity for myelination in the central nervous system. *Front Neurosci.* (2019) 13:952. doi: 10.3389/fnins.2019.00952
- 30. Fannon J, Tarmier W, Fulton D. Neuronal activity and AMPA-type glutamate receptor activation regulates the morphological development of oligodendrocyte precursor cells. *Glia.* (2015) 63:1021–35. doi: 10.1002/glia.22799

Sindi et al. 10.3389/fimmu.2025.1532877

## Glossary

4AP	4-Aminopyridine	IS/OS	Inner and Outer Segments of Photoreceptors
AMPA-PAM	AMPA-type glutamate receptor Positive Allosteric Modulator	Ki-67	Proliferation Marker Protein
AMPAR	AMPA Receptor	LFB	Luxol Fast Blue
ANOVA	Analysis of Variance	MBP	Myelin Basic Protein
BDNF	Brain-Derived Neurotrophic Factor	MOG35-55	Myelin Oligodendrocyte Glycoprotein fragment 35-55
CFA	Complete Freund's Adjuvant	MS	Multiple Sclerosis
CNS	Central Nervous System	NFL	Nerve Fiber Layer
Cuprizone (CPZ)	Copper Chelating Agent used to induce demyelination	OCT	Optical Coherence Tomography
CYP	Cytochrome P450	OMR	Optomotor Response
DAPI	4',6-Diamidin-2-phenylindol	ONL	Outer Nuclear Layer
EAE	Experimental Autoimmune Encephalomyelitis	OPC	Oligodendrocyte Progenitor Cell
ELM	External Limiting Membrane	OPL	Outer Plexiform Layer
fEPSP	Field Excitatory Postsynaptic Potential	ORL	Outer Retinal Layer
GCL	Ganglion Cell Layer	PDGFRα	Platelet-Derived Growth Factor Receptor Alpha
GEE	Generalized Estimation Equation	PTX	Pertussis Toxin
Iba1	Ionized Calcium Binding Adapter Molecule 1	RGC	Retinal Ganglion Cell
INL	Inner Nuclear Layer	RPE	Retinal Pigment Epithelium
IPL	Inner Plexiform Layer	TRT	Total Retinal Thickness
IRL	Inner Retinal Layer		

# scientific reports



#### **OPEN**

# Flecainide mediated sodium channel blockade enhances blood brain barrier integrity and promotes neuroprotection in neuroinflammation

Mustafa Sindi<sup>1</sup>, Diana Klees<sup>1</sup>, Vera Dobelmann<sup>1</sup>, Paul Disse<sup>1</sup>, Hanne Weigel<sup>1</sup>, Stefanie Lichtenberg<sup>1,5</sup>, Rebekka Ricci<sup>2</sup>, Leonie Thewes<sup>1</sup>, Gülsüm Deniz-Köseoglu<sup>1</sup>, Christina Hecker<sup>1</sup>, Thomas Müntefering<sup>1</sup>, Andrea Issberner<sup>1</sup>, Joel Gruchot<sup>1</sup>, Hans-Peter Hartung<sup>1</sup>, Tobias Ruck<sup>1</sup>, Carsten Berndt<sup>1</sup>, Thomas Kurz<sup>3</sup>, Holger Stark<sup>3</sup>, Patrick Küry<sup>1</sup>, Britta Engelhardt<sup>2</sup>, Ruth Lyck<sup>2</sup>, Sven G. Meuth<sup>1</sup>, Michael Dietrich<sup>1,6</sup> & Philipp Albrecht<sup>1,4,6</sup> ≅

Multiple Sclerosis (MS), an autoimmune disorder, is characterized by severe neuroinflammation, leading to demyelination and neuronal damage in the CNS, resulting in significant clinical impairment. MS progression involves complex pathological processes like immune cell invasion and cytokinemediated recruitment to the CNS. Experimental autoimmune encephalomyelitis (EAE), widely used as a model for MS, despite its translational limitations, has been crucial for identifying effective treatments. Recent studies have shown that sodium channel (NaV) blockers and monoamine oxidase- (MAO) B inhibitors can alleviate symptoms of EAE and optic neuritis (ON), but their mode of action remains partially unclear. To evaluate the effects and understand the action mechanism of NaV blockers and MAO-B inhibitors (rasagiline, safinamide, flecainide and phenytoin) in neurological conditions, various techniques were used, including optical coherence tomography (OCT), optomotor response measurement (OMR), flow cytometry, histological evaluations, Evans blue assay, blood-brain barrier (BBB) permeability assay, western blot, proliferations assay, and gene expression analyses. The study found that the primary therapeutic effect comes from inhibiting the NaV 1.5 sodium channel, not MAO-B inhibition. Flecainide, a NaV 1.5 channel blocker, significantly reduced EAE disability scores, mitigated neurodegeneration, preserved visual function, and restricted immune cell migration into the CNS. Importantly, blocking the NaV 1.5 channel had an effect on the BBB, limiting lymphocyte entry into the CNS. This research highlights sodium channel blockers' potential in treating EAE. The findings demonstrate induced neuroprotection and reduced disease progression, suggesting a novel therapeutic approach. Crucially, it reveals for the first time that NaV 1.5 channel blockade leads to neuroprotection primarily by affecting the BBB, a key factor in controlling immune cell migration, thus addressing a critical aspect of neuroinflammation.

**Keywords** Flecainide, Rasagiline, Safinamide, Sodium-channel blocking, MAO-B inhibition, Neuroprotection, Multiple sclerosis, Blood-brain-barrier, EAE

#### Abbreviations

(2025) 15:31032

<sup>1</sup>Department of Neurology, Medical Faculty, University Hospital Düsseldorf, Heinrich-Heine-University, Düsseldorf, Germany. <sup>2</sup>Theodor Kocher Institute, University of Bern, Bern, Switzerland. <sup>3</sup>Institute of Pharmaceutical and Medical Chemistry, Faculty of Mathematics and Natural Sciences, Heinrich-Heine University, Düsseldorf, Germany. <sup>4</sup>Department of Neurology, Maria Hilf Clinics, Mönchengladbach, Germany. <sup>5</sup>Core Facility Flow Cytometry, Medical Faculty, University Hospital Düsseldorf, Heinrich Heine University, Düsseldorf, Germany. <sup>6</sup>Michael Dietrich and Philipp Albrecht equally contributing senior authors <sup>∞</sup>email: phil.albrecht@gmail.com

ACK Ammonium-chlorid-kalium (lysis buffer)
Brn3a Brain-specific homeobox/POU domain protein 3A

BW Body weight CC Cell count

CFA Complete Freund's adjuvants
CNS Central nervous system
EBD Evan's Blue Dye

EAE Experimental autoimmune encephalomyelitis

EDSS Expanded disability status scale ELM External limiting membrane

FCS Fetal calf serum

GAPDH Glyceraldehyde 3-phosphate dehydrogenase (housekeeping gene)

GCL Ganglion cell layer

GEE Generalized estimation equation
GFAP Glial fibrillary acidic protein

IBA1 Ionized calcium-binding adaptor molecule 1 I-CAM-1 and I-CAM-2 Intercellular adhesion molecules 1 and 2

 $\begin{array}{lll} IL\text{-}1\beta & & Interleukin-1 \text{ beta} \\ INL & & Inner \text{ nuclear layer} \\ IPL & & Inner \text{ plexiform layer} \\ IRL & & Inner \text{ retinal layer} \\ IS & & Inner \text{ segment} \\ \end{array}$ 

JAM-1, JAM-2, and JAM-3
LS

Junctional adhesion molecules -1, -2 and -3
Large separation (column type in MACS)

MAO Monoamine oxidase
MACS Magnetic-activated cell sorting

MBP Myelin basic protein MD Mean difference

MOG Myelin oligodendrocyte glycoprotein

MOG35-55 Myelin oligodendrocyte glycoprotein fragment 35–55

MS Multiple sclerosis

MT Mycobacterium tuberculosis

NaV1.5/NaV1.6/NaV1.9 Voltage-gated sodium channel isoforms N-CAM-1 Neural cell adhesion molecule 1

NFL Nerve fiber layer

NOD Non-obese diabetic

OCT Optical coherence tomography

OMR Optomotor response
ON Optic neuritis
ONL Outer nuclear layer
OPL Outer plexiform layer
ORL Outer retinal layer
OS Outer segment
P Probability value

pMBMECs Primary mouse brain microvascular endothelial cells,

PECAM-1 Platelet endothelial cell adhesion molecule

PTX Pertussis toxin

RPE Retinal pigment epithelium SEM Standard error of the mean TRT Total retinal thickness

V-CAM Vascular cell adhesion molecule 1

Multiple Sclerosis (MS) is a chronic autoimmune disease that leads to inflammation, demyelination, loss of oligodendrocytes, axonal injury, and progressive neuronal degeneration within the central nervous system (CNS)<sup>1</sup>. The degenerative processes contribute significantly to the ongoing disability seen in MS patients, which often proves resistant to typical immunosuppressive and immunomodulatory treatments. Pathological changes in MS are commonly associated with lymphocyte and macrophage infiltration into CNS tissue, driving the expression of adhesion molecules and encouraging immune cell migration through the release of inflammatory cytokines. This chain of events triggers damage to glial cells and neurons, although the exact mechanisms remain incompletely understood. It is suggested that oxidative stress plays a crucial role in neuronal injury, as immune cells activated in this process may release reactive oxygen and nitrogen species<sup>2</sup>.

Additionally, the MultipleMS Consortium<sup>3</sup> highlighted that the varying severity of MS among patients could be due to distinct genetic variants, which act primarily independent of immune responses, suggesting that CNS resilience plays a crucial role in the progression of MS. In light of these findings, MS's intricate nature, influenced by genetic, environmental, and lifestyle factors, necessitates ongoing research for accurate diagnosis and effective treatment, with a primary aim to improve the quality of life for patients battling this disease.

Recent studies have highlighted additional mechanisms contributing to neuronal injury and disease progression in MS. Acid-sensing ion channels, particularly ASIC1, have been implicated in axonal degeneration through proton-gated sodium and calcium influx during tissue acidosis, as shown in experimental autoimmune

encephalomyelitis (EAE), an animal model for MS. The disruption of ASIC1 or its pharmacological inhibition using amiloride conferred neuroprotection without altering CNS inflammation, suggesting a potential therapeutic avenue for MS<sup>4</sup>. Similarly, the transient receptor potential vanilloid-type 4 (TRPV4) ion channel has been identified as a mediator of blood-brain barrier (BBB) dysfunction. Endothelial TRPV4 expression, upregulated in response to microglia-derived TNF $\alpha$ , exacerbates T cell extravasation and neuroinflammation, emphasizing its role in MS pathogenesis<sup>5</sup>. Furthermore, Th17 cells have been found to release glutamate via  $\beta$ 1-integrin-and KV1.3 channel-dependent signaling, inducing calcium-mediated neuronal damage. Inhibition of KV1.3 or glutaminase has shown promise in reducing glutamate-mediated toxicity and improving outcomes in EAE<sup>6</sup>. Finally blocking potassium channels with 4-aminopyridine has demonstrated protective effects in EAE and preclinical optic nerve damage<sup>7</sup>. These findings underscore the multifaceted roles of ion channels and immune cell signaling in driving neuroinflammation and neurodegeneration.

Sodium channel blockers are distinguished by their varied pharmacological properties, primarily modulating membrane action potentials through different mechanisms. These agents are categorized into subclasses based on their specific effects, with some exhibiting dual inhibitory actions, such as targeting sodium channels and inhibiting monoamine oxidase (MAO)-B activity. Others demonstrate selective affinity, primarily inhibiting sodium channels. The specificity among these blockers ranges from compounds targeting particular sodium channel subtypes to those affecting multiple types indiscriminately. Recent research has sparked interest in these blockers due to preliminary evidence of their beneficial effects in EAE and optic neuritis (ON), though their underlying mechanisms remain largely unexplored.

The intricate nature of EAE has prompted a myriad of investigations into its etiology and treatment. The selective MAO inhibitor, rasagiline, has been shown to induce neuroprotection in animal models of Parkinson's disease<sup>8,9</sup>, indicative of the potential therapeutic efficacy of MAO inhibitors. NaV blockade, exemplified by non-selective NaV-blocker phenytoin, has also been proposed as a potential approach for MS treatment, as it protects axons from degeneration by averting an energy deficit<sup>10</sup> and suppresses the activation of innate immune cells in the CNS<sup>11</sup>. In addition, research points to direct effects on microglial cells<sup>12</sup> and a reduction in CD45+infiltrates in the CNS upon phenytoin treatment. Safinamide, a combined MAO-B inhibitor and non-selective sodium channel blocker, has also shown promising results, as it diminished the formation of superoxide and increased GSH-level in microglia culture, leading to reduced CD68+monocytes in the spinal cord of EAE mice<sup>13</sup>. Similarly, flecainide, a sodium channel blocker, has also been found to reduce CD68+cell activation/infiltration<sup>13</sup>.

Beginning with evaluating their overall therapeutic benefits, we will progress to a detailed analysis of the most effective compound, focusing on its mechanism of action in an inflammatory setting. This understanding is crucial for exploring their potential in treating neuroinflammatory diseases. The findings from this research could significantly advance MS treatment strategies and contribute to the field.

#### Material and methods Animals, animal models, treatment

Female, six-week-old C57BL/6J mice were purchased from Janvier Labs (Le Genest-Saint-Isle, France). The NOD/ShiLtJ mice (Female, six-week-old) originate from the internal breeding facility (ZETT) at the University of Düsseldorf. EAE mouse model.

Mice were immunized with 200  $\mu$ g of myelin oligodendrocyte glycoprotein fragment 35–55 (MOG35–55), purchased from BIOTREND emulsified in 200  $\mu$ l of complete Freund's adjuvant (CFA), supplemented with 800  $\mu$ g of heat-killed Mycobacterium tuberculosis (MT) H37Ra, both purchased from BD Difco (injected subcutaneous, distributed over four spots on the hind and front flank) and additional intraperitoneal injections of 200 ng of pertussis toxin (PTX) from Sigma-Aldrich on days 0 and 2 post immunization (p.i.). The sham control group (sham) also received PTX and CFA, but no MOG35–55 peptide. The substances used for treatment, their concentration, mode of action, treatment interval and treatment start are described in Table 1. The used concentrations for each substance were adapted from recent dose finding studies found in the literature investigating the optimal dose.

Compound	Rasagiline	Safinamide	Flecainide	Phenytoin
Administration form	Oral administration	Oral administration	Subcutaneous injection	Subcutaneous injection
Concentration	5 mg/kg/bw	8 mg/kg/bw	30 mg/kg bw	50 mg/kg bw
Mode of action	Selective MAO-B inhibition	Reversible MAO-B inhibition Sodium and calcium channel blocking Glutamate release inhibition Dopamine and serotonin reuptake inhibition	Selective NaV1.5 sodium channel blocker	Unselective NaV1.1, NaV1.2, NaV1.3, NaV1.5 and NaV1.6 sodium channel blocker
Treatment interval	Daily	Daily	Daily	3 times/week
Treatment start	Directly p.i	Directly p.i	Directly p.i	Directly p.i
CAS Corresponding treatment reference	161735-79-1 (Sigma Aldrich)	202825-46-5 (Sigma Aldrich)	54143-56-5 (Sigma Aldrich)	630-93-3 (Sigma Aldrich)

Table 1. Substance treatment details.

The experimental protocol was reviewed and approved by the "State Office for Nature, Environment and Consumer Protection of North Rhine-Westphalia, Germany "Landesamt für Natur, Umwelt und Verbraucherschutz Nordrhein-Westfalen (LANUV) under approval number Az. 81-02.04.2019.A063.

The in vitro concentrations of 2  $\mu$ M and 5  $\mu$ M flecainide used for treating primary mouse brain microvascular endothelial cells (pMBMECs) were selected as part of a dose-finding approach based on previously published studies <sup>17,18</sup>. These concentrations were chosen to approximate pharmacologically relevant levels corresponding to the systemic in vivo dosage of 30 mg/kg administered subcutaneously in our EAE model, while allowing the assessment of dose-dependent effects on endothelial gene expression and barrier function.

#### **OCT** measurements

Periodic OCT measurements were conducted using the Spectralis\* HRA+OCT device (Heidelberg Engineering, Germany) with several adaptations for rodents, as previously described<sup>19</sup>. Segmentation of retinal volume scans was performed using the Heidelberg Eye Explorer software, with manual control for segmentation errors. The volume of the parapapillary region was assessed using the ETDRS grid, excluding the center with the disc, as published previously<sup>20</sup>. Inner retinal layer (IRL) thickness was examined at defined intervals after irradiation and compared with baseline measurements (IRL: NFL, GCL, and IPL layer).

For the measurements, the animals were anesthetized using isoflurane (Vaporizer from Harvard Apparatus Anesthetic Vaporizors; Isofluran from Piramal critical care). Specifically, induction was carried out at 3.5% isoflurane, followed by maintenance at 2% isoflurane, with a flow rate of 0.6 L/minute of oxygen. The gas was transferred through nose cones to the mice.

#### Optomotor response (OMR) measurements

OMR measurements were performed periodically, exclusively in C57BL/6J mice, using the OptoMotry<sup>\*</sup> device from Cerebral Mechanics, in parallel with OCT measurements. Spatial frequency was monitored as a parameter for visual function. The spatial frequency threshold was determined by randomly changing the spatial frequency to identify the threshold at which the mouse could track the grids, as previously described<sup>20,21</sup>.

#### Histology (optic nerves, retinal cross sections and retinal whole mounts)

Mice were euthanized using 100 mg/kg Ketamine und 20 mg Xylazin intraperitoneal (i.p). (in 250 μl NaCl 0,9%) followed by cardiac perfusion using phosphate-buffered saline (Gibco, Carlsbad, USA).

The optic nerves were then isolated and fixated in 4% paraformaldehyde (Carl Roth, Karlsruhe, Germany) overnight. After fixation, the optic nerves were subjected to a sucrose gradient for dehydration and subsequently embedded in O.C.T. compound (Sakura™ Finetek, Alphen aan den Rijn, Netherlands). Longitudinal sections of five micrometers were cut and prepared for fluorescence staining. Longitudinal sections of the optic nerves were used for quantifying T-Lymphocytes (CD3 (Clone 17A2), 1:400, Biolegend), assessing the state of myelination (MBP (Clone 12), Merck Millipore, 1:500), evaluating microglial activation (Iba1 (Clone GT10312), 1:500, Merck) using Leica HyD detector attached to a Leica DMi8 confocal microscope (63×objective lens magnification). Astrocytic activation (GFAP (Clone 173,004), 1:1000 Synaptic System) was assessed using retinal cross sections. Cy3 goat anti-mouse (1:500 Millipore), Cy3 goat anti-rat (1:500, Millipore) and Cy3 goat anti-rabbit (1:500, Invitrogen) were used as secondary antibodies. The numbers of cells stained with CD3 and Iba1 were analyzed using ImageJ software, applied by blinded raters, and expressed as a ratio to DAPI staining. The overall signal for MBP (positive total area in the red channel) was analyzed using ImageJ software. Cell counts for CD3 and Iba1, as well as the positive area for MBP and GFAP, were assessed in the whole field across 6–9 images per sample. The mean values were calculated and utilized for analysis.

RGC count was calculated by a semi-automated count of Brn3a+cells on retinal flat mounts. Briefly, retinae were stained with Brn3a (1:200, Santa Cruz Biotechnology, cat# sc-31984) antibody and flat-mounted on glass slides. Each retina was then divided into four quadrants (three areas per quadrant: central, mid-periphery, and far-periphery). For each eye, Brn3a+cell count was summed up from all 6–12 areas imaged.

#### Evan's Blue Dye assay

Evan's Blue Dye (EBD) is a diazo dye that binds to serum albumin, creating a large molecular complex that normally does not cross the intact BBB. However, in pathological conditions leading to increased BBB permeability, the EBD-albumin complex can cross the BBB and accumulate in brain tissue, thus providing a measurable indication of barrier disruption. At the pre-determined time points of 18 days post-immunization, the mice were injected intravenously with 4% Evan's Blue Dye in saline at a dosage of 4 ml/kg body weight. The dye was allowed to circulate for 3 h to ensure systemic distribution. After the circulation period, the mice were anesthetized and transcardially perfused with phosphate-buffered saline (PBS) to remove intravascular dye. The brains and spinal cords were then carefully extracted, weighed, and homogenized in N,N-dimethylformamide to extract the dye from the tissue. The samples were then centrifuged, and the supernatants were collected for spectrophotometric analysis. Quantification of the EBD was performed using a TECAN spectroscopic device. The absorption of the extracted solutions was measured at 565 nm, a wavelength at which EBD exhibits a distinct peak. EBD concentration was calculated from the absorbance values using a standard curve generated with known concentrations of EBD. The amount of EBD in the brain tissue was then expressed as μg of EBD per g of brain tissue. All data were collected and analyzed using appropriate statistical methods.

#### Flow cytometry analysis

Flow cytometry was used to examine the lymphocyte subpopulations in spinal cord and spleen of the EAE mice at specified time points. Spinal cords were carefully harvested and mechanically and enzymatically (Collagenase, DNAse) dissociated. Lymphocytes were then isolated from the suspension using a LymphoprepTM-gradient

Fluorochrome	Antigen	Clone	Company
BrilliantViolet421	CD4	RM4-5	BD Biosciences
BrilliantViolet605	CD8	53-6.7	Biolegend
BrilliantViolet650	CD3	17A2	Biolegend
FITC	CD11b	M1/70	Biolegend
PE-Cy5.5	Ly6G	1A8	Biolegend
PE	CD11c	N418	Biolegend
ECD	CD19	6D5	Biolegend
PE Dazzle594	CD25	PC61	BD Biosciences
APC	NK1.1	S17016D	Biolegend
Alexa Fluor 700	Ly6C	HK1.4	Biolegend
APC-Cy7	CD45	30-F11	Biolegend

**Table 2.** Antibodies used for flow cytometry analysis on CNS immune cell infiltration analysis (ex vivo experiment).

Fluorochrome	Antigen	Clone	Company
eFluor450	CD69	H1.2F3	Invitrogen
Fluor506	Viability dye	-	Invitrogen
BV605	CD8a	53-6.7	BioLegend
FITC	CD19	MB19-1	BioLegend
PerCP-Cy5.5	CD3	17A2	BioLegend
PE	CD11a	2D7	BD Biosciences
PE-Cy7	CD25	PC61	BioLegend
Alexa Fluor 647	CD4	RM4-5	BioLegend
APC/Fire750	CD49d	R1-2	BioLegend
PE-Dazzle594	Ki-67	16A8	BioLegend

**Table 3**. Antibodies used for flow cytometry analysis on lymphocyte activation, adhesion, and proliferation (in vitro experiment).

(Stemcell technologies). Spleen was collected and mechanically dissociated by passing it through a 70  $\mu$ m cell strainer. Red blood cells were lysed with ACK Lysis Buffer and suspension was again passed through a 70  $\mu$ m cell strainer.

Lymphocytes from both organs were centrifuged and resuspended in FACS buffer, containing 2 mM EDTA and 2% fetal calf serum. Cells were then stained with fluorochrome-conjugated monoclonal antibodies (Tables 2, and 3, respectively) in the dark 4 °C for 30 min. The cells were then washed with FACS buffer and prepared for analysis. Cells were analyzed on a CytoFLEX S (Beckman Coulter) and data was interpreted using Kaluza Analysis Software (Beckman Coulter). Lymphocytes were identified based on forward and side scatter properties, with specific populations determined by surface marker expression (representative gating strategy is stated in Fig. S1). Data are reported as the total cell counts (via flowrate check) of each cell type within the total lymphocyte population.

#### Isolation of pMBMECs

pMBMECs were isolated according to different protocols for performing the quantitative PCR or the permeability assay. In both procedures, the pMBMECs were never passaged between isolation and experiment. Flecainide treatment was applied for 24 h prior to qPCR analyses and for 7 days prior to Western blot analyses, starting after pMBMECs had reached confluency.

Isolation pMBMECs for quantitative PCR and western blot

We began by euthanizing six- to eight-week-old female C57BL/6 mice. After euthanasia, the brains were carefully extracted and immediately transferred onto sterile filter paper to facilitate the removal of the meninges. Following this step, the brain tissue was homogenized to a uniform consistency and subsequently processed according to the protocol of the Adult Brain Dissociation Kit (Miltenyi Biotec), which is optimized for effective dissociation of murine brain tissue. To isolate microvascular endothelial cells, the resulting single-cell suspension was subjected to magnetic-activated cell sorting (MACS). First, CD45<sup>+</sup> immune cells were labeled using CD45 MicroBeads and removed by magnetic separation via LS columns and the MACS Separator. The flow-through, containing CD45<sup>-</sup> cells, was then incubated with CD31 MicroBeads to isolate CD31<sup>+</sup> endothelial cells. These CD45<sup>-</sup>CD31<sup>+</sup> cells were collected and plated in 12-well plates for culture. Prior to seeding, the plates were coated overnight at 4 °C with a coating solution consisting of 500 µl dH<sub>2</sub>O, 400 µl collagen, and 100 µl fibronectin (200 µl per well), to enhance cell adhesion. The isolated endothelial cells were seeded in 1.5 ml of MBMEC medium per

well. For the initial two days, cells were cultured in MBMEC medium supplemented with 0.1% pyromycin (10  $\mu$ l pyromycin per 10 ml medium) to select for the desired cell population. Thereafter, the medium was replaced with pyromycin-free MBMEC medium. The MBMEC culture medium consisted of 40 ml DMEM high glucose, 10 ml fetal calf serum (FCS), 25  $\mu$ l basic fibroblast growth factor (bFGF) and 50  $\mu$ l heparin.

#### Isolation of pMBMECs for permeability assay

Cells were isolated by the method of Coisne et al.  $^{22}$  as follows: for each preparation cortices from six- to tenweeks old gender matched mice were isolated and meninges were removed. Preparations were pooled and homogenized in Hank's balanced salt solution containing 0.1% bovine serum albumin. The homogenate was mixed with 30% dextran and centrifuged at 3000g for 25 min at 10 °C. The pellet containing the vascular fraction was collected. Centrifugation and pellet harvesting was repeated once. The collected vascular fraction was then filtered through a 60  $\mu$ m nylon mesh. The capillary-enriched filtrate was digested in DNase I (10 mg/mL), TLCK (0.147 mg/mL), and collagenase/dispase (2 mg/mL) for 30 min at 37 °C. The digestion was stopped by an excess of wash buffer and filtered through a 20  $\mu$ m nylon mesh. The crude cell preparation of pMBMECs were cultured for 48 h in the presence of 4  $\mu$ g/ml puromycin, which allowed selective growth of pMBMECs only.

#### Western blot analysis of protein expression in pMBMECs

pMBMECs were cultured to confluence as described in "Isolation pMBMECs for quantitative PCR and western blot" section, then treated for 7 days with flecainide (2  $\mu$ M or 5  $\mu$ M) or vehicle. After treatment, cells were washed with PBS and lysed in NP-40 buffer (150 mM NaCl, 50 mM Tris/HCl, 1% NP-40, pH 8.0) on ice for 20 min and then scraped off using a pipette tip. Lysates were cleared by centrifugation (12,000 × g, 10 min, 4 °C), and protein concentration was determined using the BCassay kit (Interchim, France). Equal protein amounts (25  $\mu$ g) were mixed with 1×Laemmli buffer, denatured at 95 °C for 5 min, separated by SDS-PAGE, and transferred onto 0.2  $\mu$ m nitrocellulose membranes. Membranes were blocked for 10 min at room temperature with EveryBlot buffer (Bio-Rad, USA), then incubated overnight at 4 °C with the following primary antibodies: anti-Actin (Invitrogen, PA1-183, 1:4000), anti-PECAM1 (Antibodies Online, ABIN669006, 1:1000), anti- $\beta$ -Integrin (ABIN739029, 1:1000), anti-JAM3 (ABIN1386406, 1:1000), and anti-JAM2 (ABIN3187667, 1:1000). Following three washes with PBS containing 0.05% Tween-20, membranes were incubated for 1.5 h on a shaker at room temperature with IRDye-labeled secondary antibodies: Goat anti-Rabbit 680RD (LI-COR, 926-68071) and Goat anti-Mouse 800CW (LI-COR, 926-32210). Protein bands were visualized using the ChemiDoc system (Bio-Rad) and quantified with ImageLab software. Expression levels were normalized to  $\beta$ -actin and analyzed using GraphPad Prism.

#### Quantitative PCR analysis

For our qPCR analysis, we utilized the QuantStudio 3 from Thermo Fisher Scientific, employing SYBR Green as our detection chemistry. After preparing and loading our samples, we conducted the qPCR run analyzing the genes listed in Table 4 (in different experimental approaches). The machine's sophisticated technology measured DNA quantity using the fluorescence of the SYBR Green. Post-run, we processed and interpreted the data using the QuantStudio Design and Analysis Software from Thermo Fisher Scientific, enabling us to calculate relative gene expression levels using the  $\Delta\Delta$ Ct and  $\Delta$ Ct, respectively.

The treatment groups in the in vitro treatment experiments included cells exposed to 2  $\mu$ M or 5  $\mu$ M flecainide or PBS vehicle control 24 h prior to cell harvesting. The in vitro concentrations were used based on previous experiments with flecainide found in literature<sup>17,18</sup>.

V-CAM-1	JAM-1
Forward sequence GCTATGAGGATGGAAGACTCTGG	Forward sequence CACCTACTCTGGCTTCTCCTCT
Reverse sequence ACTTGTGCAGCCACCTGAGATC	Reverse SEQUENCE TGCCACTGGATGAGAAGGTGAC
I-CAM-1	JAM-2
Forward sequence AAACCAGACCCTGGAACTGCAC	Forward sequence CAGACTGGAGTGGAAGAAGGTG
Reverse sequence GCCTGGCATTTCAGAGTCTGCT	Reverse sequence GCTGACTTCACAGCGATACTCTC
I-CAM-2	JAM-3
Forward sequence GACGGTCTCAACTTTTCCTGCC	Forward sequence GCATTGCTTCCAATGACGCAGG
Reverse sequence CCATTTGGTTGTCCTGCATCGG	Reverse sequence GATGAAGCAGCCTCGTCTGTAC
PECAM-1	Occludin
Forward sequence CCAAAGCCAGTAGCATCATGGTC	Forward sequence TGGCAAGCGATCATACCCAGAG
Reverse sequence GGATGGTGAAGTTGGCTACAGG	Reverse sequence CTGCCTGAAGTCATCCACACTC
NaV1.5	NaV1.9
Forward sequence GGTTCCGAGATGGTCAGTTGCT	Forward sequence GTCTTCAGCATGTTCATTATC
Reverse sequence CAAGGACTCCTGTCCAATACGG	Reverse sequence CCACACATTATGAAGTCCTCG
NaV1.6	GAPDH
Forward sequence AAGTGGACAGCCTATGGCTTC	Forward sequence TGTGTCCGTCGTGGATCTGA
Reverse sequence AGCCAGAAGATGAGACACACC	Reverse sequence CCTGCTTCACCACCTTCTTGA

**Table 4**. List of primers used for qPCR analysis.

#### Permeability assay

Permeability assays were performed in triplicates as reported by Coisne et al.<sup>22</sup>, with minor adaptations: pMBMECs were grown on Matrigel-coated Transwell\* filter inserts (0.4  $\mu$ m pore size, 6.5 mm diameter; article number 662640, Greiner Bio-One Vacuette Schweiz GmbH, St. Gallen, Switzerland) for 6 to 8 days. Alexa Fluor 680-dextran (3 kDa, 10  $\mu$ g/ml; LuBioScience, Luzerne, Switzerland) was used as permeability tracer. Diffused dextran was quantified using the Odyssey Imaging System (LI-COR, Bad Homburg, Germany) and the clearance value (Pe, in cm/min) of the pMBMECs calculated as reported by Coisne et al. 2005. Flecainide treatment at 5  $\mu$ M was for 24 h and IL-1 $\beta$  treatment at 20 ng/ml was for 16 h. The in vitro concentrations of flecainide were used based on previous experiments found in literature<sup>17,18</sup>. After the experiment, each filter was examined for confluent growth of pMBMECs by staining with phalloidin-rhodamine and subsequent fluorescence microscopy. The inflammatory state of pMBMECs after IL-1 $\beta$  stimulation was monitored in parallel samples by staining with the homemade rat anti-mouse ICAM-1 monoclonal antibody 29G1 followed by a secondary donkey anti-rat Cy5 antibody (Jackson ImmunoResearch, Milan Analytica AG, Rheinfelden, Switzerland).

#### Isolation of splenocytes for proliferation assay and qPCR analysis

Immediately following euthanasia, spleens were aseptically removed and placed into wash buffer composed of DMEM supplemented with fetal calf serum and antibiotics. For tissue dissociation, each spleen was transferred onto a pre-wetted 40  $\mu$ m cell strainer positioned on a conical tube. The spleen was mechanically dissociated by gently pressing it through the strainer using the plunger of a syringe. The cell strainer was then rinsed with additional wash buffer to collect all cells. The resulting single-cell suspension was centrifuged at 4 °C. After removal of the supernatant, the cell pellet was resuspended in pre-warmed ACK lysis buffer to lyse erythrocytes. The suspension was incubated at room temperature, and erythrocyte lysis was subsequently stopped by adding wash buffer, followed by a second centrifugation step at 4 °C. The final cell pellet was resuspended in wash buffer and passed through a freshly rinsed 40  $\mu$ m cell strainer into a new conical tube to ensure maximal recovery of splenocytes.

#### Proliferation assay using CFSE and Ki-67

To investigate the effects of flecainide on lymphocyte proliferation, we performed a combined assay using CFSE (carboxyfluorescein succinimidyl ester) labeling and intracellular Ki-67 staining. Splenocytes were isolated as described in "Isolation of splenocytes for proliferation assay and qPCR analysis" section. Prior to culture, cells were labeled with CFSE by incubation in PBS supplemented with fetal calf serum and the dye at 37 °C in the dark. The labeling reaction was quenched by the addition of cold wash medium, followed by incubation on ice. After two washing steps, cells were resuspended in murine T cell medium composed of IMDM supplemented with fetal calf serum,  $\beta$ -mercaptoethanol, L-glutamine, and antibiotics. T cell activation was achieved by seeding the CFSE-labeled splenocytes into anti-CD3-coated 96-well plates. Cells were treated with either vehicle (containing 0,005% DMSO), 2  $\mu$ M flecainide, or 5  $\mu$ M flecainide and incubated for five days at 37 °C in a humidified CO $_2$  incubator. On day three, half of the culture medium was carefully replaced with fresh treatment medium. At the end of the incubation period, proliferation was assessed by flow cytometric analysis of CFSE dilution and intracellular Ki-67 expression. For Ki-67 staining, cells were fixed, permeabilized, and stained with a fluorochrome-conjugated anti-Ki-67 antibody according to the manufacturer's protocol. Data were acquired and analyzed within defined immune cell subsets.

#### Statistics and data interpretation

Statistical analysis was performed using Prism (version 9, Graphpad Software, Inc.) and IBM SPSS Statistics (version 20, IBM Corporation, USA). Total and percent changes of the acquired retinal parameters (OCT and OMR) were analyzed using generalized estimation equation (GEE) models, accounting for within-subject intereye correlations, to test for differences between the two groups. For non-paired data, group means analyses were compared using a one-way ANOVA with the Dunnett's post hoc test, utilizing one optic nerve per animal for the histological investigations. The thickness of the inner retinal layers, ranging from the inner limiting membrane to the bottom of the inner plexiform layer, the total retinal thickness and outer retinal layers were assessed in volume scans around the optic disc as the primary OCT-based outcome parameters. The spatial frequency served as a functional primary readout. The other histology-derived parameters were assessed as secondary outcome criteria. The severity of EAE symptoms, extending from minor hind limb weakness to complete paralysis, was assessed through a standardized scoring system (ranging from 0 to 5), providing a quantitative outcome measure of neuroinflammation and neurodegeneration. The EAE scores served as an integral part of the study, illustrating the clinical manifestation and progression of the disease, offering a real-time evaluation of the neurological impairment. QPCR was deployed for the precise quantification of targeted gene expression changes. The relative changes in gene expression levels were examined as one of the primary outcome measures, offering key insights into the molecular mechanisms. The permeability of the BBB was further evaluated by using the Evans Blue assay. This approach involved the systemic administration of Evans Blue dye, the penetration of which into the brain tissue served as a direct indicator of BBB disruption. The quantified extent of dye penetration, extracted and measured spectrophotometrically, offered a primary outcome measure of BBB integrity. The data derived from the Evans Blue assay yielded essential insights into the degree and timing of BBB permeability changes in response to neuroinflammation and following various therapeutic interventions.

#### Results

#### Assessment of clinical disability (EAE-scoring)

We aimed at determining the most promising pure sodium channel blocker for extended EAE studies in various rodent strains by conducting a preliminary screening experiment to discern the more effective candidate

between flecainide and phenytoin. Both these drugs have been previously noted for their beneficial effects in EAE models, with flecainide<sup>10,13</sup> being a selective sodium channel blocker and phenytoin<sup>11,23</sup> an unselective one.

Figure 1 demonstrates our experiment comparing two drugs' effectiveness in alleviating EAE symptoms, guiding future long-term study decisions. Flecainide emerged as the more effective of the two, demonstrating a superior ability to alleviate EAE conditions. This was quantitatively reflected in the mean difference (MD) of 0.4551 ( $\pm 0.0854$ , P: 0.0003), favoring flecainide over phenytoin. This led us to our decision to prioritize it in subsequent, more comprehensive EAE studies across different rodent strains. Rasagiline demonstrated no positive effects, whereas safinamide slightly improved EAE outcomes compared to the MOG vehicle (MD:  $0.3196\pm 0.1249$ , P: 0.0120).

C57BL/6J and non-obese-diabetic (NOD) mice exhibit distinct EAE progression patterns: the former develops a more chronic progression with a disease peak around day 18 post-immunization, while the latter shows a relapsing–remitting course with complete recovery phases. In the mentioned subsequent studies, the impact of flecainide, rasagiline, and safinamide on EAE progression in these mouse models was evaluated over a period of 90 days p.i. of EAE, induced by immunization with MOG35-55, scored clinically over time. The treatment groups were compared to the MOG EAE vehicle group, with n=9 per group. The treatments were initiated from day 0 of immunization.

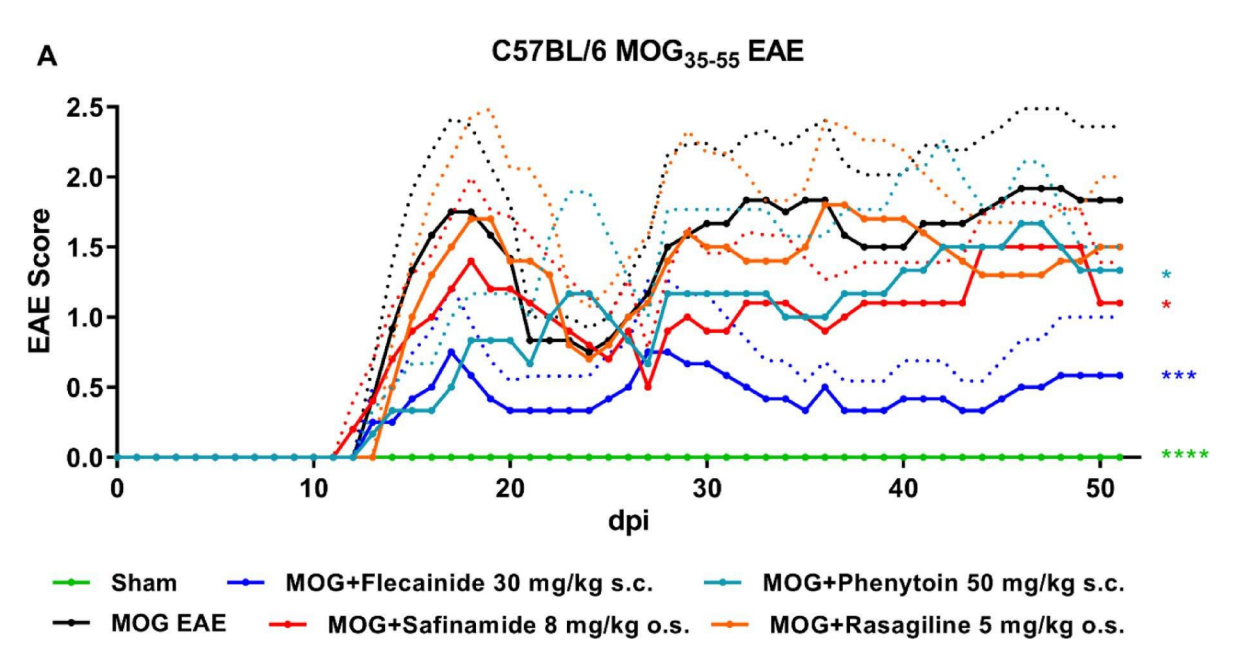
Figure 2A illustrates the clinical scores of EAE in the acute progressive C57BL/6J mouse model. Administration of flecainide (30 mg/kg subcutaneously) and safinamide (8 mg/kg orally) resulted in a significant reduction in EAE-related disability. The flecainide-treated group exhibited a MD score of  $0.7711\pm0.0649$  (P=0.0002), while the safinamide-treated group showed an MD score of  $0.2930\pm0.0753$  (P=0.0251). These findings indicate a substantial decrease in disability with both flecainide and safinamide treatment compared to the MOG-induced EAE control group.

Similarly, Fig. 2B presents the EAE clinical scores in the chronic progressive NOD mouse model. Notably, treatment with flecainide (MD:  $0.3335\pm0.0528$ , P=0.0010) and safinamide (MD:  $0.2437\pm0.0545$ , P=0.0126) also significantly reduced EAE-related disability compared to the MOG EAE control group.

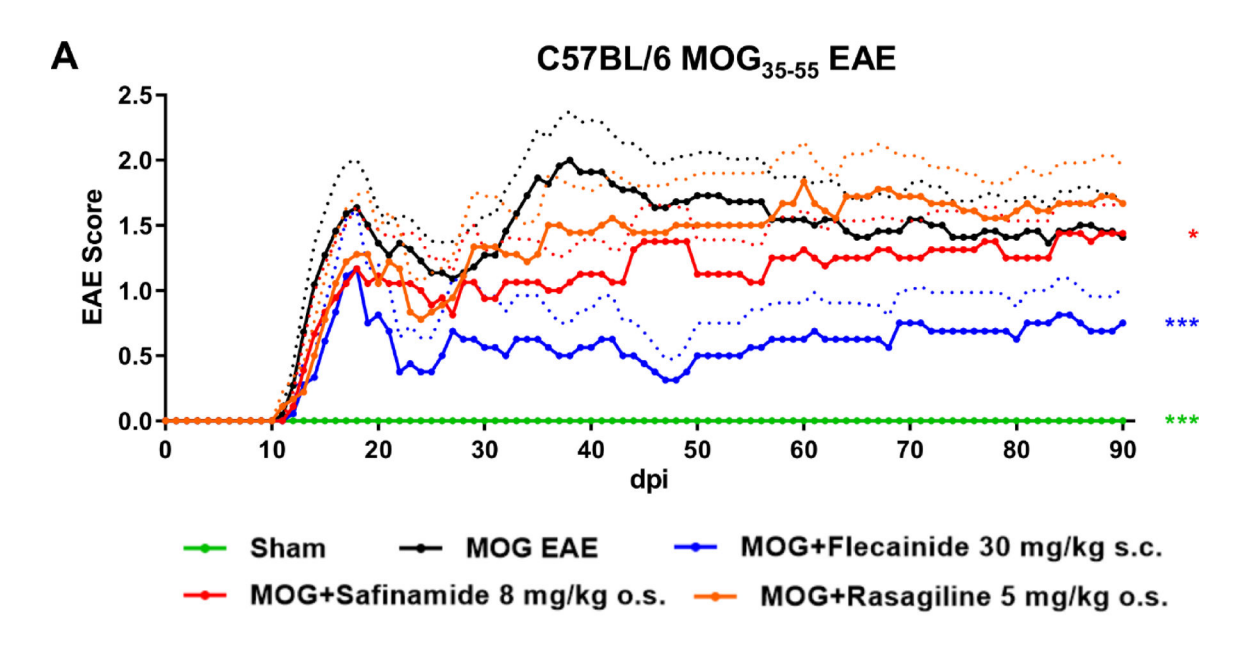
In contrast, treatment with rasagiline did not result in a significant reduction in disability in either mouse model compared to the untreated MOG EAE group.

#### Evaluation of neurodegeneration and visual function via OCT and OMR

In addition to assessing the effects of flecainide and safinamide on EAE-related disability, we conducted a longitudinal evaluation of neurodegeneration and visual function using OCT in both C57BL/6J and NOD EAE mice, as well as OMR testing in C57BL/6J EAE mice over 90 days post EAE induction (Fig. 3). NOD mice were not subjected to OMR testing, as their genetic background is associated with congenital visual impairment, limiting the reliability of behavioral vision assessments. The OCT volume scans examined the degeneration of the inner retinal layers (IRL). In C57BL/6J EAE mice, flecainide treatment significantly reduced the change in IRL thickness over the 90-day period (MD=1.940±0.7879, P=0.0004), whereas safinamide and rasagiline showed no significant differences compared to the MOG EAE vehicle group. Similarly, in NOD EAE mice, flecainide



**Fig. 1.** Flecainide shows superior beneficial effects in C57BL/6J EAE compared to phenytoin. Progression of EAE in C57BL/6J mice over 52 days post EAE induction, immunized with MOG35-55. Treatment with flecainide, safinamide, phenytoin and rasagiline was initiated from day 0. \*p<0.05; \*\*\*p<0.001, \*\*\*\*p<0.0001, area under the curve analyzed via ANOVA with Dunnett's post hoc test in comparison to MOG EAE. n = 6 per group. Dotted lines represent the standard deviation.



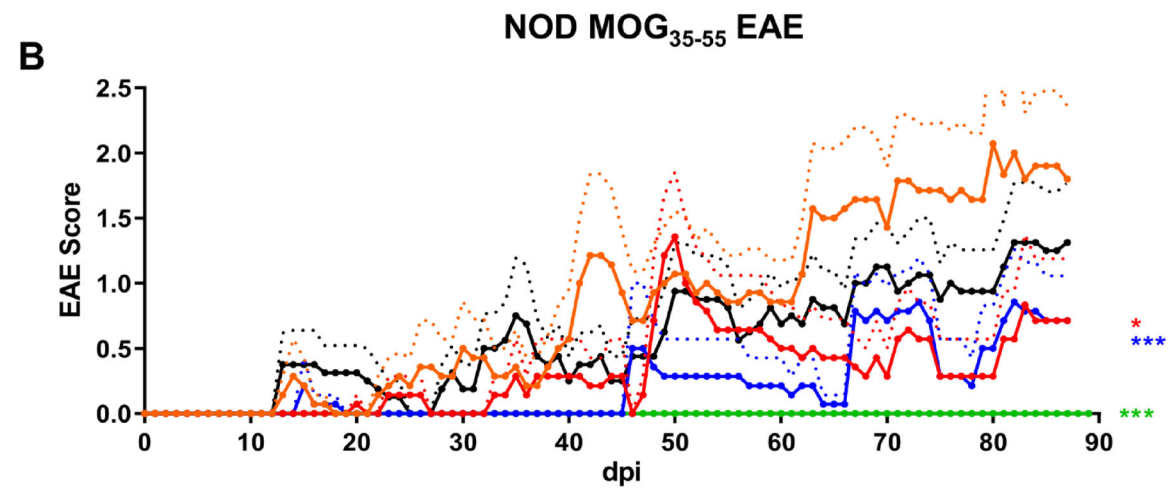


**Fig. 2.** Flecainide and safinamide mitigates clinical long-term EAE severity. Progression of EAE in C57BL/6J mice (**A**) and NOD female mice (**B**) over 90 days post EAE induction, immunized with MOG35-55. Treatment with flecainide, safinamide, and rasagiline was initiated from day 0. \*\*p < 0.01; \*\*\*p < 0.001, area under the curve analyzed via ANOVA with Dunnett's post hoc test in comparison to MOG EAE. n = 9 per group. Dotted lines represent the standard deviation.

(MD=1.844 $\pm$ 0.8840, P=0.0162) and safinamide (MD=1.473 $\pm$ 0.8223, P=0.0061) both significantly reduced IRL thickness changes. Flecainide treatment led to a significant improvement in visual function compared to the MOG vehicle group (MD=0.0458 $\pm$ 0.0347, P=0.0111), while safinamide and rasagiline did not show significant effects. These findings indicate that flecainide effectively slows neurodegeneration and preserves visual function in EAE mouse models, and safinamide also provides significant neuroprotective effects in NOD EAE mice, supporting their potential therapeutic benefits in neurodegenerative conditions like EAE.

#### Histological analyses of immunological markers in the optic nerve

We extended our investigation to the histological evaluation of immune cell markers, specifically CD3, a marker for T-cell infiltration, and Iba1 (ionized calcium-binding adaptor molecule 1), indicative of microglial activation, in longitudinal sections of optic nerves from C57BL/6J and NOD mice 90 days post-immunization. In addition, GFAP (glial fibrillary acidic protein), a marker for astroglial activation, was analyzed in retinal cross sections. Quantitative analyses (A, B, C, D, E and F) and representative illustrations (G) are presented in Fig. 4. In C57BL/6J mice, treatment with both flecainide and safinamide significantly reduced the infiltration of CD3-positive lymphocytes compared to the MOG EAE control group, with flecainide achieving a MD of  $1.8220\pm0.4116$  (P=0.0005) and safinamide achieving an MD of  $1.5323\pm0.4317$  (P=0.0048). In contrast, in NOD mice, only flecainide treatment significantly reduced CD3-positive infiltrates (MD=3.0239±1.0146, P=0.0228). No significant differences in Iba1 expression were observed among treatment groups in C57BL/6J mice. However, in NOD mice, flecainide treatment resulted in a significant reduction in Iba1-positive cells

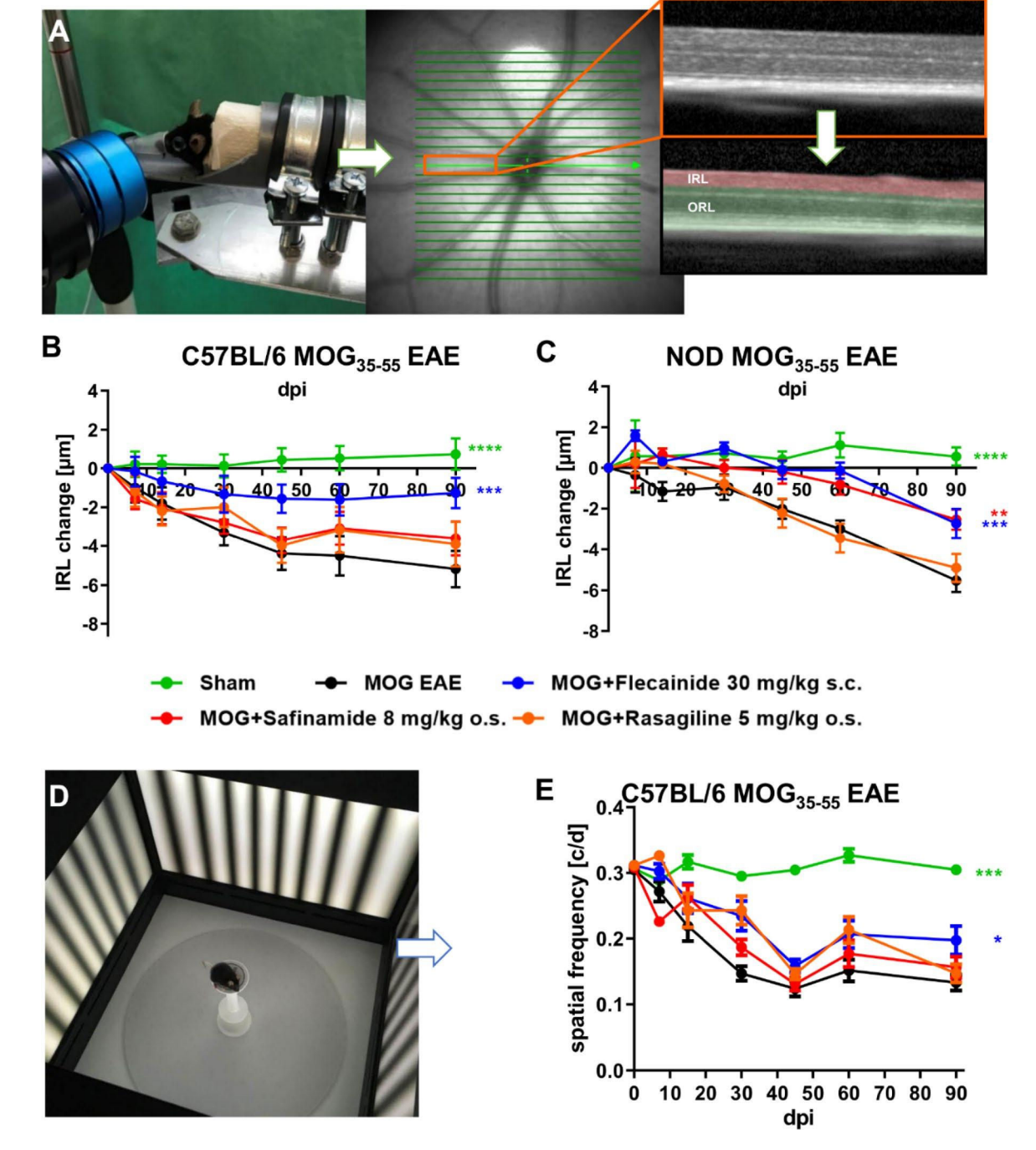


**Fig. 3.** Longitudinal evaluation of neurodegeneration and visual function via OCT and OMR reveals beneficial effects of flecainide and safinamide. OCT volume scan (**A**) of the degeneration of the inner retinal layers (IRL) (**B**, **C**), and OMR measurement of visual function (spatial frequency) (**D**) in cycles per degree (c/d) (**E**) in female C57BL/6J-EAE and NOD EAE mice over 90 days post EAE induction. \*\*p<0.01; \*\*\*p<0.001, \*\*\*\*p<0.0001, area under the curve analyzed via ANOVA with Dunnett's post hoc test in comparison to MOG EAE. n = 9 per group.

compared to the vehicle-treated EAE group (MD= $3.2844\pm0.8723$ , P=0.0036). No significant differences in GFAP expression were observed between treatment groups in either C57BL/6J or NOD mice, indicating that astrocytic activation remained unaffected by flecainide or safinamide treatment. These findings indicate that both flecainide and safinamide effectively reduce T-cell infiltration in the C57BL/6J EAE model, while flecainide additionally diminishes both T-cell infiltration and myeloid cell activation in the NOD-EAE model. This implies potential anti-inflammatory and neuroprotective effects of these treatments in the context of EAE.

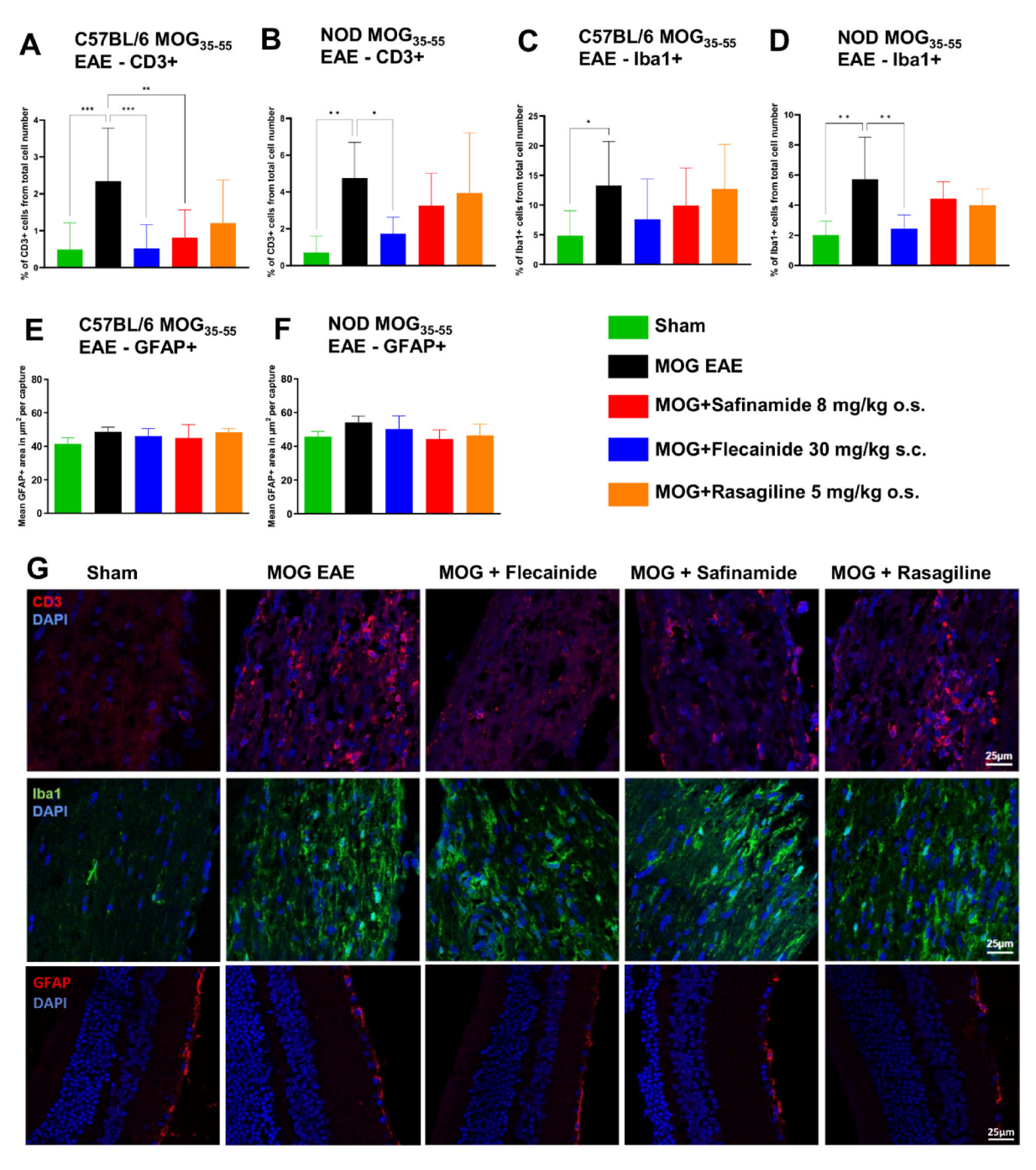


Fig. 4. Histological evaluations of immune- and glial cell markers shows immune modulating effects of flecainide. Quantitative analyses (A–F) and representative illustrations (G) of staining for T-cell infiltration (CD3), and microglial activation (Iba1) from longitudinal sections of optic nerves in C57BL/6J and NOD mice, and staining for astrocytic activation (GFAP) in retinal cross sections in C57BL/6J mice, 90 days post-immunization. Representative images show sections from C57BL/6J mice. Total cell number was measured based on automated DAPI cell counting with ImageJ2/Fiji. CD3 and Iba1 positive cells were counted by blinded raters. \*p<0.05, \*\*p<0.01, \*\*\*p<0.001, evaluated using ANOVA with Dunnett's post hoc test compared to MOG EAE. n=9 per group.

#### Histological analyses of neuronal and myelin markers in the optic nerve

In addition to assessing immune cell markers, we conducted histological evaluations of myelination and neuronal survival using Myelin Basic Protein (MBP) and Brain-specific homeobox/POU domain protein 3A (Brn3a) markers, respectively. Quantitative analyses (A, B, D, E) and representative illustrations (C) are presented in Fig. 5, based on longitudinal sections of optic nerves from C57BL/6J and NOD mice 90 days post-immunization. MBP, essential for nerve myelination, was utilized to evaluate myelin status, while Brn3a, expressed in retinal ganglion cells (RGCs), was employed to assess neuronal survival in the context of optic neuritis. Our results

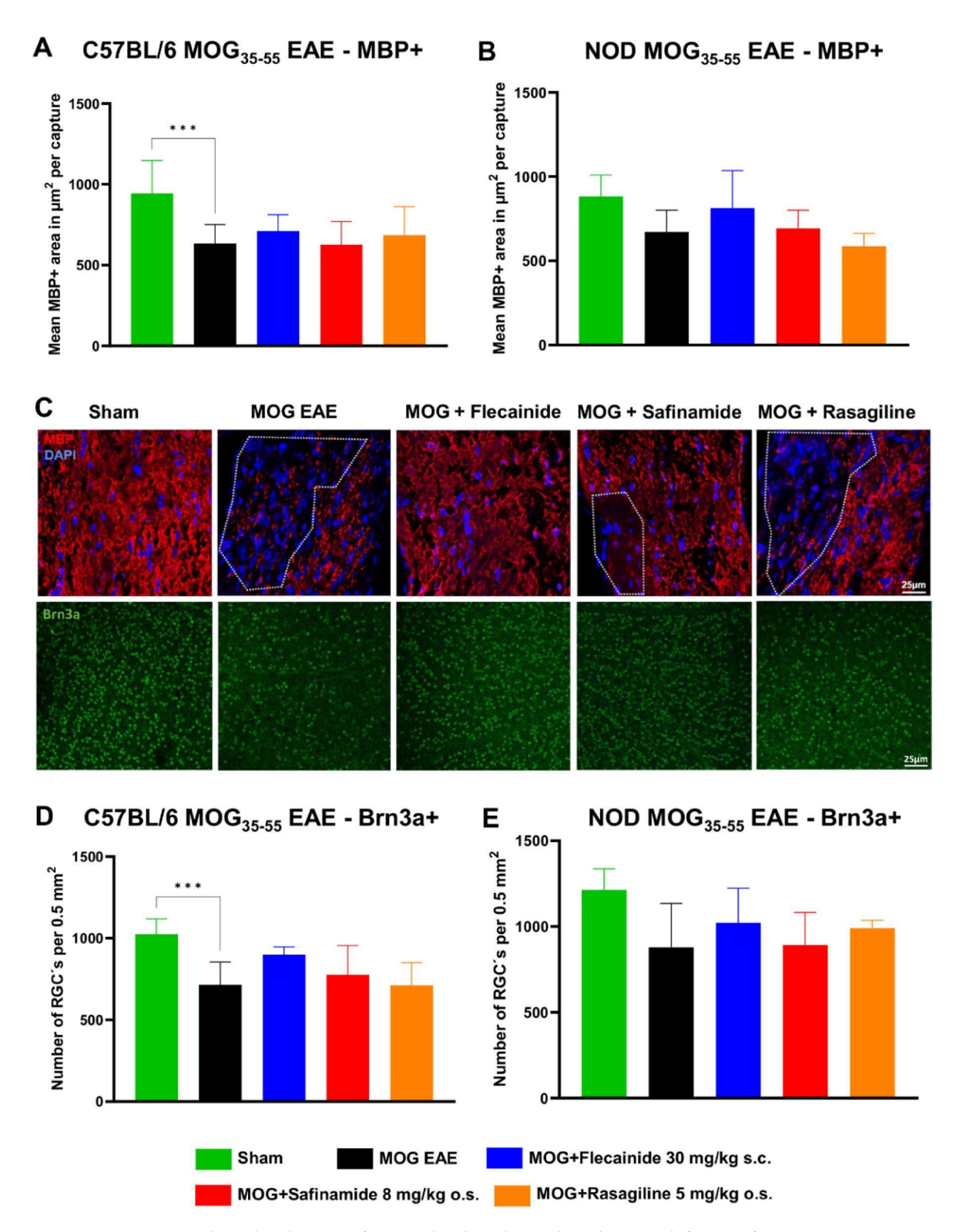
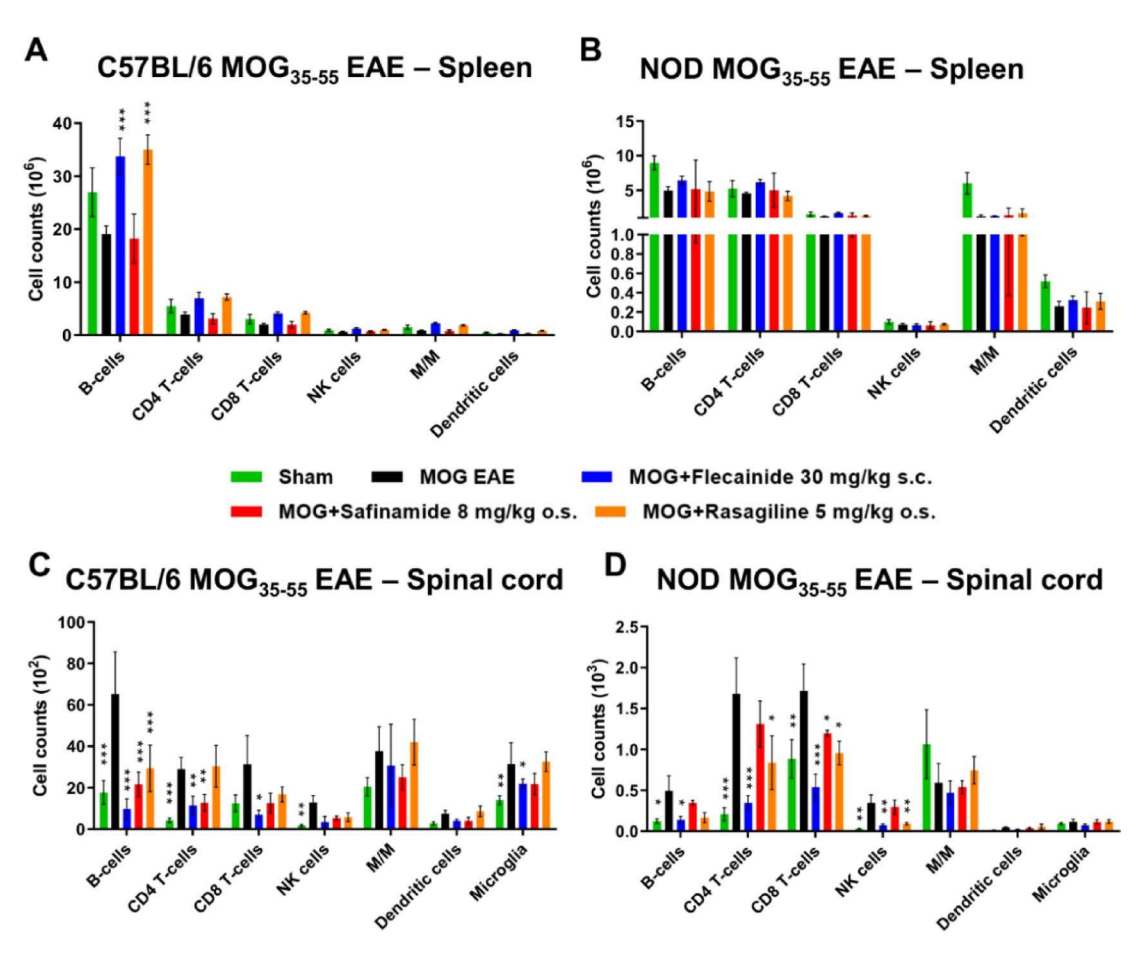


Fig. 5. Histological evaluations of neuronal and myelin markers shows no difference after treatment. Quantitative analyses (A, B, D, E) and representative illustrations (C) of staining for myelination (MBP) and neuronal survival (RGC's) (Brn3a) from longitudinal sections of optic nerves in C57BL/6J and NOD mice, 90 days post-immunization. Representative images show sections from C57BL/6J mice. The indicated  $\mu m^2$  mean of MBP+total area has been calculated out of a total 8.100  $\mu m^2$  captured area. Brn3a positive cells were counted automated by ImageJ2 / Fiji. \*\*\*p<0.001, evaluated using ANOVA with Dunnett's post hoc test compared to MOG EAE. n=9 per group.

showed no significant differences in the levels of either MBP or Brn3a across treatment groups in both mouse models. However, there was a noticeable trend suggesting that flecainide may have beneficial effects on myelination and neuronal survival, as indicated by increased MBP and Brn3a expression, though these changes did not reach statistical significance.

#### Assessment of CNS immune cell infiltration

Further investigation focused on analyzing immune cell infiltration across the BBB using immunophenotyping via flow cytometry (CD45+pre-gated). We examined the spleen (Fig. 6A,B) and spinal cord (Fig. 6C,D) of C57BL/6J and NOD EAE mice 90 days post-immunization. In the spleen of C57BL/6J mice, treatment with flecainide (MD =  $14.7039 \pm 1.5572$ , P < 0.0001) and rasagiline (MD =  $15.9590 \pm 1.4776$ , P < 0.0001) resulted in a significant increase in B cells. Additionally, there was a trend towards increased counts of CD4+T cells, NK cells, microglia, and dendritic cells with flecainide treatment, although these changes were not statistically significant. In NOD mice, flecainide treatment showed a non-significant trend of overall immune cell increase in the spleen. In contrast, immune cell infiltration in the CNS, specifically the spinal cord, exhibited different dynamics. In C57BL/6J mice, all treatment groups demonstrated significant reductions in B cells (flecainide:  $MD = 55.5006 \pm 9.5138$ , P < 0.0001; safinamide:  $MD = 43.6541 \pm 9.0240$ , P < 0.0001; rasagiline:  $MD = 35.8577 \pm 11.3321$ , P = 0.0005). Additionally, safinamide ( $MD = 16.2063 \pm 9.0249$ , P = 0.0020) and flecainide (MD=17.5004 $\pm$ 9.5138, P=0.0093) significantly reduced CD4+T cells, while flecainide also significantly decreased CD8+T cells (MD =  $24.2563 \pm 3.2195$ , P = 0.0193) and microglia (MD =  $9.5011 \pm 1.4139$ , P = 0.0215). In NOD mice, flecainide led to significant reductions in B cells (MD =  $0.3559 \pm 0.0549$ , P = 0.0395), CD4+T cells (MD=1.3310±0.0916, P=0.0007), CD8+T cells (MD=1.1782±0.1873, P=0.0004), and NK cells (MD =  $0.2775 \pm 0.0230$ , P = 0.0049). Safinamide significantly reduced CD8+T cells (MD =  $0.5181 \pm 0.0294$ , P=0.0394), while rasagiline treatment significantly reduced CD4+T cells (MD=0.8432±0.3520, P=0.0452), CD8+T cells (MD =  $0.7590 \pm 0.1819$ , P = 0.0207), and NK cells (MD =  $0.2569 \pm 0.0036$ , P = 0.0069). These findings indicate that the treatment compounds, particularly flecainide, resulted in increased numbers of immune cells in the spleen and reduced numbers in the spinal cord.



**Fig. 6.** CNS immune cell infiltration analysis revealed BBB modulating effect of flecainide. Immunophenotyping using flow cytometry (CD45+pre-gated) in C57BL/6J and NOD EAE mice 90 days post-immunization, focusing on spleen (**A**) and spinal cord (**B**). \*p < 0.05; \*\*p < 0.01; \*\*\*p < 0.001, as determined by ANOVA with Dunnett's post hoc test in comparison to untreated MOG EAE mice. n = 9 per group. M/M = Monocytes/Macrophages.

## Comprehensive analysis of BBB modulation through in vitro gene expression and permeability assay in pMBMECs and in vivo Evan's Blue Dye assay

Based on flow cytometry results showing reduced lymphocyte infiltration into the CNS after flecainide treatment, we assessed the integrity of the BBB using the EB-assay (Fig. 7). Quantification revealed a significant increase in EB perfusion in the CNS of MOG EAE mice. In contrast, flecainide treatment led to a noticeable reduction in EB perfusion (MD =  $0.0315 \pm 0.0113$ , P = 0.0167) compared to untreated MOG EAE animals.

To evaluate the impact of flecainide on gene expression in pMBMECs, we examined the RNA expression of key genes depicted in Fig. 8. These genes include *v-cam*, which facilitates leukocyte adhesion; *i-cam-1* and *i-cam-2*, involved in leukocyte trafficking; *pecam-1* (CD31), essential for angiogenesis and BBB integrity; *n-cam-1*, important for neuronal development; *jam-1*, *jam-2* and *jam-3*, critical for tight junctions and barrier function; *occludin*, a tight junction component in endothelial cells; and *integrin*  $\beta$ -3, key in cell adhesion and signal transduction<sup>24–26</sup>. In cells treated with 2  $\mu$ M flecainide, no significant differences were observed in the relative expression of these genes compared to vehicle-treated controls. However, cells treated with 5  $\mu$ M flecainide exhibited significant increases in the expression of several genes. *Pecam-1* showed a substantial increase with a MD of 0.8305±0.0059 (P=0.0004), and *jam-2* expression was elevated with an MD of 0.7141±0.0168 (P=0.0003). Additionally, *jam-3* expression significantly increased with an MD of 1.416±0.0401 (P=0.0002), and *integrin*  $\beta$ -3 demonstrated the most substantial increase with an MD of 3.111±0.0348 (P=0.0001).

To validate the transcriptional changes observed in the qPCR analysis, a subsequent Western blot was performed targeting selected molecules that had shown differential expression following flecainide treatment. Specifically, protein levels of JAM-2, JAM-3, and integrin  $\beta$ -3 were assessed, as these genes were significantly upregulated at the mRNA level upon exposure to 5  $\mu$ M flecainide. The results confirmed that JAM-2 and JAM-3 exhibited trends toward increased expression at the protein level, while integrin  $\beta$ -3 showed a significant upregulation in the 5  $\mu$ M flecainide group compared to vehicle-treated controls (MD =  $-0.1816\pm0.0607$ , P=0.0362), consistent with the qPCR findings. PECAM-1 protein could not be reliably detected under the given experimental conditions. For JAM-2 and JAM-3, protein lysates from two mice were pooled per well, resulting in one biological replicate per group. For integrin  $\beta$ -3, eight mice per group were used, pooled into four wells (two mice per well), providing a more robust dataset. These findings support the notion that flecainide modulates adhesion molecule expression in pMBMECs, not only at the transcript level, but also at the protein level (Fig. 8B,C).

We performed permeability experiments to investigate the effect of flecainide on BBB permeability under inflammatory conditions, modeled in vitro using IL-1 $\beta$ -stimulated pMBMECs (Fig. 9). IL-1 $\beta$  treatment significantly compromised the barrier properties of pMBMECs (MD=0.07833, P<0.0001)<sup>27</sup>. However,

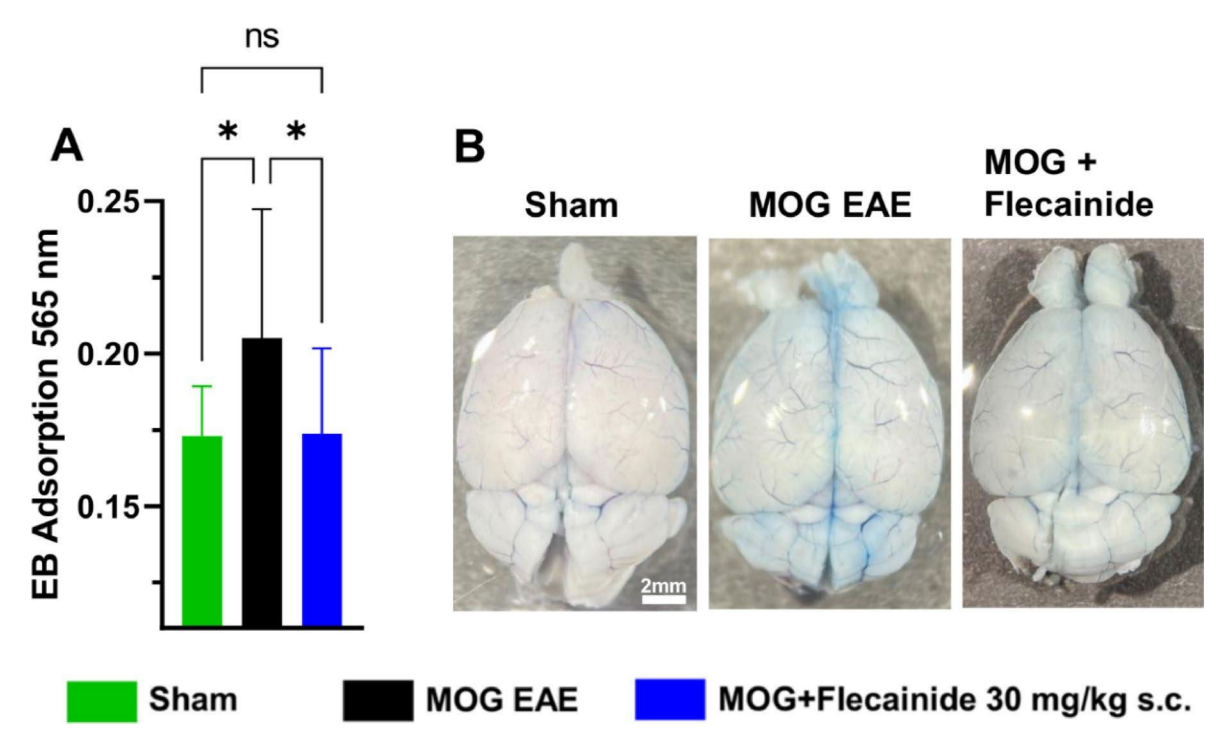
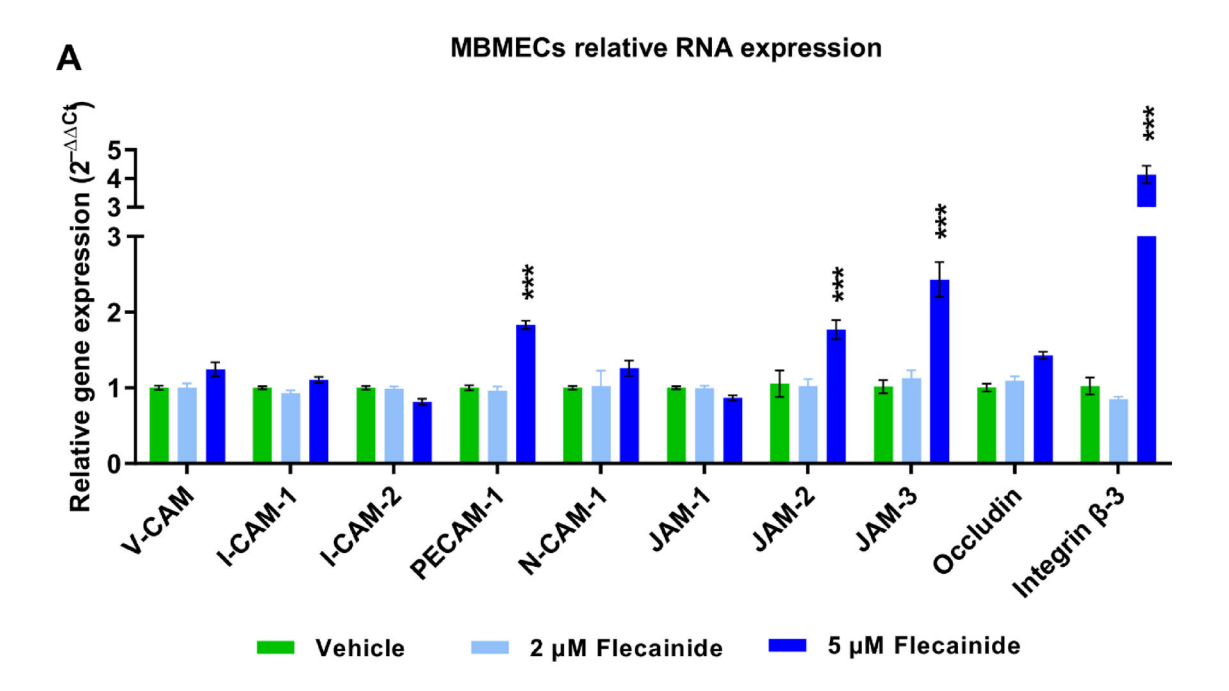


Fig. 7. Analysis of Blood–Brain Barrier permeability using Evan's Blue Assay after EAE Induction shows beneficial effects of flecainide. Quantitative data ( $\mathbf{A}$ ) and representative images ( $\mathbf{B}$ ) depict Evan's Blue (EB) absorption at 565 nm from mice whole brains homogenate after weight correction, sacrificed at day 18 post-EAE induction at the peak of disease. Statistical significance is represented by \*p < 0.05 and ns (not significant), determined by ANOVA followed by Dunnett's post hoc test comparing to untreated MOG EAE mice. N = 15 per group. Scale bar: 2mm.



#### MBMECs relative protein expression

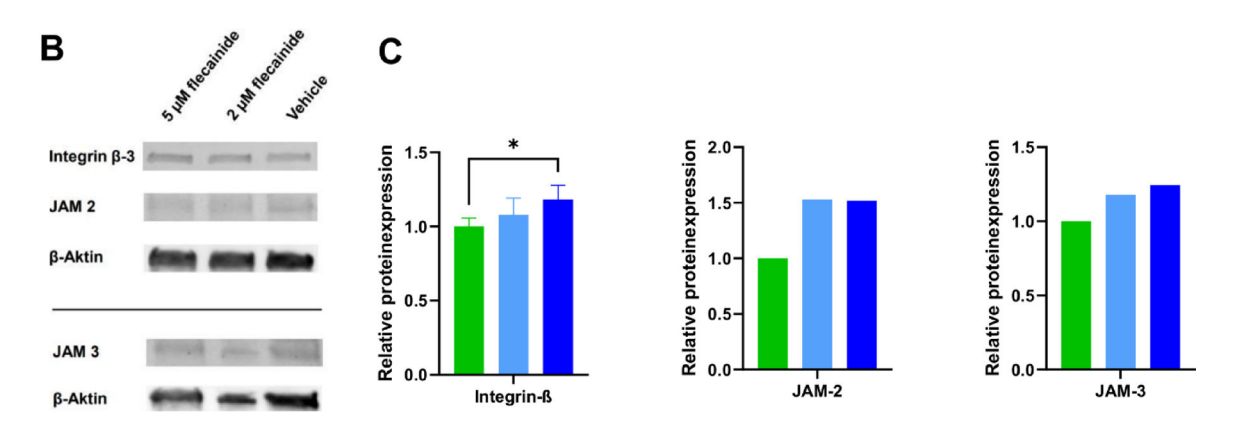


Fig. 8. In vitro flecainide treatment of pMBMECs alters gene expression profile and protein expression of important BBB integrity markers. (A) The graph depicts the  $\Delta\Delta$ Ct values (normalized to housekeeping gene GAPDH and relative to vehicle-treated controls) for a range of genes of interest (X-axis) in pMBMECs. The treatment groups include cells exposed to 2  $\mu$ M or 5  $\mu$ M flecainide or PBS vehicle control 24 h prior to cell harvesting. The bars represent the mean  $\Delta\Delta$ Ct values while error bars indicate standard error of the mean (SEM) across three independent experiments. (B) Representative Western blot images showing protein expression of integrin  $\beta$ -3, JAM2, and JAM3 in pMBMECs treated with flecainide (2  $\mu$ M or 5  $\mu$ M) or vehicle. (C) Densitometric quantification of protein expression normalized to  $\beta$ -actin and additionally to the vehicle-treated control group. Statistical significance was determined using two-way ANOVA followed by Bonferroni's post-hoc test. Asterisks denote significant differences compared to the vehicle-treated group at \*p<0.05 and \*\*\*p<0.001.

flecainide treatment did not significantly alter the permeability of IL-1 $\beta$ -stimulated pMBMECs compared to the DMSO vehicle (MD = 0.003333 ± 0.037925, P = 0.9946) or IL-1 $\beta$  treatment alone (Fig. 9).

Figure 10 illustrates flow cytometry analyses of proliferation marker (Ki-67), adhesion molecules (CD11a, CD49d), and activation markers (CD25, CD69) in CD3+, CD4+, CD8+, and CD19+splenocytes. No significant differences were observed in the expression of these markers following treatment with either 2  $\mu$ M or 5  $\mu$ M flecainide compared to vehicle-treated controls. These findings suggest that flecainide does not exert measurable immunomodulatory effects on the activation, proliferation, or adhesion molecule expression of T or B lymphocytes in the spleen. This further supports the hypothesis that the observed therapeutic effects of flecainide are not mediated via direct action on peripheral lymphocytes.

This lack of immunomodulatory activity on splenocytes is consistent with the qPCR findings shown in Fig. 11, where expression levels of voltage-gated sodium channels NaV1.5, NaV1.6, and NaV1.9 were assessed

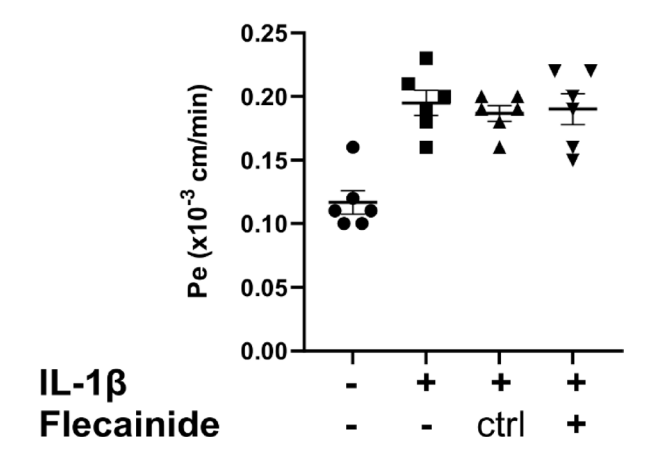


Fig. 9. Flecainide treatment does not change the permeability of IL-1 $\beta$  stimulated pMBMECs. The graph shows the permeability coefficient (Pe) value of pMBMECs to 3 kDa Dextran. Where indicated, IL-1 $\beta$  stimulation was at 20 ng/ml for 16 h, and Flecainide treatment was at 5  $\mu$ M for 24 h. Ctrl, vehicle control. For each condition, 6 data points deriving from 2 independent experiments are shown. Error bar shows  $\pm$  SEM. No significant differences were found between Flecainide and vehicle-treated groups using ordinary one-way ANOVA.

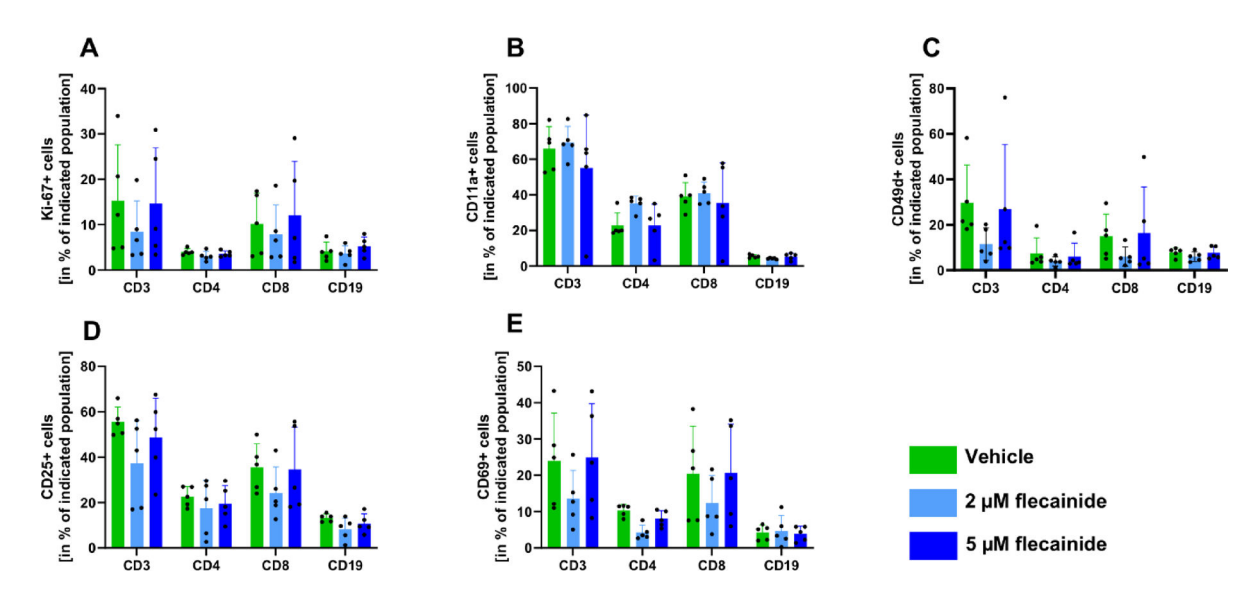


Fig. 10. Flow cytometric analysis of lymphocyte activation, adhesion, and proliferation markers after flecainide treatment. Splenocytes from mice treated with vehicle, 2  $\mu$ M, or 5  $\mu$ M flecainide were stimulated with CD3/CD28 antibodies and analyzed for expression of the proliferation marker Ki-67 (A), adhesion molecules CD11a (B) and CD49d (C), and activation markers CD25 (D) and CD69 (E) within CD3<sup>+</sup>, CD4<sup>+</sup>, CD8<sup>+</sup>, and CD19<sup>+</sup> cell populations. No significant differences were observed between treatment groups. Bars represent mean  $\pm$  SD. n=5 mice per group.

in splenocytes and pMBMECs. Notably, none of the analyzed NaV channels were detectably expressed in splenocytes, while all three showed marked expression in pMBMECs (Mean = 0.9008; SD = 0.4384). These data provide a molecular rationale for the cell type-specific action of flecainide, reinforcing the interpretation that its primary target in this context is the endothelial compartment rather than lymphocytes.

#### Discussion

EAE is a widely recognized and extensively validated animal model of MS, characterized predominantly by neuroinflammation, demyelination, and neurodegeneration<sup>1</sup>. However, it is important to acknowledge that EAE only partially recapitulates the complex immunopathology and chronic disease course observed in human MS. The translational relevance of preclinical findings must therefore be interpreted with caution, particularly in light of previous therapeutic approaches that showed efficacy in EAE but failed in clinical trials. For example, sodium channel blockers such as lamotrigine<sup>28</sup> and acid-sensing ion channel inhibitors like amiloride<sup>28</sup> demonstrated promising neuroprotective effects in animal models but did not meet endpoints in progressive MS patients. Our

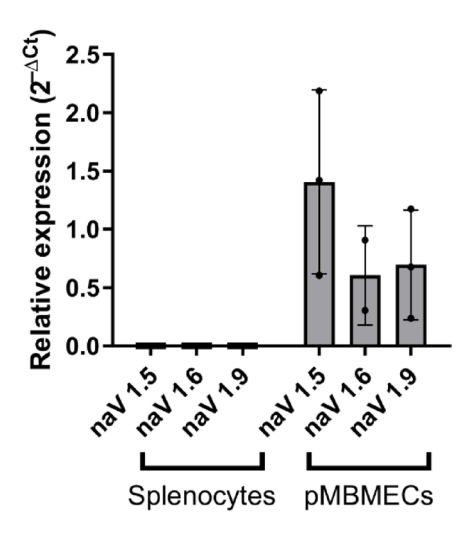


Fig. 11. Relative expression of sodium channel isoforms in splenocytes and pMBMECs. Relative expression of sodium channel isoforms in splenocytes and pMBMECs. qPCR analysis of NaV1.5, NaV1.6, and NaV1.9 expression in splenocytes and pMBMECs. While no expression of any tested NaV isoform was detected in splenocytes, all three channels were expressed in pMBMECs, with NaV1.5 showing the highest relative levels. Data are presented as  $2^{-\Delta Ct}$  values normalized to GAPDH. Bars represent mean  $\pm$  SD from n=3.

study does not include experiments on human brain tissue or human endothelial cell lines, and we refrain from making direct claims about clinical efficacy in MS. Instead, we view our findings as a preclinical proof of concept demonstrating BBB-stabilizing and neuroprotective properties of flecainide in the context of CNS inflammation, which warrant further validation in human-based systems. Notably, there are examples of NaV blockers where translational success has been achieved. Phenytoin, another sodium channel blocker that was also assessed and found effective in our study, demonstrated significant neuroprotective effects in a Phase 2 clinical trial in patients with acute optic neuritis, a common manifestation of autoimmune CNS inflammation<sup>29</sup>. This suggests that, at least in specific MS-related contexts such as optic neuritis, findings from EAE models can indeed translate into meaningful clinical benefit.

In this study, we systematically investigated the therapeutic potential of MAO-B inhibition and sodium channel blockade, both as individual interventions and in combination, across multiple murine models of EAE. Specifically, our research focused on flecainide, a Class Ic antiarrhythmic agent primarily utilized clinically for managing ventricular arrhythmias due to its potent NaV 1.5 channel blocking properties. Prior preclinical studies have demonstrated that both safinamide and flecainide exhibit beneficial effects in EAE, thus highlighting their potential therapeutic relevance for MS<sup>10,13</sup>.

NaV channels are prominently expressed in electrically excitable cells, including neurons, skeletal muscle fibers, and cardiac myocytes, where they play a fundamental role in action potential initiation and propagation. However, emerging evidence indicates their expression at significantly lower densities in various non-excitable cell populations, suggesting broader physiological roles beyond classical electrophysiological functions<sup>30</sup>. Despite extensive investigation, the precise mechanistic pathways underlying the therapeutic efficacy of sodium channel blockers such as flecainide and safinamide in EAE remain incompletely understood. In particular, uncertainty persists regarding whether their beneficial effects primarily result from direct actions on immune cells, modulation of neuronal excitability, or through influence on other cell types critically involved in disease progression, notably those contributing to the integrity of the BBB. BBB disruption represents a central pathological feature of EAE, critically influencing disease progression by facilitating inflammatory cell infiltration into the CNS. Hence, clarifying the precise cellular and molecular targets mediating the protective effects of sodium channel blockade in EAE is essential for the rational development of targeted therapeutic strategies in neuroinflammatory diseases.

Phenytoin, a Class Ib sodium channel blocker, has previously demonstrated notable beneficial effects in EAE models. Evidence from preclinical studies suggests that phenytoin effectively protects CNS axons, positioning it as a promising candidate for treating neuroinflammatory conditions<sup>29,31</sup>. The before mentioned<sup>29</sup> clinical trial investigating phenytoin in patients with acute optic neuritis yielded positive outcomes. However, our data revealed a superior therapeutic effect of flecainide over phenytoin, as shown by significantly enhanced disease mitigation and functional recovery parameters. Given these results, we choose to continue our subsequent investigations focusing on flecainide, the Class Ic sodium channel blocker, due to its demonstrated greater efficacy in alleviating EAE-associated pathology and symptoms. In this study, we introduce a novel hypothesis proposing a direct modulatory effect of sodium channel blockers on BBB integrity. Our experimental data support the conclusion that flecainide enhances BBB stability, thereby significantly reducing lymphocyte infiltration into the CNS. Furthermore, the observed protective effects of safinamide in our EAE models appear primarily mediated through sodium channel blockade rather than MAO-B inhibition, as evidenced by the lack of efficacy observed with the selective MAO-B inhibitor rasagiline. Notably, both flecainide (with substantial effects) and safinamide

(with comparatively moderate effects) demonstrated significant improvements in disability progression, neurodegeneration, visual function, immune cell infiltration, and BBB integrity.

These in vivo outcomes, particularly the pronounced effects on visual function and retinal neurodegeneration, have important clinical implications. Firstly, our results indicate that flecainide and safinamide may serve as viable candidates for clinical trials targeting acute optic neuritis, employing OCT and visual function assessments as primary endpoints. Secondly, as prior evidence has shown correlations between therapeutic outcomes in optic neuritis and effects in other CNS regions, such as the spinal cord<sup>7,21,32,33</sup>, our data may imply broader neuroprotective benefits that extend to general disability mitigation in EAE. Finally, the capacity of these agents to reduce long-term disability resulting from acute inflammatory episodes is particularly significant, given that current therapeutic strategies for inflammatory CNS diseases primarily target acute attacks without effectively preventing subsequent neurodegeneration. Despite these promising results, it remains critical to acknowledge that EAE serves only as an animal model for autoimmune CNS disorders and does not replicate every aspect of MS pathology. However, the demonstrated clinical efficacy of sodium channel blockade in human trials of acute optic neuritis with phenytoin lends strong support to the potential translatability of our findings. Our data further suggest that flecainide may represent a superior therapeutic alternative to phenytoin, thereby warranting detailed exploration in future clinical trials.

In terms of immune response, our histological analyses revealed that both flecainide and safinamide significantly reduced T-cell infiltration in the optic nerves of C57BL/6J EAE mice. T-cell infiltration is known to contribute substantially to the pathogenic mechanisms driving neuroinflammation in neuropathologic conditions such as EAE. Additionally, flecainide treatment also resulted in a significant reduction of both T-cell infiltration and microglial activation in the NOD-EAE model. These outcomes are consistent with previous reports highlighting the ability of safinamide and flecainide to mitigate microglial activation in other preclinical MS models<sup>13</sup> Notably, our study further identified that both treatments, with flecainide showing a more pronounced effect, led to increased immune cell populations in the spleen concomitant with decreased immune cell presence in the spinal cord. This suggests that sodium channel blockers potentially modulate immune cell distribution, reducing infiltration across the BBB. This immunological dichotomy aligns with gene expression analyses performed on pMBMECs following flecainide exposure. Specifically, treatment with 5 µM flecainide significantly upregulated genes known to be crucial for maintaining BBB integrity, further supporting the hypothesis of barrier modulation under neurodegenerative conditions. Interestingly, despite these transcriptional alterations, permeability assay using IL-1β-stimulated pMBMECs did not reveal immediate functional improvements in barrier integrity. This discrepancy suggests that in vivo conditions likely involve additional cellular or structural elements influencing BBB function, including interactions among endothelial cells, astrocytes, microglia, neurons, and inflammatory mediators<sup>34</sup>. Furthermore, temporal aspects must be considered, as gene expression changes may require extended periods to manifest fully as measurable functional outcomes. It should also be noted that while  $IL\text{-}1\beta$ is widely used to model inflammation-induced BBB dysfunction in vitro<sup>35,36</sup>, it represents only a subset of the pro-inflammatory stimuli active in EAE. In particular, T cells and their secreted cytokines are likely to contribute significantly to the endothelial response in vivo. Therefore, the lack of flecainide effects under IL-1 $\beta$  conditions may reflect the limited scope of the model. Moreover, the absence of glial and immune cell interactions in such monocellular systems further constrains their ability to detect complex, indirect mechanisms—such as the gliamediated BBB stabilization. This interpretation is supported by our in vivo assessments of BBB permeability using Evans Blue dye, which revealed reduced vascular leakage following flecainide treatment in the MOG-EAE model. While we acknowledge that Evans Blue provides a coarse and unspecific measure of global endothelial permeability—and does not allow conclusions regarding the precise anatomical sites of immune cell transmigration—the observed reduction in dye extravasation is consistent with a more intact vascular barrier. Importantly, this decrease in leakage correlated with diminished immune cell infiltration as shown by flow cytometry, supporting the notion of overall improved barrier function. These findings underline the complexity of BBB regulation in vivo and emphasize the necessity of physiologically integrated models when evaluating therapeutic interventions in neuroinflammation. No significant differences were observed in myelination and neuronal survival analyzed histologically across the treatment groups. While there were trends towards benefits from flecainide treatment, this aspect of our findings warrants further investigation.

In previous studies, significant efforts have been made to understanding the mechanisms underlying the beneficial effects of sodium channel blockers in neuroinflammatory conditions. Bechtold et al. <sup>10</sup> initially proposed a critical relationship between the extent of neuroinflammation and subsequent axonal degeneration, suggesting that inflammatory mediators may induce an intra-axonal accumulation of sodium and calcium ions, thereby triggering axonal injury. This hypothesis provided an important conceptual foundation for the exploration of sodium channel blockers as therapeutic agents aimed at mitigating neurodegeneration. Furthermore, Craner et al. <sup>12</sup> elaborated on this idea by emphasizing the significant role played by activated microglia and macrophages in neuroinflammatory processes. Their work suggested that sodium influx via voltage-gated sodium channels could facilitate increased intracellular calcium concentrations within microglia, consequently enhancing their inflammatory responses and exacerbating neuronal injury. Building upon these insights, the research by Morsali et al. <sup>13</sup> demonstrated that safinamide and flecainide, offer substantial neuroprotective benefits through their dual actions on reducing microglial activation and protecting axonal integrity. Although the precise molecular mechanisms underlying these protective effects remain incompletely characterized, their findings clearly show the potential clinical value of sodium channel blockade in preserving white matter integrity in neuroinflammatory contexts.

Our present findings expand on these earlier insights, providing compelling evidence that sodium channel blockers may also exert significant therapeutic effects through the modulation of BBB integrity. We suggest that BBB stabilization represents an important additional pathway, complementing the known axonal and immunomodulatory mechanisms. Our data strongly support the idea that the beneficial effects observed with

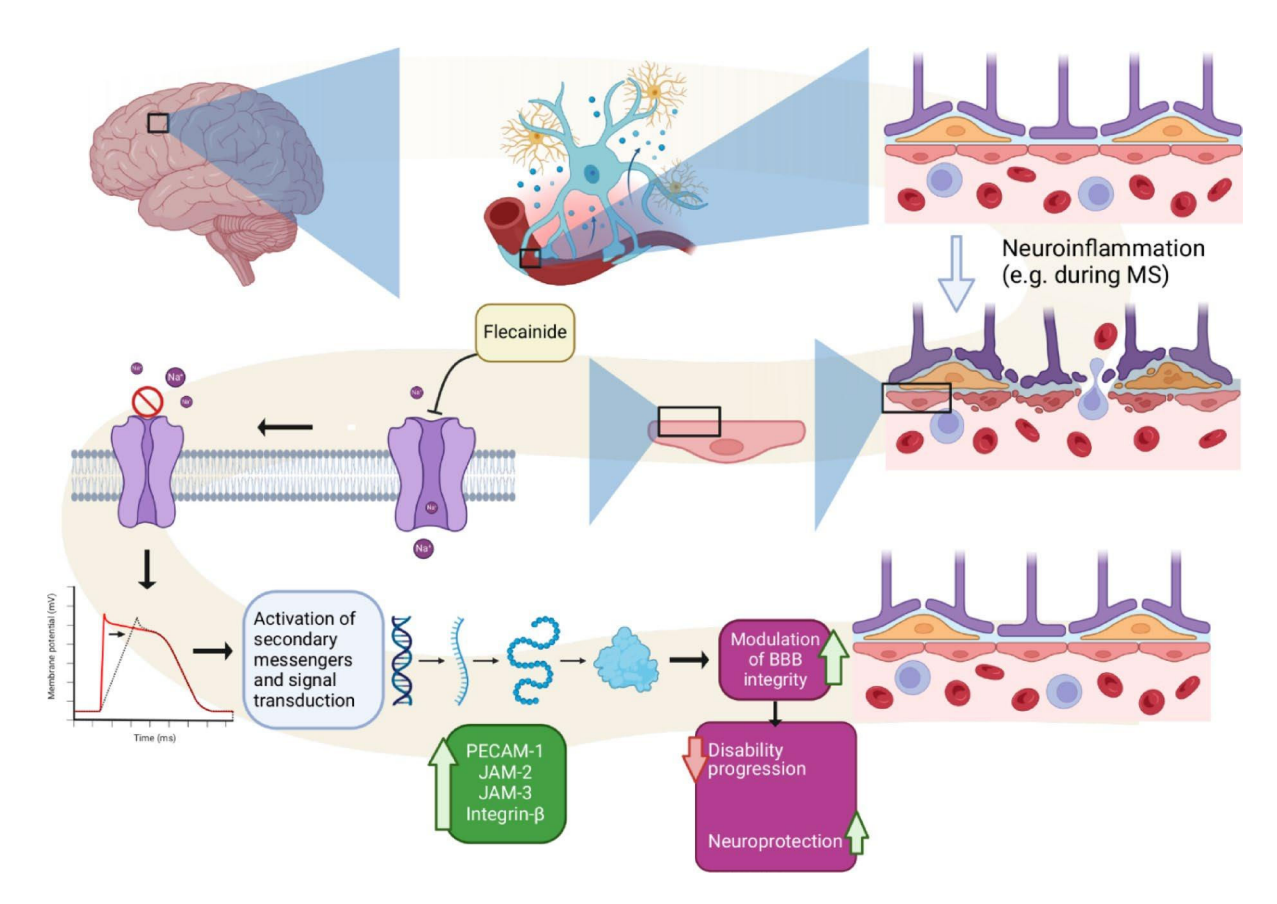


**Fig. 12.** Proposed mechanism of action of flecainide under neuroinflammatory conditions: Flecainide, a Class Ic antiarrhythmic agent, confers neuroprotection in the context of neuroinflammation by selectively inhibiting endothelial NaV 1.5. This targeted blockade leads to upregulation of junctional and adhesion molecules, thereby enhancing BBB integrity. As a result, immune cell infiltration into the central nervous system is reduced, attenuating neuroinflammation and contributing to improved functional outcomes.

flecainide and, to a lesser extent, safinamide, in EAE models can be attributed, at least in part, to their influence on BBB integrity. Thus, sodium channel blockers emerge as particularly attractive therapeutic candidates due to their multifaceted mode of action, encompassing not only direct neuronal and immunological effects but also the novel, substantial modulation of the BBB. This integrated mechanistic view reinforces the potential of sodium channel blockers as promising therapeutic strategies in the clinical management of neuroinflammatory disorders.

Flecainide, phenytoin, and safinamide each demonstrate considerable therapeutic potential in the context of neuroinflammatory conditions, by effectively mitigating disease progression and exerting neuroprotective effects by modulating immune responses in the CNS through maintaining the integrity of the BBB, as summarized in Fig. 12. Previous investigations suggest that the neuroprotective properties of these sodium channel blockers may involve mechanisms such as enhanced antioxidant defenses, decreased microglial superoxide production, and elevated glutathione levels, although the complete molecular pathways responsible for these effects are not clarified<sup>13</sup>.

To investigate the cellular target of flecainide, we performed a qPCR-based screen for various isoforms of NaVs in splenocytes. In line with previous reports  $^{37}$ , none of the analyzed isoforms were detectably expressed in these immune cells, suggesting a lack of functionally relevant sodium channel activity. Consistent with this molecular profile, flecainide treatment did not alter splenocyte proliferation, activation status, or adhesion molecule expression, arguing against a direct immunomodulatory effect on peripheral immune cells via NaV1.5. In contrast, robust expression of NaV1.5, NaV1.6, and NaV1.9 was observed in pMBMECs. Given the pivotal role of brain endothelial cells in maintaining BBB integrity, these data support the hypothesis that flecainide exerts its effects primarily through modulation of endothelial function. This interpretation is further supported by Western blot analyses demonstrating elevated protein levels of several adhesion- and junction-associated molecules—specifically integrin- $\beta$ -3, JAM-2, and JAM-3—following flecainide treatment. Recent studies highlight a central role of glial cells in regulating BBB function during neuroinflammation  $^{38,39}$ . Performed GFAP staining of optic nerve tissue of EAE mice revealed no differences between flecainide- and vehicle-treated animals, indicating no effect on astrocytic activation. In contrast, Iba1 staining showed reduced microglial activation in the flecainide group, which likely reflects an indirect consequence of diminished immune cell infiltration into the CNS rather than direct modulation of microglia. Taken together, these findings support the conclusion that pMBMECs,

rather than immune or glial cells, represent the primary target of flecainide, mediating its neuroprotective effects by stabilizing the BBB and limiting CNS inflammation.

Our findings highlight flecainide, a potent sodium channel 1.5 blocker, as particularly promising due to its pronounced modulatory effects on BBB integrity, in addition to its known effects on axonal protection and immune cell regulation. Collectively, these multi-dimensional therapeutic actions position NaV blockers as attractive candidates for a comprehensive treatment strategy in neuroinflammatory conditions. This multifaceted therapeutic profile not only aligns with and extends existing conceptual frameworks but also broadens the therapeutic scope by addressing multiple pathological targets simultaneously. Therefore, further research is essential to clarify detailed mechanistic pathways, optimize treatment strategies, and fully leverage the therapeutic potential of NaV blockers in the clinical management of neuroinflammatory disorders.

#### Data availability

All data from this study can be made available upon request to qualified researchers by contacting Mustafa Sindi at must.sindi@gmail.com.

Received: 30 October 2024; Accepted: 7 August 2025

Published online: 23 August 2025

#### References

- 1. Reich, D. S., Lucchinetti, C. F. & Calabresi, P. A. Multiple sclerosis. N. Engl. J. Med. 378, 169-180 (2018).
- 2. Fischer, M. T. et al. NADPH oxidase expression in active multiple sclerosis lesions in relation to oxidative tissue damage and mitochondrial injury. Brain 135, 886-899 (2012).
- 3. International Multiple Sclerosis Genetics Consortium & MultipleMS Consortium. Locus for severity implicates CNS resilience in progression of multiple sclerosis. Nature https://doi.org/10.1038/s41586-023-06250-x (2023).
- 4. Friese, M. A. et al. Acid-sensing ion channel-1 contributes to axonal degeneration in autoimmune inflammation of the central nervous system. Nat. Med. 13, 1483-1489 (2007).
- 5. Hansen, C. E. et al. Inflammation-induced TRPV4 channels exacerbate blood-brain barrier dysfunction in multiple sclerosis. J. Neuroinflamm. 21, 72 (2024).
- 6. Birkner, K. et al. β1-Integrin- and KV1.3 channel-dependent signaling stimulates glutamate release from Th17 cells. J. Clin. Invest. 130, 715-732 (2020).
- $7. \ \ Dietrich, M.\ et\ al.\ Protective\ effects\ of\ 4-aminopyridine\ in\ experimental\ optic\ neuritis\ and\ multiple\ sclerosis.\ \textit{Brain}\ 143,\ 1127-1142$ (2020).
- 8. Naoi, M., Maruyama, W. & Shamoto-Nagai, M. Rasagiline and selegiline modulate mitochondrial homeostasis, intervene apoptosis system and mitigate α-synuclein cytotoxicity in disease-modifying therapy for Parkinson's disease. J. Neural Transm. (Vienna) 127, 131-147 (2020)
- 9. Naoi, M., Maruyama, W. & Shamoto-Nagai, M. Neuroprotective function of rasagiline and selegiline, inhibitors of Type B monoamine oxidase, and role of monoamine oxidases in synucleinopathies. Int. J. Mol. Sci. 23, 11059 (2022)
- Bechtold, D. A., Kapoor, R. & Smith, K. J. Axonal protection using flecainide in experimental autoimmune encephalomyelitis. Ann. Neurol. 55, 607-616 (2004).
- 11. Hashiba, N. et al. Phenytoin at optimum doses ameliorates experimental autoimmune encephalomyelitis via modulation of immunoregulatory cells. J. Neuroimmunol. 233, 112-119 (2011).
- 12. Craner, M. J. et al. Sodium channels contribute to microglia/macrophage activation and function in EAE and MS. Glia 49, 220–229 (2005)
- 13. Morsali, D. et al. Safinamide and flecainide protect axons and reduce microglial activation in models of multiple sclerosis. Brain **136**, 1067–1082 (2013). 14. Okano, M., Takahata, K., Sugimoto, J. & Muraoka, S. Selegiline recovers synaptic plasticity in the medial prefrontal cortex and
- improves corresponding depression-like behavior in a mouse model of Parkinson's disease. Front. Behav. Neurosci. 13, 176 (2019).

  15. Thébault, J. J., Guillaume, M. & Levy, R. Tolerability, safety, pharmacodynamics, and pharmacokinetics of rasagiline: A potent,
- selective, and irreversible monoamine oxidase type B inhibitor. Pharmacotherapy 24, 1295-1305 (2004).
- 16. Morari, M. et al. Safinamide differentially modulates in vivo glutamate and GABA release in the rat hippocampus and Basal Ganglia. *J. Pharmacol. Exp. Ther.* **364**, 198–206 (2018).

  17. Hwang, H. S., Baldo, M. P., Rodriguez, J. P., Faggioni, M. & Knollmann, B. C. Efficacy of flecainide in catecholaminergic
- polymorphic ventricular tachycardia is mutation-independent but reduced by calcium overload. Front. Physiol. 10, 992 (2019).
- 18. Kryshtal, D. O. et al. RyR2 inhibition by flecainide determines antiarrhythmic activity in CPVT. Biophys. J. 118, 567a (2020).
- 19. Dietrich, M. et al. Whole-body positional manipulators for ocular imaging of anaesthetised mice and rats: a do-it-yourself guide. BMJ Open Ophthalmol. 1, e000008 (2017).
- 20. Dietrich, M. et al. Increased remyelination and proregenerative microglia under siponimod therapy in mechanistic models. Neurol. Neuroimmunol. Neuroinflamm. 9, e1161 (2022).
- 21. Hecker, C., Dietrich, M., Issberner, A., Hartung, H.-P. & Albrecht, P. Comparison of different optomotor response readouts for visual testing in experimental autoimmune encephalomyelitis-optic neuritis. J. Neuroinflamm. 17, 216 (2020).
- 22. Coisne, C. et al. Mouse syngenic in vitro blood-brain barrier model: A new tool to examine inflammatory events in cerebral endothelium. Lab. Invest. 85, 734-746 (2005).
- Liu, S., Zwinger, P., Black, J. A. & Waxman, S. G. Tapered withdrawal of phenytoin removes protective effect in EAE without inflammatory rebound and mortality. *J. Neurol. Sci.* **341**, 8–12 (2014).
- Bazzoni, G. The JAM family of junctional adhesion molecules. Curr. Opin. Cell Biol. 15, 525-530 (2003).
- Luo, B.-H., Carman, C. V. & Springer, T. A. Structural basis of integrin regulation and signaling. Annu. Rev. Immunol. 25, 619-647
- 26. Ohtsuki, S. & Terasaki, T. Contribution of carrier-mediated transport systems to the blood-brain barrier as a supporting and protecting interface for the brain; importance for CNS drug discovery and development. Pharm. Res. 24, 1745–1758 (2007)
- Abadier, M. et al. Cell surface levels of endothelial ICAM-1 influence the transcellular or paracellular T-cell diapedesis across the blood-brain barrier, Eur. I. Immunol. 45, 1043-1058 (2015).
- 28. Kapoor, R. et al. Lamotrigine for neuroprotection in secondary progressive multiple sclerosis: A randomised, double-blind, placebo-controlled, parallel-group trial. Lancet Neurol. 9, 681-688 (2010).
- Raftopoulos, R. et al. Phenytoin for neuroprotection in patients with acute optic neuritis: A randomised, placebo-controlled, phase 2 trial. Lancet Neurol. 15, 259-269 (2016).
- Vasylyev, D. V., Liu, C.-J. & Waxman, S. G. Sodium channels in non-excitable cells: Powerful actions and therapeutic targets beyond Hodgkin and Huxley. Trends Cell Biol. https://doi.org/10.1016/j.tcb.2024.11.009 (2024).

- 31. Black, J. A., Liu, S., Hains, B. C., Saab, C. Y. & Waxman, S. G. Long-term protection of central axons with phenytoin in monophasic and chronic-relapsing EAE. *Brain* 129, 3196–3208 (2006).
- 32. Albrecht, P. et al. Retinal neurodegeneration in Wilson's disease revealed by spectral domain optical coherence tomography. *PLoS ONE* 7, e49825 (2012).
- 33. Dietrich, M. et al. Early alpha-lipoic acid therapy protects from degeneration of the inner retinal layers and vision loss in an experimental autoimmune encephalomyelitis-optic neuritis model. *J. Neuroinflamm.* 15, 71 (2018).
- 34. Abbott, N. J., Rönnbäck, L. & Hansson, E. Astrocyte-endothelial interactions at the blood-brain barrier. *Nat. Rev. Neurosci.* 7, 41–53 (2006).
- 35. Fetsko, A. R., Sebo, D. J., Budzynski, L. B., Scharbarth, A. & Taylor, M. R. IL-1β disrupts the initiation of blood-brain barrier development by inhibiting endothelial Wnt/β-catenin signaling. iScience 27, 109651 (2024).
- 36. Saltarin, F. et al. Compromised blood-brain barrier junctions enhance melanoma cell intercalation and extravasation. *Cancers* 15, 5071 (2023).
- 37. DeCoursey, T. E., Chandy, K. G., Gupta, S. & Cahalan, M. D. Voltage-dependent ion channels in T-lymphocytes. *J. Neuroimmunol.* 10, 71–95 (1985).
- 38. Alvarez, J. I., Katayama, T. & Prat, A. Glial influence on the blood brain barrier. Glia 61, 1939-1958 (2013).
- 39. Burkhart, A. et al. Activation of glial cells induces proinflammatory properties in brain capillary endothelial cells in vitro. Sci. Rep. 14, 26580 (2024).

#### **Acknowledgements**

This project was funded by the "Forschungskommission" of the Heinrich-Heine University Düsseldorf. Graphic 12 was created by tools of biorender.com.

#### **Author contributions**

MS, MD, CH, AI, TM, RR, DK, PD, HW, LT, SL, GDK and VD performed the experiments and/or analyzed the data; MS, MD and PA wrote the manuscript; MS, CH, AI, TM, RR, DK, PD, JG, TK, HW, LT, SL, VD, SGM, TR, HPH, PK, PA, HS, RL, BE, CB, GDK and MD were involved in revising the manuscript critically for important intellectual content and made substantial contributions to interpretation of data. PA and MD conceived the study and supervised experiments. All authors read and approved the final manuscript.

#### Funding

Open Access funding enabled and organized by Projekt DEAL. This work was supported by grants from the "Research commission of the medical faculty of the Heinrich-Heine-University Düsseldorf" (Forschungskommission der Medizinischen Fakultät der Heinrich-Heine-Universität Düsseldorf) to Michael Dietrich.

#### **Declarations**

#### **Competing interests**

The work was funded by a research grant from the Forschungskommission of the Heinrich-Heine-University Düsseldorf to Michael Dietrich. Mustafa Sindi is funded by a DFG grant to Philipp Albrecht, number AL 1769/6-1. Apart from this, the authors declare that they have no additional conflict of interest related to the work presented. The following financial disclosures are unrelated to the work: SGM received honoraria for lecturing and travel expenses for 34 attending meetings from Almirall, Amicus Therapeutics Germany, Bayer Health Care, Biogen, Celgene, Diamed, Genzyme, MedDay Pharmaceuticals, Merck Serono, Novartis, Novo Nordisk, ONO Pharma, Roche, Sanofi-Aventis, Chugai Pharma, QuintilesIMS, and Teva. His research is funded by the German Ministry for Education and Research (BMBF), Deutsche Forschungsgemeinschaft (DFG), Else Kröner Fresenius Foundation, German Academic Exchange Service, Hertie Foundation, Interdisciplinary Center for Clinical Studies (IZKF) Muenster, German Foundation Neurology, and by Almirall, Amicus Therapeutics Germany, Biogen, Diamed, Fresenius Medical Care, Genzyme, Merck Serono, Novartis, ONO Pharma, Roche, and Teva. MD received speaker honoraria from Merck and Novartis. PA received compensation for serving on Scientific Advisory Boards for Ipsen, Novartis, Biogen; he received speaker honoraria and travel support from Novartis, Teva, Biogen, Merz Pharmaceuticals, Ipsen, Allergan, Bayer Healthcare, Esai, UCB and Glaxo Smith Kline; he received research support from Novartis, Biogen, Teva, Merz Pharmaceuticals, Ipsen, Bristol-Myers Squibb and Roche. The other authors report no disclosures. TR reports grants from German Ministry of Education, Science, Research and Technology, during the conduct of the study; grants and personal fees from Sanofi-Genzyme; personal fees from Biogen; personal fees and nonfinancial support from Merck Serono; personal fees from Roche, Teva, Alexion, Argenx, UCB, and BMS outside the submitted work. Author Philipp Albrecht is employed by Maria Hilf Clinics GmbH, Mönchengladbach. The remaining authors declare that the research was conducted in the absence of any commercial or financial relationships that could be construed as a potential conflict of interest.

#### **Ethical approval**

All animal experiments in this study were conducted in strict compliance with the ethical guidelines and regulations of the State Office for Nature, Environment and Consumer Protection of North Rhine-Westphalia, Germany "Landesamt für Natur, Umwelt und Verbraucherschutz Nordrhein-Westfalen, Deutschland". The study protocol was reviewed and approved under the approval number Az. 81-02.04.2019.A063. We confirm that all experiments were performed in accordance with relevant guidelines and regulations and are reported following the ARRIVE guidelines (PLoS Biol 8(6), e1000412, 2010). The mice used in this study, as described in "Animals, animal models, treatment" section of this manuscript, included C57BL/6J mice obtained from Janvier Labs and NOD/ShiLtJ mice bred in the animal facility at the University of Düsseldorf (ZETT). Both strains had ad libitum access to chow and drinking water, and measures were taken to minimize suffering.

Anesthesia and euthanasia were administered in accordance with AVMA guidelines to ensure humane treatment. Statistical analyses appropriate for each outcome were conducted to assess the results. No client-owned animals were involved in this study; therefore, informed consent from owners was not required.

#### Additional information

Supplementary Information The online version contains supplementary material available at https://doi.org/1 0.1038/s41598-025-15430-w.

Correspondence and requests for materials should be addressed to P.A.

Reprints and permissions information is available at www.nature.com/reprints.

**Publisher's note** Springer Nature remains neutral with regard to jurisdictional claims in published maps and institutional affiliations.

**Open Access** This article is licensed under a Creative Commons Attribution 4.0 International License, which permits use, sharing, adaptation, distribution and reproduction in any medium or format, as long as you give appropriate credit to the original author(s) and the source, provide a link to the Creative Commons licence, and indicate if changes were made. The images or other third party material in this article are included in the article's Creative Commons licence, unless indicated otherwise in a credit line to the material. If material is not included in the article's Creative Commons licence and your intended use is not permitted by statutory regulation or exceeds the permitted use, you will need to obtain permission directly from the copyright holder. To view a copy of this licence, visit <a href="https://creativecommons.org/licenses/by/4.0/">https://creativecommons.org/licenses/by/4.0/</a>.

© The Author(s) 2025

#### 3. Discussion

# 3.1. Longitudinal, translational in-vivo readouts of the visual system and models of choice

The studies demonstrated that longitudinal in vivo measurements using OCT, cSLO, and OMR correlated well with clinical, histological, immunological and molecular evaluations. These findings align with results from other researchers, reinforcing the validity of these methods (Alnawaiseh et al., 2016; Bliss O'Bryhim, 2023; Dietrich et al., 2019; Galetta et al., 2011; Gatto et al., 2018; Hecker et al., 2020; Rojas et al., 2019; Sotirchos & Saidha, 2018). Therefore, the mentioned techniques are well-established for investigating neuroprotective strategies in experimental MS models. Their ability to provide consistent, reliable data makes them invaluable tools in the preclinical assessment of disease progression and therapeutic efficacy.

Although these methods cover structural (OCT), cellular (cSLO), and functional (OMR) evaluations, incorporating a translational functional methodology such as visual evoked potentials (VEP) would provide a valuable addition. We initially decided against this due to its high invasiveness. However, recent studies have shown that non-invasive and semi-invasive VEP measurements yield promising results (Marenna et al., 2019). This suggests that these modified VEP techniques could be considered in future studies to enhance the comprehensive evaluation of neuroprotective strategies through visual system readouts.

MS encompasses numerous aspects, which must be studied depending on the specific research question. For investigating neuroinflammation, we selected the C57BL/6 (BL6) model with MOG35-55 peptide immunization and the NOD model with the same peptide to represent primary progressive and relapsing-remitting forms of MS, respectively. These models accurately represent the neuroinflammatory component of the disease but have limitations. Unlike MS, where both B and T cells are involved, EAE is primarily driven by T cells with less B cell involvement (Glatigny & Bettelli, 2018). Moreover, EAE presents more inflammatory plaques in the spinal cord and fewer in the brain, unlike MS, making brain pathology analysis challenging (Constantinescu et al., 2011). Thus, analyzing the visual system is advantageous as it mirrors inflammation seen in both the retina and optic nerve, acting as a miniature representation of the brain and spinal cord.

#### 3.2. A multifaceted disease requires multifaceted therapeutically strategies

Recent state-of-the-art MS treatments primarily target the immune system, either through modulation or depletion (Du Pasquier et al., 2014). However, studies have shown that MS-related disease progression can occur independently of MS relapse activity (PIRA), particularly in chronic phases (Sharrad et al., 2023). Additionally, immunomodulatory treatments are often ineffective in reversing damage to already destroyed tissue, which contributes to disability. Consequently, there is a significant demand for therapies that not only offer immunomodulation and reduction of the relapse rates, but also promote neuroprotection, remyelination and regeneration for patients with MS. This underscores the necessity for innovative therapeutic approaches to address these unmet clinical needs.

The primary substance classes utilized in our studies include selective agonists of the S1P1 and S1P5 receptors, AMPA-positive allosteric modulators (AMPA-PAM), MAO-B inhibitors, and sodium channel (Nav) blockers. The targeted action of these compounds offers potential benefits in modulating neuroinflammation, enhancing neuronal survival, and protecting against neurodegenerative processes, aligning with our research aim objective.

Selective agonists of the S1P1 and S1P5 receptors function by binding to the S1P receptors on lymphocytes, causing their internalization and degradation. This process sequesters lymphocytes in lymph nodes, reducing their exit and subsequent infiltration into the CNS, thereby decreasing neuroinflammation and protecting myelin (McGinley & Cohen, 2021). On a cellular level, this reduces the overall immune attack on CNS tissues, preserving myelin integrity and preventing further neuronal damage. Our study, published in Frontiers in Immunology (Sindi et al., 2023), assessed the protective capacity of the S1PR-1/-5 modulator RP-101074 in a photoreceptor degeneration model induced by light overstimulation. Standardized conditions were maintained for all mice during treatment. Key findings revealed that an intermediate dose (1 mg/kg BW) of RP-101074 provided more pronounced protection against visual function loss compared to a higher dose (5 mg/kg BW), aligning with previous studies on similar modulators (Dietrich et al., 2022; Messias et al., 2016). This bell-shaped dose-response curve suggests that higher doses may lead to more receptor internalization and degradation, affecting immune responses and other cellular functions (Subei & Cohen, 2015).

RP-101074 showed significant protection from retinal degeneration, particularly in the inner retinal layers, suggesting it may protect both photoreceptors and ganglion cells. Increased Sox2-

positive neural stem cells indicate potential recruitment of neural progenitors and modulation of inflammatory responses. Histological analyses showed increased myelination and progenitor cell numbers with RP-101074, suggesting a regenerative effect. The study concluded that RP-101074's protective effects might extend beyond immunomodulation to include neural protection.

AMPA-positive allosteric modulators (AMPA-PAMs) enhance synaptic transmission by binding to AMPA receptors on neuronal membranes. This binding increases the receptors' response to glutamate (Bretin et al., 2017). This modulation supports the formation and maintenance of synaptic connections, critical for cognitive and motor function (Fannon et al., 2015; K. Lee et al., 2016; Partin, 2015). Within our work, submitted to Frontiers in Immunology, we found that PF4778574, an AMPA-PAM, mitigated clinical disability and reduced demyelination, suggesting its neuroprotective effects extend beyond neurotransmission (Destot-Wong et al., 2009). However, PF4778574 did not affect microglial activity, indicating it has limited anti-inflammatory effects compared to AMPA antagonists (Bonnet et al., 2015). The lower dose of PF4778574 proved more effective, possibly due to a hormesis response, where higher doses may lead to excitotoxicity (Calabrese, 2008). The lack of additive benefits with fingolimod could be due to drug interactions involving cytochrome P450 metabolism. These findings highlight PF4778574's potential in reducing excitotoxicity and demyelination in MS.

MAO-B inhibitors prevent the enzymatic breakdown of dopamine by inhibiting monoamine oxidase B. This action reduces oxidative stress by decreasing the production of reactive oxygen species associated with dopamine metabolism. The preservation of dopamine levels and reduction of oxidative stress protect dopaminergic neurons from degeneration, crucial for maintaining motor control and cognitive function (Nagatsu & Sawada, 2006; Y.-Y. Tan et al., 2022). Sodium channel blockers inhibit the voltage-gated sodium channels on neuronal membranes. By modulating these channels, the blockers prevent excessive sodium influx, which can lead to excitotoxicity and subsequent neuronal damage. This action maintains neuronal excitability within safe limits, protecting neurons from hyperexcitability-induced damage (Li et al., 2019; Taylor & Narasimhan, 1997). Our work, submitted to Nature's Scientific Reports, investigated the therapeutic effects of MAO-B inhibition and sodium channel blocking in EAE using murine models. Flecainide, a sodium channel blocker, demonstrated superior efficacy over phenytoin in enhancing BBB integrity and reducing

lymphocyte infiltration into the CNS. The hypothesized mode of action involves enhancing BBB integrity and reducing excitability and hyperpolarizing membrane potentials.

The observed benefits primarily stem from sodium channel blocking rather than MAO-B inhibition - as Rasagiline (a MAO-B inhibitor) shows limited effects - significantly affecting disability progression, neurodegeneration, and immune cell infiltration. Previous studies (Bechtold et al., 2004; Morsali et al., 2013) support the neuroprotective role of sodium channel blockers, although, postulating a different mode of action. This study highlights the potential of flecainide in modulating the BBB, aligning with and expanding upon existing theories regarding sodium channel blockers in neuroinflammatory conditions.

#### 3.3. Future directions in the field of MS therapeutic interventions

Current research strategies for addressing remyelination, regeneration, and neuroprotection in MS involve multidisciplinary approaches. For example, in recent years, researchers have made significant progress using stem cell therapies. Specifically, mesenchymal stem cells (MSCs) have garnered attention due to their ability to differentiate into oligodendrocytes, the cells responsible for myelination in the CNS. Efforts to stimulate endogenous oligodendrocyte progenitor cells (OPCs) have also seen significant advancements. Modulating signaling pathways like Wnt, Notch, and Sonic Hedgehog (Shh) have been key. Inhibiting Wnt and Notch pathways, for example, can enhance OPC differentiation, while activating Shh signaling promotes OPC proliferation (Ferent et al., 2013; Tilborg et al., 2018; Traiffort et al., 2016). Molecules like ciliary neurotrophic factor (CNTF) and leukemia inhibitory factor (LIF) are also being explored to stimulate endogenous OPCs (Ishibashi et al., 2009).

Pharmacological agents are critical in promoting remyelination. Anti-LINGO-1 antibodies, such as BIIB033, inhibit LINGO-1, a molecule that suppresses OPC differentiation, thereby promoting remyelination, showed promising results in preclinical studies (Moradbeygi et al., 2021) but failed in recent clinical trials (Cadavid et al., 2019). Studies have shown that GSK3 $\beta$  inhibitors like lithium can activate the Wnt pathway, enhancing remyelination, while  $\gamma$ -secretase inhibitors enhance OPC differentiation by blocking the Notch pathway (Fang et al., 2016; Makoukji et al., 2012). Furthermore, recent studies have shown promising results on remyelination by inhibition of G protein-coupled receptor 17 (GPR-17) activity (Dziedzic et al., 2020; Satoh et al., 2017).

Neuroprotective strategies are equally important, focusing on reducing oxidative stress and modulating immune responses. Researchers have highlighted the benefits of antioxidants like N-acetylcysteine (NAC) (Khalatbari Mohseni et al., 2023; Wen et al., 2016), which acts as a precursor to the antioxidant glutathione, coenzyme Q10 (Khalilian et al., 2021; Moccia et al., 2019; Sanoobar et al., 2016), which supports mitochondrial function, in mitigating oxidative damage and alpha lipoic acid (Dietrich et al., 2018), which helps to protect against vision loss and degeneration of the inner retinal layers in models of optic neuritis and autoimmune encephalomyelitis.

Immunomodulatory targeting has shown the greatest development in the recent years with high efficiency agents such as Alemtuzumab, Ofatumumab, Ocrelizumab, Ublituximab and Natalizumab (Samjoo et al., 2021). Recently, bruton's tyrosine kinase (BTK) inhibitors showed very promising preclinical results (Evonuk et al., 2023; Krämer & Wiendl, 2024, 2024). In clinical trials, the BTKi tolebrutinib demonstrated a 31% delay in time to onset of SPMS (*GEMINI Trial*, 2024), but failed to meet primary endpoints (Wood, 2024).

On the regeneration front, neurotrophic factors like BDNF, NGF, and GDNF show to support neuronal survival and growth by activating receptor-mediated pathways (Gao et al., 2016; Kopec et al., 2020). Transcranial Magnetic Stimulation (TMS) has shown promise as a painless, non-invasive treatment for MS, potentially improving patient quality of life. However, more randomized controlled trials are necessary to confirm its therapeutic efficacy and safety, and to develop an optimized treatment protocol for widespread clinical use.

Gene therapy using viral vectors and CRISPR/Cas9, although controversial, is being explored and holds promise as a therapeutic approach for managing autoimmune diseases by targeting genes related to cytokines and T cell factors, potentially offering treatments for autoimmune disease such as MS. However, human studies are required to address technical challenges such as off-target activity and in vivo delivery before it can be widely applied (M. H. Lee et al., 2022).

Additionally, nutritional interventions rich in omega-3 fatty acids (AlAmmar et al., 2021; Siegert et al., 2017) and regular exercise are being investigated for their potential to support brain health and myelination (Motl et al., 2017; Wooliscroft et al., 2023).

Genetic studies, proteomics, and metabolomics continue to identify novel targets (Zhou et al., 2021). Future MS therapies should focus on combining primary immunomodulatory treatments with agents promoting neuroprotection, remyelination and regeneration, addressing both

inflammatory and neurodegenerative components of the disease. This approach is especially critical for SPMS and PPMS patients, as it could mitigate ongoing neurodegeneration, enhance recovery of lost functions, and improve overall quality of life. Continued basic and preclinical research on therapeutic strategies is essential for developing effective treatments for MS:

The future of MS therapies is likely to emphasize personalized treatment strategies, combining immunomodulators with non-immunomodulatory neuroprotective substances, tailored to the individual patient's specific disease course and condition. This personalized combinatory approach aims to address both the immune dysregulation and the neurodegenerative aspects of MS, potentially enhancing therapeutic efficacy and patient outcomes.

### 4. Other publications

#### 4.1. Publications as co-author

Gruchot, J., Lewen, I., Dietrich, M., Reiche, L., Sindi, M., Hecker, C., Herrero, F., Charvet, B., Weber-Stadlbauer, U., Hartung, H.-P., Albrecht, P., Perron, H., Meyer, U., & Küry, P. (2023). Transgenic expression of the HERV-W envelope protein leads to polarized glial cell populations and a neurodegenerative environment. Proceedings of the National Academy of Sciences of the United States of America, 120(38), Article 38.

https://doi.org/10.1073/pnas.2308187120

**Status: Published** 

**Contribution to the work:** Conducting parts of the EAE experiments.

Frenger, M. J., Hecker, C., Sindi, M., Issberner, A., Hartung, H.-P., Meuth, S. G., Dietrich, M., & Albrecht, P. (2021). Semi-Automated Live Tracking of Microglial Activation in CX3CR1GFP Mice During Experimental Autoimmune Encephalomyelitis by Confocal Scanning Laser Ophthalmoscopy. Frontiers in Immunology, 12, 761776. https://doi.org/10.3389/fimmu.2021.761776

**Status: Published** 

**Contribution to the work:** Conducting parts of the OCT / cSLO measurements. Revising the manuscript.

#### 4.2. Review articles publications as first author

Sindi, M., Oertel, F. C., Paul, F., Meuth, S. G., & Albrecht, P. (2024). Das visuelle System als Modell in der translationalen Forschung. Klinische Neurophysiologie, 55, 139–146. https://doi.org/10.1055/a-2331-0668

Status: Published

**Contribution to the work:** Writing and revising the review.

Übersicht

## Das visuelle System als Modell in der translationalen Forschung The Visual System as a Model in Translational Research

#### Autorinnen/Autoren

Mustafa Sindi<sup>1</sup>, Frederike Cosima Oertel<sup>2, 3, 4</sup>, Friedemann Paul<sup>2, 3, 4</sup>, Sven G Meuth<sup>1</sup>, Philipp Albrecht<sup>5</sup>

#### Institute

- 1 Klinik für Neurologie, Universitätsklinikum Düsseldorf, Düsseldorf, Germany
- 2 Körperschaftsmitglied der Freien Universität Berlin und der Humboldt-Universität zu Berlin, Max Delbrück Centrum für Molekulare Medizin Experimental and Clinical Research Center, Berlin, Germany
- 3 Neurologisches Klinisches Forschungszentrum, Charite Universitatsmedizin Berlin, Berlin, Germany
- 4 Abteilung für Neurologie, Charite Universitatsmedizin Berlin, Berlin, Germany
- 5 Klinik für Neurologie, Kliniken Maria Hilf GmbH, Monchengladbach, Germany

#### Schlüsselwörter

OCT, VEP, Visuelles System, Retina, Translationale Evaluierungsmethoden

#### Keywords

OCT, VEP, visual system, retina, translational evaluation methods

#### Bibliografie

Klin Neurophysiol 2024; 55: 139–146

DOI 10.1055/a-2331-0668

ISSN 1434-0275

© 2024. Thieme. All rights reserved.

Georg Thieme Verlag KG, Rüdigerstraße 14, 70469 Stuttgart, Germany

#### Korrespondenzadresse

Prof. Philipp Albrecht
Heinrich-Heine-Universitat Dusseldorf
Neurology, Moorenstr. 5
40225 Dusseldorf
Germany
phil.albrecht@gmail.com

#### ZUSAMMENFASSUNG

Das visuelle System bietet einzigartige Einblicke in die komplexen Mechanismen neurologischer Erkrankungen und stellt daher ein zentrales Modell in der translationalen Forschung dar. Die Netzhaut, als Teil des zentralen Nervensystems, dient als präzises Fenster, das es ermöglicht, neurodegenerative und neuroinflammatorische Prozesse zu untersuchen. Dieser Artikel beleuchtet die Anwendung des visuellen Systems in der translationalen Erforschung neurologischer Erkrankungen durch verschiedene experimentelle Modelle und Analysemethoden. Besonderes Augenmerk liegt auf der Untersuchung entzündlicher Modelle wie der Experimentellen Autoimmunen Enzephalomyelitis Optikusneuritis (EAEON), nicht-entzündlichen degenerativen Modellen wie dem Optic Nerve Crush und dem lichtinduzierten Photorezeptorverlust sowie demyelinisierenden Modellen wie dem Cuprizone-Modell sowie neurodegenerative Erkrankungen wie Demenz vom Alzheimer-Typ und idiopathisches Parkinson-Syndrom. Der Artikel stellt zudem diagnostische und funktionelle Evaluierungsmethoden wie die Optische Kohärenztomographie (OCT), konfokale Scanning Laser Ophthalmoskopie (cSLO), optomotorische Reaktions-Messung (OMR) und die Messung Visuell Evozierter Potentiale (VEP) vor. Abschließend werden ein kurzer Ausblick gegeben und die Limitationen, insbesondere bezüglich der Übertragbarkeit der Ergebnisse zwischen Tiermodellen und dem Menschen, erläutert.

#### **ABSTRACT**

The visual system provides unique insights into the complex mechanisms of neurological diseases, thus serving as a central model in translational research. The retina, as part of the central nervous system, acts as a precise window that enables the study of neurodegenerative and neuroinflammatory processes. This article highlights the application of the visual system in the translational research of neurological diseases through various experimental models and analytical methods. Special emphasis is placed on the examination of inflammatory models such as Experimental Autoimmune Encephalomyelitis Optic Neuritis (EAEON), non-inflammatory degenerative models like Optic Nerve Crush and light-induced photoreceptor loss, as well as demyelinating models like the Cuprizone model, in addition to neurodegenerative diseases such as Alzheimer's type dementia and idiopathic Parkinson's syndrome. The article also presents diagnostic and functional evaluation methods such as Optical Coherence Tomography (OCT), confocal Scanning Laser Ophthalmoscopy (cSLO), optomotor response (OMR) measurements, and the measurement of Visually Evoked Potentials (VEP). Furthermore, a brief outlook is provided, as well as the limitations, especially regarding the extrapolatability of results from animal models to humans and vice versa.

Die Retina, ein wichtiger Teil des Zentralnervensystems (ZNS), spielt eine zentrale Rolle in der neurologischen Forschung und klinischen Praxis. Sie bietet ein präzises diagnostisches Fenster, das tiefe Einblicke in neuronale Pathologien gewährt. Dies macht sie zu einem wichtigen Werkzeug in der Prognose und Diagnose von neurologischen Erkrankungen. Ihre Rolle bei der Identifizierung von Biomarkern ist entscheidend für die Früherkennung und das Monitoring des Krankheitsverlaufs sowie für die Bewertung der therapeutischen Effizienz. Die gute Konservierung retinaler Strukturen (> Abb. 1) im Laufe der Evolution ermöglicht die translationale Validierung präklinischer Befunde in klinische Realität und vice versa, was ihre Relevanz in der Neurologie unterstreicht.

Dieser Artikel beleuchtet die Rolle des visuellen Systems als ein wichtiges Paradigma in der translationalen Forschung, mit einem besonderen Fokus auf experimentelle Modelle, Analysemethoden und deren Implikationen für die Evaluierung neurologischer Zustände.

## Experimentelle Modelle neurologischer Zustände

#### **Entzündliches Modell**

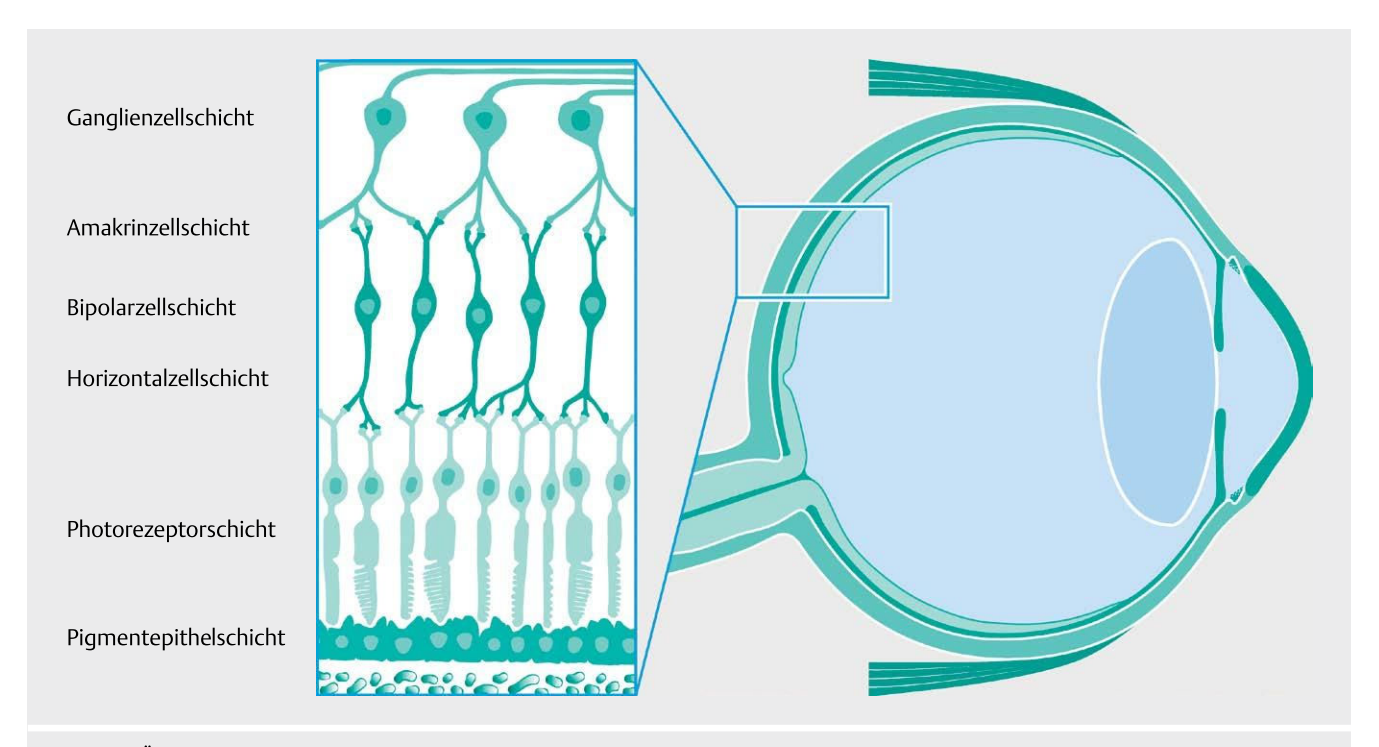
Bei der Experimentellen Autoimmunen Enzephalomyelitis Optikusneuritis (EAEON) handelt es sich um eine induzierbare, entzündliche demyelinisierende Erkrankung des ZNS [1]. Es wird hauptsächlich bei Nagetieren eingesetzt und ist als Tiermodell der menschlichen demyelinisierenden Erkrankungen des ZNS, einschließlich Multipler Sklerose weit verbreitet. Die EAEON kann in C57BI/6]

Mäusen mittels Injektion des Myelin-Oligodendrozyten-Glykoprotein (MOG) [2] bzw. dessen Peptid mit den Aminosäuren 35–55, oder mit dem Protein Myelin-Proteolipid-Protein (PLP) bzw. dessen Peptid 139–151 [3], induziert werden. Ebenso ist die Nachbildung eines chronisch, progredienten Verlaufs von großer klinischer Relevanz, da sie die Pathologie von Patienten mit primär progredienter Multipler Sklerose (PPMS) präziser als das C57Bl/6 J EAEON Modell abbildet. Dieser kann beispielsweise durch die Immunisierung mittels MOG35–55 in NOD/ShiLtJ Mäusen simuliert werden [4, 5].

#### Nicht-entzündliche, degenerative Modelle

#### Optic Nerve Crush

In den Modellen der EAE lässt sich auch bei der therapeutischen Gabe nicht mit letzter Sicherheit unterscheiden, ob beobachtete positive Effekte einer Substanz tatsächlich über neuroprotektive Mechanismen oder auch durch eine immunmodulatorische Wirkung zustande kommen. Da jedoch Substanzen mit neuroprotektiver Wirkung nicht nur für die Behandlung der Neuroinflammation von größtem Interesse sind, ist es wichtig, die neuroprotektiven Effekte auch in nicht inflammatorischen Modellen axonalen Schadens und neuronaler Degeneration zu untersuchen. Ein weit verbreitetes, gut etabliertes und für diesen Zweck bestens geeignetes Modell ist der optic nerve (ON)-crush. Bei diesem Modell wird zumeist in Mäusen oder Ratten der Sehnerv ca. 1 mm hinter dem Bulbus für 3 Sekunden mit einer Pinzette "gequetscht". Diese Prozedur führt innerhalb von 1 Woche zu einer Degeneration von ca. 80% der retinalen Ganglienzellen, was sich mittels optische Kohärenztomographie (OCT) oder histologisch, nachweisen lässt [6-8].



▶ **Abb. 1** Übersicht des menschlichen Auges mit Detailansicht der Netzhautschichten. Links: Gesamter Querschnitt des Auges, mit Hauptstrukturen und Sehnerv. Rechts: Vergrößerter Ausschnitt der Netzhaut, der von außen nach innen die Pigmentepithelschicht, Photorezeptorschicht, Horizontalzellschicht, Bipolarzellschicht, Amakrinzellschicht und Ganglienzellschicht inkl. Nervenfaserschicht zeigt.

#### Neurodegeneration bei Überaktivierung

Ebenso wie der oben genannte ON-crush eignet sich der sog. "lichtinduzierte-Phtorezeptorverlust" (Li-PRL) zur Herbeiführung eines nicht-inflammatorischen Schadens in der Retina [6]. Dabei werden die Augen mit einer starken Lichtquelle bestimmten Typs, Dauer und Abstand bestrahlt. Die Bestrahlung führt zu einer Schädigung der Nervenzellen in der Retina durch die Überaktivierung der Photorezeptoren [9].

#### **Demyelinisierendes Modell**

#### Cuprizone Modell

Die Remyelinisierungskapazität nimmt im verletzten und kranken ZNS mit fortschreitender Erkrankung und auch im alternden Nervensystem ab, da Vorläufer- und Stammzellen oft nicht mehr in der Lage sind, neue Oligodendrozyten zu generieren. Die zugrundeliegenden Ursachen für die mangelnde Bereitstellung einer langfristigen Myelinreparatur und einer funktionellen Wiederherstellung sind noch nicht hinreichend geklärt. Das Cuprizone-Mausmodell ist ein sehr zuverlässiges und reproduzierbares Demyelinisierungs-Modell [10, 11]. Dabei werden Mäuse mit 0,2 % Cuprizon (Bis-Cyclohexanonoxaldihydrazon)-haltigen Pellets gefüttert, um eine vollständige Demyelinisierung innerhalb von 5 Wochen zu induzieren. Dieses Modell ermöglicht es, die Reparatur nach Demyelinisierung zu untersuchen, da nach der Umstellung auf eine normale Ernährung nach der Cuprizon-Behandlung ein natürlicher, endogener und regenerativer Mechanismus bei diesen Mäusen erfolgt.

#### Primär neurodegenerative Erkrankungen

Mehrere Arbeiten der vergangenen Jahre konnten bereits die Relevanz der OCT und OCT-Angiographie (OCTA) Methoden bei der Untersuchung neurodegenerativer Veränderungen, die mit Alzheimer [12, 13], Parkinson [14, 15], amyotropher Lateralsklerose (ALS) [16, 17] und Huntington-Krankheit [18, 19] assoziiert sind, aufzeigen. Die Unterscheidung zwischen den OCT- und OCTA-Befunden bietet einen umfassenden Einblick in die neuroophthalmologischen Manifestationen dieser Krankheiten und betont den diagnostischen sowie Monitoring Nutzen dieser Methoden. Diese Ergebnisse, die eine Schrumpfung retinaler Schichten in Alzheimer- und Parkinson-Modellen zeigen, sowie die mikrovaskulären Veränderungen, die durch OCTA evaluiert wurden [20], bieten wertvolle Informationen über die zugrundeliegenden neurodegenerativen Prozesse, die möglicherweise eine verbesserte Diagnose, Prognose und Überwachung dieser Krankheiten ermöglichen.

#### Parkinson Modell

Bei Patienten mit idiopathischem Parkinson-Syndrom konnten retinale Veränderungen sowohl im OCT, wie auch histologisch nachgewiesen werden [21, 22]. Präklinische Studien wurden überwiegend am toxischen 1-Methyl-4-phenyl-1,2,3,6-tetrahydropyridin (MPTP)-Modell durchgeführt. Das MPTP-Mausmodell wird für die präklinische Untersuchung der Parkinson-Krankheit verwendet. Es wendet die intraperitoneale Injektion des Neurotoxins MPTP an, um selektiv dopaminerge Neuronen zu schädigen. Durch diese Methode wird die Degeneration dopaminerger Neurone im ZNS induziert, was eine eine detaillierte Untersuchung der Auswirkungen auf die Retina ermöglicht, einschließlich Verzögerungen in oszillatorischen Potentialen und Veränderungen in der Struktur der äu-

ßeren plexiformen Schicht. Diese Veränderungen deuten auf eine Beeinträchtigung der dopaminergen Amakrinzellen hin, ein Befund, der durch die Anwendung von L-DOPA und die daraus resultierende Milderung der funktionellen Defizite weiter untermauert wird. Die umfassende Analyse, die elektroretinographische Aufzeichnungen, OCT und Tyrosinhydroxylase-Immunhistochemie (TH-IHC) kombiniert, liefert ein tiefgehendes Verständnis der spezifischen retinalen Auswirkungen bei diesem Modell, indem sie unterschiedliche Aspekte der retinalen Funktion und Struktur erfasst, was letztendlich mit dem Zustand des restlichen ZNS in Korrelation gebracht werden kann: Elektroretinographie ermöglicht die Beurteilung der elektrischen Reaktionen der Retina auf Lichtstimuli, OCT liefert präzise Bilder von der retinalen Schichtdicke und Morphologie, und TH-IHC hilft, die Verteilung und Dichte dopaminerger Neurone zu identifizieren und zu quantifizieren. Dieses Modell ist daher von großem Wert für die Entwicklung spezifischer therapeutischer Ansätze, und bietet wichtige Einblicke in die potenziellen therapeutischen Strategien, die diese spezifischen pathologischen Veränderungen adressieren könnten [23].

#### Alzheimer Modell

Im APP/PS1-Mausmodell, das zur Untersuchung von Alzheimerspezifischen neuropathologischen Veränderungen eingesetzt wird, ermöglicht die transgene Expression von Mutationen im Amyloid-Precursor Protein (APP) und Presenilin-1 (PS1) die Induktion von Alzheimer-ähnlichen Zuständen, einschließlich der Bildung von Amyloid-β-Plaques [24]. Die Untersuchung der Retina mittels OCT und OCTA bietet eine detaillierte Einsicht in strukturelle und vaskuläre Veränderungen, die auf Neurodegeneration hinweisen könnten. Diese Erkenntnisse demonstrieren, wie retinale Veränderungen als Biomarker für zerebrale neurodegenerative Prozesse dienen könnten [24].

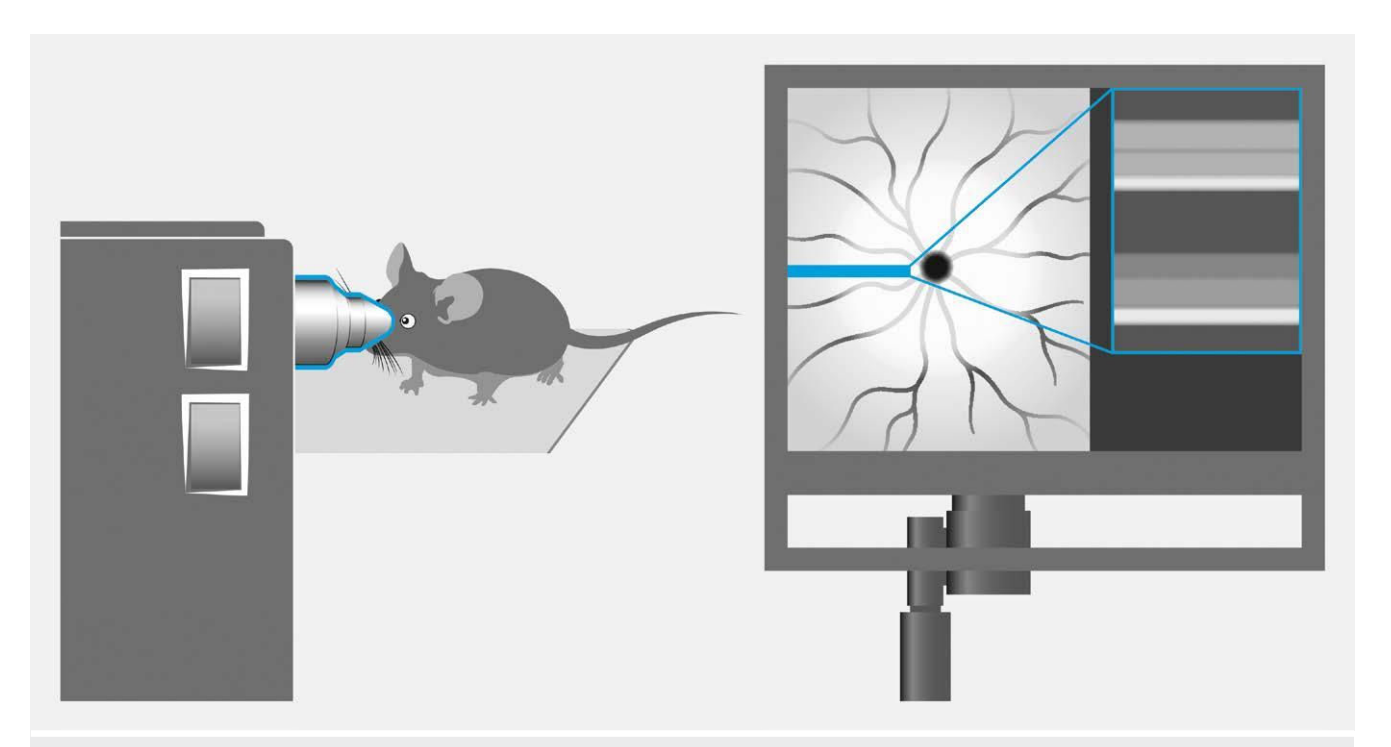
#### Ceroid Lipofuszinose Modell

Die Untersuchung von retinalen Veränderungen in Mausmodellen der neuronalen Ceroidlipofuszinose mittels OCT bietet weitere Einblicke in die translationalen Möglichkeiten der visuellen Systemmodelle [25]. Die spezifischen Modelle, Ppt1-/- und Cln3-/- Mäuse, repräsentieren die infantile und juvenile Form der neuronalen Ceroidlipofuszinose. Die OCT-Aufnahmen dieser Modelle offenbaren eine erhöhte Akkumulation von autofluoreszierender Ablagerungen, sowie eine Reduktion der Netzhautdicke, was auf signifikante neuronale Veränderungen hinweist.

# Strukturelle und funktionelle Evaluierungsmethoden

#### Optische Kohärenztomographie

Verantwortlich für die nur mäßigen Behandlungsmöglichkeiten neurodegenerativer Erkrankungen ist einerseits der Zeitverlauf der Neurodegeneration, die meist erst im späteren Erkrankungsstadium zum Tragen kommt und sich sehr langsam vollzieht, anderseits die Schwierigkeit, degenerative Prozesse nachzuweisen. Seit den 90er Jahren steht mit der optischen Kohärenztomographie eine relativ einfache, schnelle und nicht-invasive Methode (> Abb. 2) zur



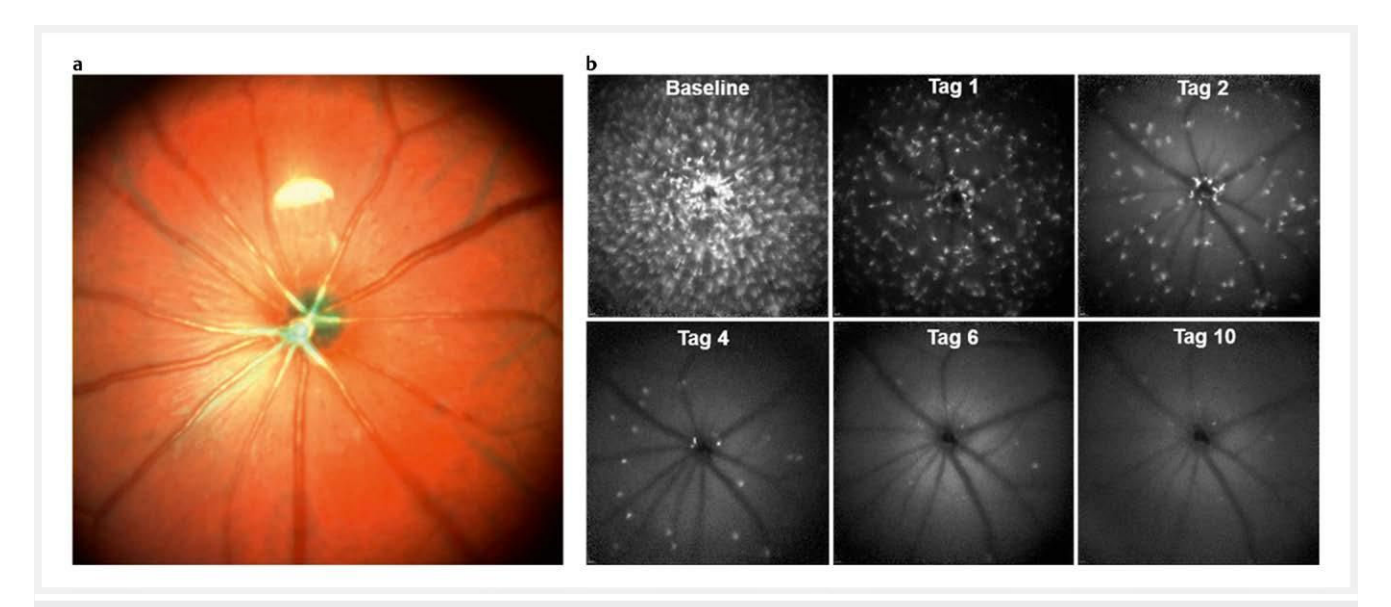
▶ **Abb. 2** Darstellung einer OCT-Messapparatur bei einer Maus. Die Messung erfolgt am anästhesierten Tier durch die mit einer Kontaktlinse bedeckte und weitgetropfte Pupille (A). Skizzenhafte Darstellung einer OCT-Messung des Mäuseauges, mit hervorgehobenen inneren Netzhautschichten (IRL) und äußere Netzhausschichten (ORL), analysiert durch eine KI-gestützte Software (C).

genauen Untersuchung der Retina im Auge zur Verfügung [26]. Ursprünglich in der Ophthalmologie verwendet, eröffnete OCT neue Möglichkeiten in der Neurologie, insbesondere bei der Untersuchung von primär neurodegenerative Erkrankungen aber auch sekundär neurodegenerative Erkrankungen wie der MS, bei der neurodegenerative Prozesse eine zentrale Rolle in späteren, chronischen Phasen spielen.

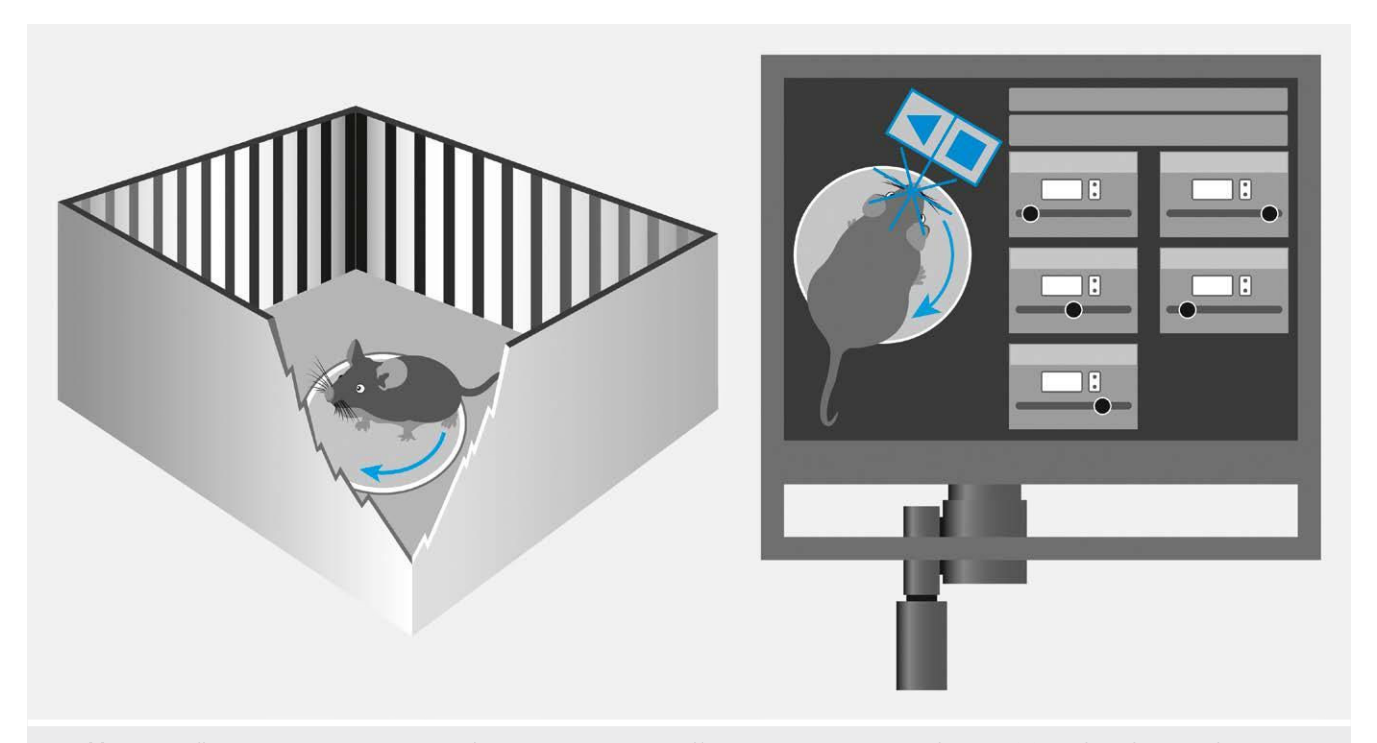
Nachdem bereits 1999 eine erste Studie mit Hilfe der inzwischen kommerziell erhältlichen OCT-Technologie eine Degeneration der retinalen Nervenfaserschicht (RNFL) bei MS-Patienten mit stattgehabter Sehnerventzündung (Retrobulbärneuritis) nachgewiesen hatte [27], konnten im Verlauf auch eine Degeneration der RNFL bei MS-Patienten unabhängig von einer Retrobulbärneuritis nachgewiesen werden [28, 29]. Die neue Generation der OCT Geräte mit der sogenannten Spectral Domain Technologie, die sich die unterschiedlichen Brechungseigenschaften des retinalen Gewebes für Licht verschiedener Wellenlängen zunutze macht, lässt sich eine deutlich höhere Auflösung von bis zu 1−2 µm erreichen, sodass heutzutage neben der RNFL eine Quantifizierung auch aller anderen retinalen Schichten möglich ist [21, 30, 31] und neue morphologische Veränderungen der retinalen Struktur, wie Mikrozysten in der inneren Körnerzellschicht (INL) identifiziert werden können [32]. Aufgrund ihrer hohen Auflösung erlaubt die Spectral Domain OCT-Technologie des weiteren die genaue Messung retinaler Strukturen in Mäusen und Ratten [31, 33, 34]. So lässt sich die retinale Neurodegeneration bzw. Schwellung von bestimmten Zellschichten in Tiermodellen untersuchen. Gegenüber histologischen Methoden hat dies den entscheidenden Vorteil, dass longitudinale Messungen möglich sind, sodass weniger Versuchstiere nötig sind und die experimentelle Variabilität reduziert wird, da die inter-Tier Variabilität wegfällt. Darüber hinaus erfolgt die Messung direkt in vivo, sodass es im Gegensatz zur Histologie, nicht zu Artefakten oder Änderungen der retinalen Schichtdicken durch Färbung und Fixierung kommen kann. Die Software des OCT-Geräts generiert darüber hinaus aus vielen einzelnen Querscans volumetrische Daten der gesamten Retina, sodass im Gegensatz zur Histologie nicht nur an einzelnen Punkten gemessen wird, sondern fast die gesamte Netzhaut volumetrisch analysiert wird. Gegenüber Magnetresonanztomographie (MRT) Messungen des Hirnvolumens stellt die Methode einen erheblich geringeren Aufwand dar und hat den Vorteil, dass es sich bei der Retina mit ihren unterschiedlichen Schichten um ein einfacheres und klar definiertes System handelt, in dem sich Atrophie und Degeneration besser quantifizieren lassen. Daher eignet sich die Untersuchung retinaler Degeneration mittels longitudinaler OCT-Untersuchungen und histologischer Evaluation als Endpunkt ideal, aber auch um bei nicht-inflammatorischen Modellen, Schäden zu untersuchen. OCT-Messungen zeigen eine signifikante Korrelation mit MRT-Daten und klinischen Evaluationen [35-40]. Obwohl ein vollständiger Ersatz der MRT durch OCT unrealistisch ist, ergänzt die OCT die diagnostische und prognostische Landschaft um wichtige quantitative Informationen, besonders im Bereich der Neurodegeneration. Aufgrund ihrer Kosteneffizienz könnte die OCT eine engmaschige Überwachung der Patienten erlauben, was zu einer früheren Identifizierung von Anomalien und einer schnelleren Anpassung der Therapiestrategien führt.

#### Konfokale Scanning Laser Ophthalmoskopie (cSLO)

Die konfokale Scanning Laser Ophthalmoskopie, ermöglicht die gleichzeitige konfokale Abbildung mit Infrarot, grünen und blauen



▶ **Abb. 3** Unter Verwendung eines grünen, roten und blauen Lasers wird ein Multicolor-Abbildung der Retina einer C57BL/6J-Maus durch Mittelung von 100 Bildern erzeugt (A). cSLO-Bildgebung von GFP-markierten Mikroglia. Mit dem grünen Laser und dem Fluoreszenzangiographiefilter wurden retinale Ganglienzellen in einer transgenen CX3CR1-GFP Maus abgebildet. Die Mikroglia wurden mit dem CSF-1R-Antagonisten PLX3397 depletiert (B).



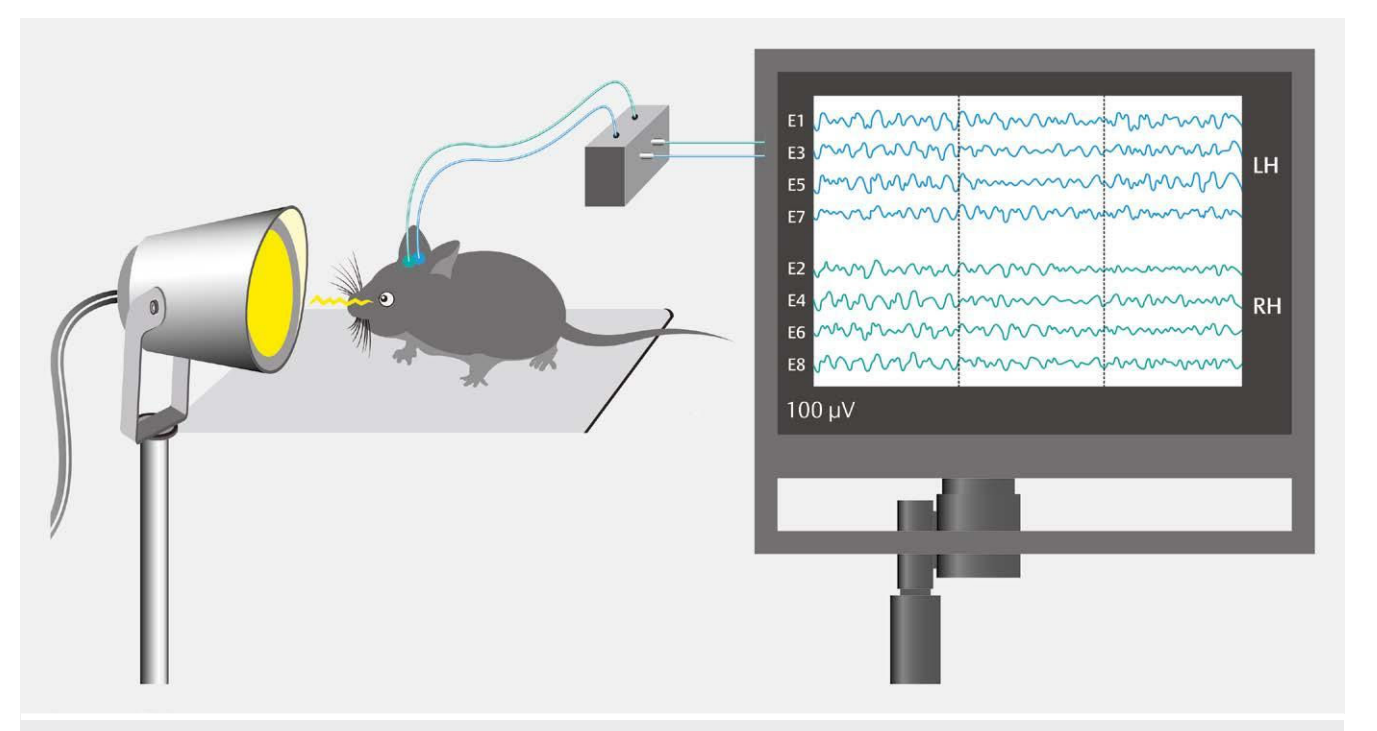
▶ **Abb. 4** Darstellung einer OMR-Messapparatur bei einer Maus. Eine C57Bl/6 J Maus in einer OMR-Messkammer (A). Tracking der Versuchstiere erfolgt in temporal nasaler Richtung. Skizzenhafte Darstellung einer OMR-Messung zur Beurteilung der Sehfähigkeit bei einer Maus (B).

Lasern (488, 514, 788 und 820 nm). Diese Aufnahmen können Informationen über verschiedene Netzhautpathologien oder Veränderungen des retinalen Pigmentepithels liefern. "Multicolor" Bilder der Netzhaut dienen dazu, den allgemeinen Gesundheitszustand des Gewebes und der Nervenfasern während inflammatorischen, degenerativen und ischämischen Modellen zu bewerten. Außerdem können longitudinal, in vivo-Abbildungen von verschiedenen

Fluorophoren wie GFP markierten retinalen Zellen erzeugt werden [9, 41], um dynamische Prozesse zu beobachten (> **Abb. 3**).

### **Optomotorische Reaktions-Messung**

Bei Mäusen und Ratten kann die Funktion des visuellen Systems mittels optomotorischer Reaktions-Messung (OMR) beurteilt werden. Die Tiere werden hierzu auf eine Plattform in der Mitte eines



▶ **Abb. 5** Darstellung einer VEP-Messapparatur bei einer Maus. Visuelle Stimuli induzieren elektrische Aktivitäten im Gehirn, deren Nervenleitgeschwindigkeit und Verarbeitungsqualität durch Elektroden aufgezeichnet, weiterverarbeitet, und auf einem Monitor zur Bewertung visualisiert werden.

Quadrats von Bildschirmen platziert ( Abb. 4). Mittels einer Software wird ein virtueller Zylinder mit umlaufenden Gittern erzeugt. Die Tiere verfolgen dieses Gitter unwillkürlich mit reflexiven Kopfund Halsbewegungen. Diese Tracking-Bewegungen können über eine Kamera oberhalb des Tiers mittels einer Software gemessen werden. Die optomotorische Reaktion wird bei Sehstörungen reduziert oder vollständig behindert. Da das Tracking der Tiere nur in temporal-nasaler Richtung erfolgt, kann zwischen der Funktion beider Augen unterschieden werden. Damit kann die funktionelle Konsequenz struktureller Neurodegeneration auch in vivo analysiert werden [42].

Ebenso wie die OCT-Messung hat die OMR-Methode den Vorteil, dass longitudinale Messungen möglich sind, sodass weniger Versuchstiere nötig sind und die experimentelle Variabilität reduziert wird. Darüber hinaus müssen die Tiere hierbei nicht fixiert oder anästhesiert werden, sodass eine Belastung der Versuchstiere stark reduziert wird.

### Visuell Evozierte Potentiale

Die Messung visuell evozierter Potentiale (VEP) ist eine neurophysiologische Untersuchungsmethode, bei der die elektrische Aktivität des Gehirns in Antwort auf visuelle Reize gemessen wird (> Abb. 5). Diese Methode wird häufig verwendet, um die Funktion des Sehnervs und der Sehbahn im Gehirn zu beurteilen. Diese Methode ist besonders nützlich, um quantifizierbare Aussagen insbesondere über den Myelinisierungszustand der Axone des Sehnervens auf funktioneller Ebene zu treffen. Die Möglichkeit, longitudinale Messungen durchzuführen und ebenso die mögliche Translation des gewählten Settings in die Klinik zu übertragen, macht es zu einem wertvollen Tool. Als Beispiel wäre hier die EAE

erwähnenswert: VEP-Messungen können in vivo quantifizierbare Aussagen zum Myelinisierungszustand des Sehnervens geben und beispielsweise so die Wirksamkeit von remyelinisierenden Therapien bewerten. Die Studien von Cordano et al., 2022 und Marenna et al., 2023 [10, 43], hebt die Nutzung von VEPs als eine nicht-invasive Methode hervor, um neurophysiologische Veränderungen im EAE Mausmodell zu evaluieren. Die Beobachtungen, dass Veränderungen in den VEP-Komponenten P1 und P2 sowie in ihren Latenzzeiten vor den Veränderungen der N1-Komponente auftreten, signalisieren eine frühe intrakortikale Dysfunktion. Die Validität des Modells wird durch die Parallelität vieler beobachteter neurophysiologischer Veränderungen und therapeutischer Effekte im EAE-Modell mit denjenigen bei MS-Patienten gestärkt. Trotz der inhärenten Unterschiede zwischen dem Modell und der menschlichen Erkrankung bietet es wertvolle Einblicke in die Pathophysiologie der MS und dient als ein wichtiges Werkzeug für die Identifizierung und Bewertung potenzieller Behandlungsansätze. Wie auch die OCT- Untersuchung, bietet die VEP-Untersuchung optimale translationale Bedingungen, da die erfassten Parameter und methodischen Setting sich zwischen Tiermodell und Patient sehr ähneln. Die möglichen Limitationen bei der Anwendung von VEPs in der Klinik umfassen Fehlinterpretationen durch fehlende Patientenkooperation oder extreme Müdigkeit des Patienten, sowie Fehlplatzierungen des Cursors, was die Genauigkeit bei der Bestimmung von Latenz und Amplitude beeinträchtigt.

## Bedeutung

Diese Beispiele untermauern, dass bildgebende und funktionelle Untersuchungen des visuellen Systems wertvolle und valide Instrumente in der neurologischen Forschung darstellen. Sie ermöglichen ein tieferes Verständnis der Pathologie und des Verlaufs neurodegenerativer Erkrankungen. Die hierbei generierten Daten bieten nicht nur zuverlässige Indikatoren für die Krankheitsaktivität bei neurologischen Erkrankungen, sondern eröffnen auch wichtige Einblicke in die Mechanismen der Krankheitsentwicklung und -progression. Diese Modelle erweitern die Möglichkeiten für den translationalen Einsatz in Diagnostik, Prognostik und Monitoring neurodegenerativer und neuroinflammatorischer Zustände und unterstreichen die Wichtigkeit translationaler Bestrebungen in der Neurologie.

Zudem bieten Fortschritte im Bereich der künstlichen Intelligenz neue Perspektiven: Durch maschinelles Lernen mittels tomographischer und physiologischer Daten, könnten dank verbesserter Analysegenauigkeit und der präziseren Erkennung pathologischer Merkmale sowie beschleunigten Analysekapazitäten, ein signifikanter Entwicklungsimpuls in diesem Bereich gesetzt werden, wie Arbeiten und Analysen von Li & Wan, 2022; Ortiz et al., 2023; Przybyszewski et al., 2023 und Wagner et al., 2023 [22, 44–46], eindrucksvoll zeigen konnten. Solche Fortentwicklungen sind ausschlaggebend, um das visuelle System dauerhaft in den routinemäßigen klinischen Alltag zu integrieren.

### Limitationen

Obwohl Modelle des visuellen Systems entscheidende Einblicke in neurologische Erkrankungen bieten, sind sie nicht ohne Limitationen. Ein wesentlicher Nachteil ist die teilweise mangelnde Übertragbarkeit der aus Tiermodellen gewonnenen Ergebnisse auf den Menschen. Trotz der evolutionären Konservierung retinaler Strukturen unterscheiden diese sich zwischen Tieren und Menschen doch in einigen Aspekten [47], was die direkte Übertragung der Forschungsergebnisse auf menschliche Patienten einschränken kann.

Zum Beispiel handelt es sich bei Ratten und Mäusen um afoveate Säugetiere, deren Retina keine Fovea Zentralis (beim Menschen der Punkt des schärfsten Sehens) aufweist. Daher werden im Mausmodell die quantitativen Messungen der retinalen Schichten meist auf den Sehnervenkopf zentriert, während bei Menschen meist die Fovea anvisiert wird.

Ein weiteres Problem stellt die Nutzung transgener Modelle, wie CX3CR1-GFP Mäuse oder SOX10-GFP Mauslinien dar, in denen Gliazellen live via cSLO-Methodik beobachtet werden können. Diese Möglichkeiten sind in der klinischen Praxis bei Patienten natürlicherweise nicht umsetzbar.

Ein kritischer Punkt ist auch, dass Tiermodelle, wie das EAE-Modell oder verschiedene Parkinson-Modelle [48], menschliche Krankheiten nicht vollständig abbilden. Solche Modelle können spezifische Aspekte einer Krankheit simulieren, erfassen jedoch nicht die gesamte Komplexität menschlicher pathologischer Zustände. Die daraus resultierenden Erkenntnisse können daher nur bedingt zur Diagnose, Krankheitsprognose oder Vorhersage der Wirksamkeit von Therapien beim Menschen herangezogen werden.

Schließlich ist die eingeschränkte Skalierbarkeit von Forschungsergebnissen eine bedeutende Limitation. Während Modelle des visuellen Systems in kontrollierten Laborumgebungen funktionieren, können die variierenden klinischen Settings und die genetische Vielfalt des Menschen dazu führen, dass die Ergebnisse nicht universell anwendbar sind. Die individuellen Unterschiede zwischen Patienten, wie genetische Variationen, Lebensstilfaktoren und Komorbiditäten, erschweren die direkte Übertragung von im Tiermodell gewonnenen Erkenntnissen auf die allgemeine Patientenpopulation.

Zusammenfassend sind die Modelle des visuellen Systems zwar ein wertvolles Werkzeug in der neurologischen Forschung, doch es ist entscheidend, ihre Grenzen zu kennen und die Ergebnisse im Kontext der genannten Einschränkungen zu interpretieren. Die kontinuierliche Entwicklung und Verfeinerung dieser Modelle sind essentiell, um die translationale Vergleichbarkeit zu optimieren.

#### Interessenkonflikt

Die Autorinnen/Autoren geben an, dass kein Interessenkonflikt besteht.

#### Literatur

- Oertel FC, Hastermann M, Paul F. Delimiting MOGAD as a disease entity using translational imaging. Front Neurol 2023; 14: 1216477. DOI: 10.3389/fneur.2023.1216477
- [2] Dietrich M, Koska V, Hecker C et al. Protective effects of 4-aminopyridine in experimental optic neuritis and multiple sclerosis. Brain 2020; 143: 1127–1142. DOI: 10.1093/brain/awaa062
- [3] Ingwersen J, De Santi L, Wingerath B et al. Nimodipine confers clinical improvement in two models of experimental autoimmune encephalomyelitis. J Neurochem 2018. DOI: 10.1111/jnc.14324
- [4] Levy H, Assaf Y, Frenkel D. Characterization of brain lesions in a mouse model of progressive multiple sclerosis. Exp Neurol 2010; 226: 148–158. DOI: 10.1016/j.expneurol.2010.08.017
- [5] Rothhammer V, Kenison JE, Tjon E et al. Sphingosine 1-phosphate receptor modulation suppresses pathogenic astrocyte activation and chronic progressive CNS inflammation. Proc Natl Acad Sci USA 2017; 114: 2012–2017. DOI: 10.1073/pnas.1615413114
- [6] Dietrich M, Hecker C, Nasiri M et al. Neuroprotective Properties of Dimethyl Fumarate Measured by Optical Coherence Tomography in Non-inflammatory Animal Models. Front Neurol 2020; 11: 601628. DOI: 10.3389/fneur.2020.601628
- [7] Hilla AM, Diekmann H, Fischer D. Microglia Are Irrelevant for Neuronal Degeneration and Axon Regeneration after Acute Injury. J Neurosci 2017; 37: 6113–6124. DOI: 10.1523/JNEUROSCI.0584-17.2017
- [8] Meyer R, Weissert R, Diem R et al. Acute neuronal apoptosis in a rat model of multiple sclerosis. J Neurosci 2001; 21: 6214–6220. DOI: 10.1523/JNEUROSCI.21-16-06214.2001
- [9] Sindi M, Hecker C, Issberner A et al. S1PR-1/5 modulator RP-101074 shows beneficial effects in a model of central nervous system degeneration. Front Immunol 2023; 14: 1234984. DOI: 10.3389/ fimmu.2023.1234984
- [10] Cordano C, Sin JH, Timmons G et al. Validating visual evoked potentials as a preclinical, quantitative biomarker for remyelination efficacy. Brain 2022: 145: 3943–3952. DOI: 10.1093/brain/awac207
- [11] Marenna S, Huang S-C, Dalla Costa G et al. Visual Evoked Potentials to Monitor Myelin Cuprizone-Induced Functional Changes. Front Neurosci 2022; 16: 820155. DOI: 10.3389/fnins.2022.820155
- [12] Parisi V, Restuccia R, Fattapposta F et al. Morphological and functional retinal impairment in Alzheimer's disease patients. Clin Neurophysiol 2001; 112: 1860–1867. DOI: 10.1016/s1388-2457(01)00620-4

- [13] Loh EH-T, Ong Y-T, Venketasubramanian N et al. Repeatability and Reproducibility of Retinal Neuronal and Axonal Measures on Spectral-Domain Optical Coherence Tomography in Patients with Cognitive Impairment. Front Neurol 2017; 8: 359. DOI: 10.3389/ fneur.2017.00359
- [14] Garcia-Martin E, Larrosa JM, Polo V et al. Distribution of retinal layer atrophy in patients with Parkinson disease and association with disease severity and duration. Am J Ophthalmol 2014; 157: 470–478.e2. DOI: 10.1016/j.ajo.2013.09.028
- [15] Satue M, Obis J, Alarcia R et al. Retinal and Choroidal Changes in Patients with Parkinson's Disease Detected by Swept-Source Optical Coherence Tomography. Curr Eye Res 2018; 43: 109–115. DOI: 10.1080/02713683.2017.1370116
- [16] Simonett J, Chou J, Siddique N et al. Ocular Manifestations and Optic Nerve Changes in Patients with Amyotrophic Lateral Sclerosis (ALS). Investigative Ophthalmology & Visual Science 2013; 54: 4382–4382
- [17] Mukherjee N, McBurney-Lin S, Kuo A et al. Retinal thinning in amyotrophic lateral sclerosis patients without ophthalmic disease. PLoS One 2017; 12: e0185242. DOI: 10.1371/journal.pone.0185242
- [18] Kersten HM, Danesh-Meyer HV, Kilfoyle DH et al. Optical coherence tomography findings in Huntington's disease: a potential biomarker of disease progression. J Neurol 2015; 262: 2457–2465. DOI: 10.1007/ s00415-015-7869-2
- [19] Gatto E, Parisi V, Persi G et al. Optical coherence tomography (OCT) study in Argentinean Huntington's disease patients. Int J Neurosci 2018; 128: 1157–1162. DOI: 10.1080/00207454.2018.1489807
- [20] Tsokolas G, Tsaousis KT, Diakonis VF et al. Optical Coherence Tomography Angiography in Neurodegenerative Diseases: A Review. Eye Brain 2020; 12: 73–87. DOI: 10.2147/EB.S193026
- [21] Albrecht P, Müller A-K, Südmeyer M et al. Optical coherence tomography in parkinsonian syndromes. PLoS One 2012; 7: e34891. DOI: 10.1371/journal.pone.0034891
- [22] Wagner SK, Romero-Bascones D, Cortina-Borja M et al. Retinal Optical Coherence Tomography Features Associated With Incident and Prevalent Parkinson Disease. Neurology 2023; 101: e1581–e1593. DOI: 10.1212/WNL.0000000000207727
- [23] Tran KKN, Wong VHY, Lim JKH et al. Characterization of retinal function and structure in the MPTP murine model of Parkinson's disease. Sci Rep 2022; 12: 7610. DOI: 10.1038/s41598-022-11495-z
- [24] Harper DJ, Augustin M, Lichtenegger A et al. Retinal analysis of a mouse model of Alzheimer's disease with multicontrast optical coherence tomography. Neurophotonics 2020; 7: 015006. DOI: 10.1117/1.NPh.7.1.015006
- [25] Groh J, Stadler D, Buttmann M et al. Non-invasive assessment of retinal alterations in mouse models of infantile and juvenile neuronal ceroid lipofuscinosis by spectral domain optical coherence tomography. Acta Neuropathol Commun 2014; 2: 54. DOI: 10.1186/2051-5960-2-54
- [26] Huang D, Swanson EA, Lin CP et al. Optical coherence tomography. Science 1991; 254: 1178–1181. DOI: 10.1126/science.1957169
- [27] Parisi V, Manni G, Spadaro M et al. Correlation between morphological and functional retinal impairment in multiple sclerosis patients. Invest Ophthalmol Vis Sci 1999; 40: 2520–2527
- [28] Albrecht P, Fröhlich R, Hartung H-P et al. Optical coherence tomography measures axonal loss in multiple sclerosis independently of optic neuritis. J Neurol 2007; 254: 1595–1596. DOI: 10.1007/ s00415-007-0538-3
- [29] Costello F, Hodge W, Pan YI et al. Differences in retinal nerve fiber layer atrophy between multiple sclerosis subtypes. J Neurol Sci 2009; 281: 74–79. DOI: 10.1016/j.jns.2009.02.354
- [30] Albrecht P, Müller A-K, Ringelstein M et al. Retinal neurodegeneration in Wilson's disease revealed by spectral domain optical coherence tomography. PLoS One 2012; 7: e49825. DOI: 10.1371/journal. pone.0049825

- [31] Albrecht P, Ringelstein M, Müller AK et al. Degeneration of retinal layers in multiple sclerosis subtypes quantified by optical coherence tomography. Mult Scler 2012; 18: 1422–1429. DOI: 10.1177/1352458512439237
- [32] Saidha S, Sotirchos ES, Ibrahim MA et al. Microcystic macular oedema, thickness of the inner nuclear layer of the retina, and disease characteristics in multiple sclerosis: a retrospective study. Lancet Neurol 2012; 11: 963–972. DOI: 10.1016/S1474-4422(12)70213-2
- [33] Dietrich M, Hecker C, Hilla A et al. Using Optical Coherence Tomography and Optokinetic Response As Structural and Functional Visual System Readouts in Mice and Rats. | Vis Exp 2019. DOI: 10.3791/58571
- [34] Fischer MD, Huber G, Beck SC et al. Noninvasive, in vivo assessment of mouse retinal structure using optical coherence tomography. PLoS One 2009; 4: e7507. DOI: 10.1371/journal.pone.0007507
- [35] Sotirchos ES, Saidha S. OCT is an alternative to MRI for monitoring MS YES. Mult Scler 2018; 24: 701–703. DOI: 10.1177/1352458517753722
- [36] Saidha S, Calabresi PA. Optical coherence tomography should be part of the routine monitoring of patients with multiple sclerosis: yes. Mult Scler 2014; 20: 1296–1298. DOI: 10.1177/1352458514541509
- [37] Castonguay A, Lefebvre J, Lesage F et al. Comparing three-dimensional serial optical coherence tomography histology to MRI imaging in the entire mouse brain. J Biomed Opt 2018; 23: 1–9. DOI: 10.1117/1. JBO.23.1.016008
- [38] Manogaran P, Hanson JVM, Olbert ED et al. Optical Coherence Tomography and Magnetic Resonance Imaging in Multiple Sclerosis and Neuromyelitis Optica Spectrum Disorder. Int J Mol Sci 2016; 17: 1894. DOI: 10.3390/ijms17111894
- [39] Brandt AU, Martinez-Lapiscina EH, Nolan R et al. Monitoring the Course of MS With Optical Coherence Tomography. Curr Treat Options Neurol 2017; 19: 15. DOI: 10.1007/s11940-017-0452-7
- [40] Oh J, Sotirchos ES, Saidha S et al. Relationships between quantitative spinal cord MRI and retinal layers in multiple sclerosis. Neurology 2015; 84: 720–728. DOI: 10.1212/WNL.000000000001257
- [41] Frenger MJ, Hecker C, Sindi M et al. Semi-Automated Live Tracking of Microglial Activation in CX3CR1GFP Mice During Experimental Autoimmune Encephalomyelitis by Confocal Scanning Laser Ophthalmoscopy. Front Immunol 2021; 12: 761776. DOI: 10.3389/ fimmu.2021.761776
- [42] Hecker C, Dietrich M, Issberner A et al. Comparison of different optomotor response readouts for visual testing in experimental autoimmune encephalomyelitis-optic neuritis. J Neuroinflammation 2020; 17: 216. DOI: 10.1186/s12974-020-01889-z
- [43] Marenna S, Rossi E, Huang S-C et al. Visual evoked potentials waveform analysis to measure intracortical damage in a preclinical model of multiple sclerosis. Front Cell Neurosci 2023; 17: 1186110. DOI: 10.3389/fncel.2023.1186110
- [44] Li M, Wan C. The use of deep learning technology for the detection of optic neuropathy. Quant Imaging Med Surg 2022; 12: 2129–2143. DOI: 10.21037/qims-21-728
- [45] Ortiz M, Mallen V, Boquete L et al. Diagnosis of multiple sclerosis using optical coherence tomography supported by artificial intelligence. Mult Scler Relat Disord 2023; 74: 104725. DOI: 10.1016/j. msard.2023.104725
- [46] Przybyszewski AW, Śledzianowski A, Chudzik A et al. Machine Learning and Eye Movements Give Insights into Neurodegenerative Disease Mechanisms. Sensors (Basel) 2023; 23: 2145. DOI: 10.3390/s23042145
- [47] Volland S, Esteve-Rudd J, Hoo J et al. A comparison of some organizational characteristics of the mouse central retina and the human macula. PLoS One 2015; 10: e0125631. DOI: 10.1371/journal.pone.0125631
- [48] Lama J, Buhidma Y, Fletcher EJR et al. Animal models of Parkinson's disease: a guide to selecting the optimal model for your research. Neuronal Signal 2021; 5: NS20210026. DOI: 10.1042/NS20210026

## 5. References

- AlAmmar, W. A., Albeesh, F. H., Ibrahim, L. M., Algindan, Y. Y., Yamani, L. Z., & Khattab, R. Y. (2021). Effect of omega-3 fatty acids and fish oil supplementation on multiple sclerosis: A systematic review. *Nutritional Neuroscience*, 24(7), 569–579. https://doi.org/10.1080/1028415X.2019.1659560
- Albrecht, P., Ringelstein, M., Muller, A. K., Keser, N., Dietlein, T., Lappas, A., Foerster, A., Hartung, H. P., Aktas, O., & Methner, A. (2012). Degeneration of retinal layers in multiple sclerosis subtypes quantified by optical coherence tomography. *Multiple Sclerosis Journal*, *18*(10), 1422–1429. https://doi.org/10.1177/1352458512439237
- Alnawaiseh, M., Rosentreter, A., Hillmann, A., Alex, A. F., Niekämper, D., Heiduschka, P., Pap, T., & Eter, N. (2016). OCT angiography in the mouse: A novel evaluation method for vascular pathologies of the mouse retina. *Experimental Eye Research*, *145*, 417–423. https://doi.org/10.1016/j.exer.2016.02.012
- Bechtold, D. A., Kapoor, R., & Smith, K. J. (2004). Axonal protection using flecainide in experimental autoimmune encephalomyelitis. *Annals of Neurology*, *55*(5), 607–616. https://doi.org/10.1002/ana.20045
- Bliss O'Bryhim, B. O. (2023). *Use of OCT in Neurodegenerative Diseases— Https://eyewiki.aao.org/Use\_of\_OCT\_in\_Neurodegenerative\_Diseases*.

  https://eyewiki.aao.org/Use\_of\_OCT\_in\_Neurodegenerative\_Diseases
- Bonnet, C. S., Williams, A. S., Gilbert, S. J., Harvey, A. K., Evans, B. A., & Mason, D. J. (2015). AMPA/kainate glutamate receptors contribute to inflammation, degeneration and pain related behaviour in inflammatory stages of arthritis. *Annals of the Rheumatic Diseases*, 74(1), 242–251. https://doi.org/10.1136/annrheumdis-2013-203670
- Bretin, S., Louis, C., Seguin, L., Wagner, S., Thomas, J.-Y., Challal, S., Rogez, N., Albinet, K., Iop, F., Villain, N., Bertrand, S., Krazem, A., Bérachochéa, D., Billiald, S., Tordjman, C., Cordi, A., Bertrand, D., Lestage, P., & Danober, L. (2017). Pharmacological characterisation of S 47445, a novel positive allosteric modulator of AMPA receptors. *PLoS ONE*, 12(9), e0184429. https://doi.org/10.1371/journal.pone.0184429
- Buhler, L. A., Samara, R., Guzman, E., Wilson, C. L., Krizanac-Bengez, L., Janigro, D., & Ethell, D. W. (2009). Matrix metalloproteinase-7 facilitates immune access to the CNS in experimental autoimmune encephalomyelitis. *BMC Neuroscience*, 10, 17. https://doi.org/10.1186/1471-2202-10-17
- Cadavid, D., Mellion, M., Hupperts, R., Edwards, K. R., Calabresi, P. A., Drulović, J., Giovannoni, G., Hartung, H.-P., Arnold, D. L., Fisher, E., Rudick, R., Mi, S., Chai, Y., Li, J., Zhang, Y., Cheng, W., Xu, L., Zhu, B., Green, S. M., ... SYNERGY study investigators. (2019). Safety and efficacy of opicinumab in patients with relapsing multiple sclerosis (SYNERGY): A randomised, placebo-controlled, phase 2 trial. *The Lancet. Neurology*, 18(9), 845–856. https://doi.org/10.1016/S1474-4422(19)30137-1
- Calabrese, E. J. (2008). Hormesis: Why it is important to toxicology and toxicologists. *Environmental Toxicology and Chemistry*, 27(7), 1451–1474. https://doi.org/10.1897/07-541
- Constantinescu, C. S., Farooqi, N., O'Brien, K., & Gran, B. (2011). Experimental autoimmune encephalomyelitis (EAE) as a model for multiple sclerosis (MS): EAE as model for MS. *British Journal of Pharmacology*, *164*(4), 1079–1106. https://doi.org/10.1111/j.1476-5381.2011.01302.x
- Dedoni, S., Scherma, M., Camoglio, C., Siddi, C., Dazzi, L., Puliga, R., Frau, J., Cocco, E., & Fadda, P. (2023). An overall view of the most common experimental models for multiple sclerosis. *Neurobiology of Disease*, *184*, 106230. https://doi.org/10.1016/j.nbd.2023.106230
- Destot-Wong, K.-D., Liang, K., Gupta, S. K., Favrais, G., Schwendimann, L., Pansiot, J., Baud, O., Spedding, M., Lelièvre, V., Mani, S., & Gressens, P. (2009). The AMPA receptor positive allosteric modulator, S18986, is neuroprotective against neonatal excitotoxic and inflammatory brain damage through BDNF synthesis. *Neuropharmacology*, *57*(3), 277–286. https://doi.org/10.1016/j.neuropharm.2009.05.010
- Dietrich, M., Hecker, C., Hilla, A., Cruz-Herranz, A., Hartung, H.-P., Fischer, D., Green, A., & Albrecht, P. (2019). Using Optical Coherence Tomography and Optokinetic Response As Structural and Functional Visual System Readouts in Mice and Rats. *Journal of Visualized Experiments: JoVE*, 143. https://doi.org/10.3791/58571

- Dietrich, M., Hecker, C., Martin, E., Langui, D., Gliem, M., Stankoff, B., Lubetzki, C., Gruchot, J., Göttle, P.,
  Issberner, A., Nasiri, M., Ramseier, P., Beerli, C., Tisserand, S., Beckmann, N., Shimshek, D., Petzsch,
  P., Akbar, D., Levkau, B., ... Albrecht, P. (2022). Increased Remyelination and Proregenerative
  Microglia Under Siponimod Therapy in Mechanistic Models. Neurology(R) Neuroimmunology & Neuroinflammation, 9(3), e1161. https://doi.org/10.1212/NXI.0000000000001161
- Dietrich, M., Helling, N., Hilla, A., Heskamp, A., Issberner, A., Hildebrandt, T., Kohne, Z., Küry, P., Berndt, C., Aktas, O., Fischer, D., Hartung, H.-P., & Albrecht, P. (2018). Early alpha-lipoic acid therapy protects from degeneration of the inner retinal layers and vision loss in an experimental autoimmune encephalomyelitis-optic neuritis model. *Journal of Neuroinflammation*, *15*(1), 71. https://doi.org/10.1186/s12974-018-1111-y
- Disanto, G., Morahan, J. M., & Ramagopalan, S. V. (2012). Multiple sclerosis: Risk factors and their interactions. *CNS & Neurological Disorders Drug Targets*, *11*(5), 545–555. https://doi.org/10.2174/187152712801661266
- Du Pasquier, R. A., Pinschewer, D. D., & Merkler, D. (2014). Immunological mechanism of action and clinical profile of disease-modifying treatments in multiple sclerosis. *CNS Drugs*, 28(6), 535–558. https://doi.org/10.1007/s40263-014-0160-8
- Dziedzic, A., Miller, E., Saluk-Bijak, J., & Bijak, M. (2020). The GPR17 Receptor-A Promising Goal for Therapy and a Potential Marker of the Neurodegenerative Process in Multiple Sclerosis. *International Journal of Molecular Sciences*, 21(5), 1852. https://doi.org/10.3390/ijms21051852
- Edinger, A., & Habibi, M. (2024). The evolution of multiple sclerosis disease-modifying therapies: An update for pharmacists. *American Journal of Health-System Pharmacy: AJHP: Official Journal of the American Society of Health-System Pharmacists*, 81(2), 37–55. https://doi.org/10.1093/ajhp/zxad247
- Evonuk, K. S., Wang, S., Mattie, J., Cracchiolo, C. J., Mager, R., Ferenčić, Ž., Sprague, E., Carrier, B., Schofield, K., Martinez, E., Stewart, Z., Petrosino, T., Johnson, G. A., Yusuf, I., Plaisted, W., Naiman, Z., Delp, T., Carter, L., & Marušić, S. (2023). Bruton's tyrosine kinase inhibition reduces disease severity in a model of secondary progressive autoimmune demyelination. *Acta Neuropathologica Communications*, 11(1), 115. https://doi.org/10.1186/s40478-023-01614-w
- Fang, X.-Y., Zhang, W.-M., Zhang, C.-F., Wong, W.-M., Li, W., Wu, W., & Lin, J.-H. (2016). Lithium accelerates functional motor recovery by improving remyelination of regenerating axons following ventral root avulsion and reimplantation. *Neuroscience*, *329*, 213–225. https://doi.org/10.1016/j.neuroscience.2016.05.010
- Fannon, J., Tarmier, W., & Fulton, D. (2015). Neuronal activity and AMPA-type glutamate receptor activation regulates the morphological development of oligodendrocyte precursor cells. *Glia*, *63*(6), 1021–1035. https://doi.org/10.1002/glia.22799
- Ferent, J., Zimmer, C., Durbec, P., Ruat, M., & Traiffort, E. (2013). Sonic Hedgehog Signaling Is a Positive Oligodendrocyte Regulator during Demyelination. *The Journal of Neuroscience*, *33*(5), 1759. https://doi.org/10.1523/JNEUROSCI.3334-12.2013
- Galetta, K. M., Calabresi, P. A., Frohman, E. M., & Balcer, L. J. (2011). Optical coherence tomography (OCT): Imaging the visual pathway as a model for neurodegeneration. *Neurotherapeutics: The Journal of the American Society for Experimental NeuroTherapeutics*, 8(1), 117–132. https://doi.org/10.1007/s13311-010-0005-1
- Gao, X., Deng, L., Wang, Y., Yin, L., Yang, C., Du, J., & Yuan, Q. (2016). GDNF Enhances Therapeutic Efficiency of Neural Stem Cells-Based Therapy in Chronic Experimental Allergic Encephalomyelitis in Rat. *Stem Cells International*, 2016, 1431349. https://doi.org/10.1155/2016/1431349
- Gatto, E., Parisi, V., Persi, G., Fernandez Rey, E., Cesarini, M., Luis Etcheverry, J., Rivera, P., & Squitieri, F. (2018). Optical coherence tomography (OCT) study in Argentinean Huntington's disease patients. *The International Journal of Neuroscience*, 128(12), 1157–1162. https://doi.org/10.1080/00207454.2018.1489807
- Glatigny, S., & Bettelli, E. (2018). Experimental Autoimmune Encephalomyelitis (EAE) as Animal Models of Multiple Sclerosis (MS). *Cold Spring Harbor Perspectives in Medicine*, 8(11), a028977. https://doi.org/10.1101/cshperspect.a028977

- Greer, J. M., Sobel, R. A., Sette, A., Southwood, S., Lees, M. B., & Kuchroo, V. K. (1996). Immunogenic and encephalitogenic epitope clusters of myelin proteolipid protein. *Journal of Immunology (Baltimore, Md.: 1950)*, 156(1), 371–379.
- Guo, L., Li, Y., Lin, H., Ji, X., Li, J., Que, L., Zhang, Y., Rong, Y., & Wang, J. (2004). Evaluation of a rat model of experimental autoimmune encephalomyelitis with human MBP as antigen. *Cellular & Molecular Immunology*, *1*(5), 387–391.
- Haines, J. D., Inglese, M., & Casaccia, P. (2011). Axonal Damage in Multiple Sclerosis. *The Mount Sinai Journal of Medicine*, *New York*, 78(2), 231–243. https://doi.org/10.1002/msj.20246
- Hauser, S. L., & Oksenberg, J. R. (2006). The neurobiology of multiple sclerosis: Genes, inflammation, and neurodegeneration. *Neuron*, *52*(1), 61–76. https://doi.org/10.1016/j.neuron.2006.09.011
- Hecker, C., Dietrich, M., Issberner, A., Hartung, H.-P., & Albrecht, P. (2020). Comparison of different optomotor response readouts for visual testing in experimental autoimmune encephalomyelitis-optic neuritis. *Journal of Neuroinflammation*, 17(1), 216. https://doi.org/10.1186/s12974-020-01889-z
- Ishibashi, T., Lee, P. R., Baba, H., & Fields, R. D. (2009). Leukemia inhibitory factor regulates the timing of oligodendrocyte development and myelination in the postnatal optic nerve. *Journal of Neuroscience Research*, 87(15), 3343. https://doi.org/10.1002/jnr.22173
- Kaufmann, M., Schaupp, A.-L., Sun, R., Coscia, F., Dendrou, C. A., Cortes, A., Kaur, G., Evans, H. G., Mollbrink, A., Navarro, J. F., Sonner, J. K., Mayer, C., DeLuca, G. C., Lundeberg, J., Matthews, P. M., Attfield, K. E., Friese, M. A., Mann, M., & Fugger, L. (2022). Identification of early neurodegenerative pathways in progressive multiple sclerosis. *Nature Neuroscience*, 25(7), 944–955. https://doi.org/10.1038/s41593-022-01097-3
- Khalatbari Mohseni, G., Hosseini, S. A., Majdinasab, N., & Cheraghian, B. (2023). Effects of N-acetylcysteine on oxidative stress biomarkers, depression, and anxiety symptoms in patients with multiple sclerosis. *Neuropsychopharmacology Reports*, 43(3), 382–390. https://doi.org/10.1002/npr2.12360
- Khalilian, B., Madadi, S., Fattahi, N., & Abouhamzeh, B. (2021). Coenzyme Q10 enhances remyelination and regulate inflammation effects of cuprizone in corpus callosum of chronic model of multiple sclerosis. *Journal of Molecular Histology*, 52(1), 125–134. https://doi.org/10.1007/s10735-020-09929-x
- Kopec, B. M., Kiptoo, P., Zhao, L., Rosa-Molinar, E., & Siahaan, T. J. (2020). Noninvasive Brain Delivery and Efficacy of BDNF to Stimulate Neuroregeneration and Suppression of Disease Relapse in EAE Mice. *Molecular Pharmaceutics*, *17*(2), 404–416. https://doi.org/10.1021/acs.molpharmaceut.9b00644
- Krämer, J., Balloff, C., Weise, M., Koska, V., Uthmeier, Y., Esderts, I., Nguyen-Minh, M., Zimmerhof, M., Hartmann, A., Dietrich, M., Ingwersen, J., Lee, J.-I., Havla, J., Kümpfel, T., Kerschensteiner, M., Häußler, V., Heesen, C., Stellmann, J.-P., Zimmermann, H. G., ... Albrecht, P. (2024). Evolution of retinal degeneration and prediction of disease activity in relapsing and progressive multiple sclerosis. *Nature Communications*, *15*(1), 5243. https://doi.org/10.1038/s41467-024-49309-7
- Krämer, J., & Wiendl, H. (2024). Bruton tyrosine kinase inhibitors in multiple sclerosis: Evidence and expectations. *Current Opinion in Neurology*, *37*(3), 237–244. https://doi.org/10.1097/WCO.0000000000001269
- Kwilasz, A. J., Clements, M. A., Larson, T. A., Harris, K. M., Litwiler, S. T., Woodall, B. J., Todd, L. S., Schrama, A. E. W., Mitten, E. H., Maier, S. F., Van Dam, A.-M., Rice, K. C., & Watkins, L. R. (2022). Involvement of TLR2-TLR4, NLRP3, and IL-17 in pain induced by a novel Sprague-Dawley rat model of experimental autoimmune encephalomyelitis. *Frontiers in Pain Research (Lausanne, Switzerland)*, 3, 932530. https://doi.org/10.3389/fpain.2022.932530
- Lee, K., Goodman, L., Fourie, C., Schenk, S., Leitch, B., & Montgomery, J. M. (2016). AMPA Receptors as Therapeutic Targets for Neurological Disorders. *Advances in Protein Chemistry and Structural Biology*, 103, 203–261. https://doi.org/10.1016/bs.apcsb.2015.10.004
- Lee, M. H., Shin, J. I., Yang, J. W., Lee, K. H., Cha, D. H., Hong, J. B., Park, Y., Choi, E., Tizaoui, K., Koyanagi, A., Jacob, L., Park, S., Kim, J. H., & Smith, L. (2022). Genome Editing Using CRISPR-Cas9 and Autoimmune Diseases: A Comprehensive Review. *International Journal of Molecular Sciences*, 23(3), 1337. https://doi.org/10.3390/ijms23031337
- Li, Z.-M., Chen, L.-X., & Li, H. (2019). Voltage-gated Sodium Channels and Blockers: An Overview and Where Will They Go? *Current Medical Science*, *39*(6), 863–873. https://doi.org/10.1007/s11596-019-2117-0

- Liu, R., Du, S., Zhao, L., Jain, S., Sahay, K., Rizvanov, A., Lezhnyova, V., Khaibullin, T., Martynova, E., Khaibullina, S., & Baranwal, M. (2022). Autoreactive lymphocytes in multiple sclerosis: Pathogenesis and treatment target. *Frontiers in Immunology*, *13*. https://doi.org/10.3389/fimmu.2022.996469
- Lyons, J. A., Ramsbottom, M. J., Trotter, J. L., & Cross, A. H. (2002). Identification of the encephalitogenic epitopes of CNS proteolipid protein in BALB/c mice. *Journal of Autoimmunity*, 19(4), 195–201. https://doi.org/10.1006/jaut.2002.0619
- Makoukji, J., Belle, M., Meffre, D., Stassart, R., Grenier, J., Shackleford, G., Fledrich, R., Fonte, C., Branchu, J., Goulard, M., de Waele, C., Charbonnier, F., Sereda, M. W., Baulieu, E.-E., Schumacher, M., Bernard, S., & Massaad, C. (2012). Lithium enhances remyelination of peripheral nerves. *Proceedings of the National Academy of Sciences of the United States of America*, 109(10), 3973–3978. https://doi.org/10.1073/pnas.1121367109
- Manouchehri, N., Salinas, V. H., Rabi Yeganeh, N., Pitt, D., Hussain, R. Z., & Stuve, O. (2022). Efficacy of Disease Modifying Therapies in Progressive MS and How Immune Senescence May Explain Their Failure. *Frontiers in Neurology*, *13*. https://doi.org/10.3389/fneur.2022.854390
- Marenna, S., Castoldi, V., d'Isa, R., Marco, C., Comi, G., & Leocani, L. (2019). Semi-invasive and non-invasive recording of visual evoked potentials in mice. *Documenta Ophthalmologica. Advances in Ophthalmology*, 138(3), 169–179. https://doi.org/10.1007/s10633-019-09680-z
- Markovic-Plese, S., Pinilla, C., & Martin, R. (2004). The initiation of the autoimmune response in multiple sclerosis. *Clinical Neurology and Neurosurgery*, *106*(3), 218–222. https://doi.org/10.1016/j.clineuro.2004.02.018
- McGinley, M. P., & Cohen, J. A. (2021). Sphingosine 1-phosphate receptor modulators in multiple sclerosis and other conditions. *Lancet (London, England)*, 398(10306), 1184–1194. https://doi.org/10.1016/S0140-6736(21)00244-0
- McPherson, R. C., Cambrook, H. E., O'Connor, R. A., & Anderton, S. M. (2014). Induction of passive EAE using myelin-reactive CD4+ T cells. *Methods in Molecular Biology (Clifton, N.J.)*, 1193, 187–198. https://doi.org/10.1007/978-1-4939-1212-4 17
- Mendel, I., Kerlero de Rosbo, N., & Ben-Nun, A. (1995). A myelin oligodendrocyte glycoprotein peptide induces typical chronic experimental autoimmune encephalomyelitis in H-2b mice: Fine specificity and T cell receptor V beta expression of encephalitogenic T cells. *European Journal of Immunology*, 25(7), 1951–1959. https://doi.org/10.1002/eji.1830250723
- Messias, C. V., Santana-Van-Vliet, E., Lemos, J. P., Moreira, O. C., Cotta-de-Almeida, V., Savino, W., & Mendes-da-Cruz, D. A. (2016). Sphingosine-1-Phosphate Induces Dose-Dependent Chemotaxis or Fugetaxis of T-ALL Blasts through S1P1 Activation. *PloS One*, 11(1), e0148137. https://doi.org/10.1371/journal.pone.0148137
- Moccia, M., Capacchione, A., Lanzillo, R., Carbone, F., Micillo, T., Perna, F., De Rosa, A., Carotenuto, A., Albero, R., Matarese, G., Palladino, R., & Brescia Morra, V. (2019). Coenzyme Q10 supplementation reduces peripheral oxidative stress and inflammation in interferon-β1a-treated multiple sclerosis. *Therapeutic Advances in Neurological Disorders*, 12, 1756286418819074. https://doi.org/10.1177/1756286418819074
- Moradbeygi, K., Parviz, M., Rezaeizadeh, H., Zargaran, A., Sahraian, M. A., Mehrabadi, S., Nikbakhtzadeh, M., & Zahedi, E. (2021). Anti-LINGO-1 improved remyelination and neurobehavioral deficit in cuprizone-induced demyelination. *Iranian Journal of Basic Medical Sciences*, 24(7), 900–907. https://doi.org/10.22038/ijbms.2021.53531.12043
- Morsali, D., Bechtold, D., Lee, W., Chauhdry, S., Palchaudhuri, U., Hassoon, P., Snell, D. M., Malpass, K., Piers, T., Pocock, J., Roach, A., & Smith, K. J. (2013). Safinamide and flecainide protect axons and reduce microglial activation in models of multiple sclerosis. *Brain: A Journal of Neurology*, *136*(Pt 4), 1067–1082. https://doi.org/10.1093/brain/awt041
- Motl, R. W., Sandroff, B. M., Kwakkel, G., Dalgas, U., Feinstein, A., Heesen, C., Feys, P., & Thompson, A. J. (2017). Exercise in patients with multiple sclerosis. *The Lancet. Neurology*, *16*(10), 848–856. https://doi.org/10.1016/S1474-4422(17)30281-8
- Nagatsu, T., & Sawada, M. (2006). Molecular mechanism of the relation of monoamine oxidase B and its inhibitors to Parkinson's disease: Possible implications of glial cells. *Journal of Neural Transmission*. *Supplementum*, 71, 53–65. https://doi.org/10.1007/978-3-211-33328-0\_7

- Nikbin, B., Bonab, M. M., Khosravi, F., & Talebian, F. (2007). Role of B cells in pathogenesis of multiple sclerosis. *International Review of Neurobiology*, 79, 13–42. https://doi.org/10.1016/S0074-7742(07)79002-5
- Partin, K. M. (2015). AMPA receptor potentiators: From drug design to cognitive enhancement. *Current Opinion in Pharmacology*, 20, 46–53. https://doi.org/10.1016/j.coph.2014.11.002
- Popescu, B. F. Gh., Pirko, I., & Lucchinetti, C. F. (2013). Pathology of Multiple Sclerosis: Where Do We Stand? *Continuum: Lifelong Learning in Neurology*, 19(4 Multiple Sclerosis), 901–921. https://doi.org/10.1212/01.CON.0000433291.23091.65
- Press Release: Tolebrutinib demonstrated a 31% delay in time to onset of confirmed disability progression in non-relapsing secondary progressive multiple sclerosis phase 3 study. (n.d.). Retrieved January 7, 2025, from https://www.sanofi.com/en/media-room/press-releases/2024/2024-09-20-09-30-00-2949552
- Rojas, P., de Hoz, R., Ramírez, A. I., Ferreras, A., Salobrar-Garcia, E., Muñoz-Blanco, J. L., Urcelay-Segura, J. L., Salazar, J. J., & Ramírez, J. M. (2019). Changes in Retinal OCT and Their Correlations with Neurological Disability in Early ALS Patients, a Follow-Up Study. *Brain Sciences*, 9(12), 337. https://doi.org/10.3390/brainsci9120337
- Samjoo, I. A., Worthington, E., Drudge, C., Zhao, M., Cameron, C., Häring, D. A., Stoneman, D., Klotz, L., & Adlard, N. (2021). Efficacy classification of modern therapies in multiple sclerosis. *Journal of Comparative Effectiveness Research*, 10(6), 495–507. https://doi.org/10.2217/cer-2020-0267
- Sanoobar, M., Dehghan, P., Khalili, M., Azimi, A., & Seifar, F. (2016). Coenzyme Q10 as a treatment for fatigue and depression in multiple sclerosis patients: A double blind randomized clinical trial. *Nutritional Neuroscience*, 19(3), 138–143. https://doi.org/10.1179/1476830515Y.0000000002
- Satoh, J., Kino, Y., Yanaizu, M., Tosaki, Y., Sakai, K., Ishida, T., & Saito, Y. (2017). Expression of GPR17, a regulator of oligodendrocyte differentiation and maturation, in Nasu-Hakola disease brains. *Intractable & Rare Diseases Research*, 6(1), 50–54. https://doi.org/10.5582/irdr.2016.01097
- Sharrad, D., Chugh, P., Slee, M., & Bacchi, S. (2023). Defining progression independent of relapse activity (PIRA) in adult patients with relapsing multiple sclerosis: A systematic review . *Multiple Sclerosis and Related Disorders*, 78, 104899. https://doi.org/10.1016/j.msard.2023.104899
- Shin, T., Ahn, M., & Matsumoto, Y. (2012). Mechanism of experimental autoimmune encephalomyelitis in Lewis rats: Recent insights from macrophages. *Anatomy & Cell Biology*, 45(3), 141–148. https://doi.org/10.5115/acb.2012.45.3.141
- Siegert, E., Paul, F., Rothe, M., & Weylandt, K. H. (2017). The effect of omega-3 fatty acids on central nervous system remyelination in fat-1 mice. *BMC Neuroscience*, 18(1), 19. https://doi.org/10.1186/s12868-016-0312-5
- Sindi, M., Hecker, C., Issberner, A., Ruck, T., Meuth, S. G., Albrecht, P., & Dietrich, M. (2023). S1PR-1/5 modulator RP-101074 shows beneficial effects in a model of central nervous system degeneration. *Frontiers in Immunology*, *14*, 1234984. https://doi.org/10.3389/fimmu.2023.1234984
- Smith, K. J., & McDonald, W. I. (1999). The pathophysiology of multiple sclerosis: The mechanisms underlying the production of symptoms and the natural history of the disease. *Philosophical Transactions of the Royal Society of London. Series B, Biological Sciences*, *354*(1390), 1649–1673. https://doi.org/10.1098/rstb.1999.0510
- Sotirchos, E. S., & Saidha, S. (2018). OCT is an alternative to MRI for monitoring MS YES. *Multiple Sclerosis* (Houndmills, Basingstoke, England), 24(6), 701–703. https://doi.org/10.1177/1352458517753722
- Stefferl, A., Brehm, U., Storch, M., Lambracht-Washington, D., Bourquin, C., Wonigeit, K., Lassmann, H., & Linington, C. (1999). Myelin Oligodendrocyte Glycoprotein Induces Experimental Autoimmune Encephalomyelitis in the "Resistant" Brown Norway Rat: Disease Susceptibility Is Determined by MHC and MHC-Linked Effects on the B Cell Response1. *The Journal of Immunology*, *163*(1), 40–49. https://doi.org/10.4049/jimmunol.163.1.40
- STOSIC-GRUJICIC, S., RAMIC, Z., BUMBASIREVIC, V., HARHAJI, L., & MOSTARICA-STOJKOVIC, M. (2004). Induction of experimental autoimmune encephalomyelitis in Dark Agouti rats without adjuvant. *Clinical and Experimental Immunology*, *136*(1), 49–55. https://doi.org/10.1111/j.1365-2249.2004.02418.x
- Subei, A. M., & Cohen, J. A. (2015). Sphingosine 1-Phosphate Receptor Modulators in Multiple Sclerosis. *CNS Drugs*, 29(7), 565–575. https://doi.org/10.1007/s40263-015-0261-z

- Szpakowski, P., Ksiazek-Winiarek, D., & Glabinski, A. (2021). Targeting Antigen-Presenting Cells in Multiple Sclerosis Treatment. *Applied Sciences*, 11(18), Article 18. https://doi.org/10.3390/app11188557
- Tan, L. J., Kennedy, M. K., & Miller, S. D. (1992). Regulation of the effector stages of experimental autoimmune encephalomyelitis via neuroantigen-specific tolerance induction. II. Fine specificity of effector T cell inhibition. *Journal of Immunology (Baltimore, Md.: 1950)*, 148(9), 2748–2755.
- Tan, Y.-Y., Jenner, P., & Chen, S.-D. (2022). Monoamine Oxidase-B Inhibitors for the Treatment of Parkinson's Disease: Past, Present, and Future. *Journal of Parkinson's Disease*, 12(2), 477–493. https://doi.org/10.3233/JPD-212976
- Taylor, C. P., & Narasimhan, L. S. (1997). Sodium channels and therapy of central nervous system diseases. *Advances in Pharmacology (San Diego, Calif.)*, *39*, 47–98.
- Terry, R. L., Ifergan, I., & Miller, S. D. (2016). Experimental Autoimmune Encephalomyelitis in Mice. *Methods in Molecular Biology (Clifton, N.J.)*, 1304, 145–160. https://doi.org/10.1007/7651 2014 88
- Tilborg, E. van, Theije, C. G. M. de, Hal, M. van, Wagenaar, N., Vries, L. S. de, Benders, M. J., Rowitch, D. H., & Nijboer, C. H. (2018). Origin and dynamics of oligodendrocytes in the developing brain:

  Implications for perinatal white matter injury. *Glia*, 66(2), 221. https://doi.org/10.1002/glia.23256
- Tompkins, S. M., Padilla, J., Dal Canto, M. C., Ting, J. P.-Y., Van Kaer, L., & Miller, S. D. (2002). De novo central nervous system processing of myelin antigen is required for the initiation of experimental autoimmune encephalomyelitis. *Journal of Immunology (Baltimore, Md.: 1950)*, *168*(8), 4173–4183. https://doi.org/10.4049/jimmunol.168.8.4173
- Traiffort, E., Zakaria, M., Laouarem, Y., & Ferent, J. (2016). Hedgehog: A Key Signaling in the Development of the Oligodendrocyte Lineage. *Journal of Developmental Biology*, 4(3). https://doi.org/10.3390/jdb4030028
- Walton, C., King, R., Rechtman, L., Kaye, W., Leray, E., Marrie, R. A., Robertson, N., La Rocca, N., Uitdehaag, B., van der Mei, I., Wallin, M., Helme, A., Angood Napier, C., Rijke, N., & Baneke, P. (2020). Rising prevalence of multiple sclerosis worldwide: Insights from the Atlas of MS, third edition. *Multiple Sclerosis (Houndmills, Basingstoke, England)*, 26(14), 1816–1821. https://doi.org/10.1177/1352458520970841
- Wen, J., Ariyannur, P. S., Ribeiro, R., Tanaka, M., Moffett, J. R., Kirmani, B. F., Namboodiri, A. M. A., & Zhang, Y. (2016). Efficacy of N-Acetylserotonin and Melatonin in the EAE Model of Multiple Sclerosis. *Journal of Neuroimmune Pharmacology: The Official Journal of the Society on NeuroImmune Pharmacology*, 11(4), 763–773. https://doi.org/10.1007/s11481-016-9702-9
- Werner, S. R., Dotzlaf, J. E., & Smith, R. C. (2008). MMP-28 as a regulator of myelination. *BMC Neuroscience*, 9, 83. https://doi.org/10.1186/1471-2202-9-83
- Wood, H. (2024). BTK inhibitor falters in multiple sclerosis trials. *Nature Reviews. Neurology*, 20(5), 255. https://doi.org/10.1038/s41582-024-00958-8
- Wooliscroft, L., McCoy, S., Hildebrand, A., Rooney, W., Oken, B. S., Spain, R. I., Kuehl, K. S., Bourdette, D., & Cameron, M. (2023). Protocol for an exploratory, randomised, single-blind clinical trial of aerobic exercise to promote remyelination in multiple sclerosis. *BMJ Open*, 13(1), e061539. https://doi.org/10.1136/bmjopen-2022-061539
- Zhou, Y., Cuellar-Partida, G., Simpson Yap, S., Lin, X., Claflin, S., Burdon, K., Charlesworth, J., & Taylor, B. (2021). Utilising multi-large omics data to elucidate biological mechanisms within multiple sclerosis genetic susceptibility loci. *Multiple Sclerosis (Houndmills, Basingstoke, England)*, 27(14), 2141–2149. https://doi.org/10.1177/13524585211004422

## 6. Appendix

AMPA-PAM: AMPA-positive allosteric modulator

BDNF: Brain-derived neurotrophic factor

Brn3a: Brain-specific homeobox/POU domain protein 3A

BTK: Bruton's tyrosine kinase

BW: Body weight CC: Cell count

CFA: Complete Freund's adjuvants CNS: Central nervous system CNTF: Ciliary neurotrophic factor

CSLO: Confocal scanning laser ophthalmoscopy CX3CL1: Chemokine (C-X3-C motif) ligand 1

CX3CR1: CX3C chemokine receptor 1

CYP: Cytochrome P450

EAE: Experimental autoimmune encephalomyelitis

EBD: Evan's Blue Dye

EDSS: Expanded disability status scale

EGF: Epidermal growth factor ELM: External limiting membrane

(E)GFP: (Enhanced) green fluorescent protein

EBV: Epstein-Barr virus

FGF-2: Fibroblast growth factor-2

Fingo: Fingolimod

GCL: Ganglion cell layer

GDNF: Glial cell line-derived neurotrophic factor

GEE: Generalized estimation equation GPR-17: G protein-coupled receptor 17

HGF: Hepatocyte growth factor

HHI-LI-PRL: High-intensity light induced photoreceptor loss

IBA1: Ionized calcium-binding adaptor molecule 1

I-CAM-1 and I-CAM-2: Intercellular Adhesion Molecules 1 and 2

IGF-1: Insulin-like growth factor-1

IL-1β: Interleukin-1 beta IL-10: Interleukin-10 INL: Inner nuclear layer IPL: Inner plexiform layer IRL: Inner retinal layer

JAM-1, JAM-2, and JAM-3: Junctional Adhesion Molecules -1, -2 and -3

LI: Light induced

IS: Inner segment

LIF: Leukemia inhibitory factor

LWI-LI-PRL: Low-intensity light induced photoreceptor loss

MAO: Monoamine Oxidase MAO-B: Monoamine Oxidase B MBP: Myelin basic protein MD: Mean Difference

MOG: Myelin oligodendrocyte glycoprotein

MOG35-55: Myelin oligodendrocyte glycoprotein fragment 35-55

mOL's: Myelinating oligodendrocytes

MP: Mega pixels

MSCs: Mesenchymal stem cells

MS: Multiple sclerosis NAC: N-acetylcysteine

N-CAM-1: Neural Cell Adhesion Molecule 1

NFL: Nerve fiber layer NGF: Nerve growth factor NOD: Non-obese diabetic

OCT: Optical coherence tomography

OMR: Optomotor response

ON: Optic neuritis

ONL: Outer nuclear layer

OPC's: Oligodendrocytes progenitor cells

OPL: Outer plexiform layer ORL: Outer retinal layer OS: Outer segment P: Probability value

pMBMECs: Primary mouse brain microvascular endothelial cells

PDGF-A: Platelet-derived growth factor A PDGF-AA: Platelet-derived growth factor AA

PECAM-1: Platelet Endothelial Cell Adhesion Molecule

PF4778574: AMPA-PAM

P.i.: Post irradiation

PIRA: Progression independent of relapse activity

PRL: Photoreceptor loss PTX: Pertussis toxin

RPE: Retinal pigment epithelium

Shh: Sonic Hedgehog

S1P1: Sphingosine-1-phosphate receptor 1 S1P5: Sphingosine-1-phosphate receptor 5 Sox-2: Sex determining region Y (SRY) - box 2 TGF-β: Transforming growth factor-beta

TNF-α: Tumor necrosis factor-alpha
TMS: Transcranial Magnetic Stimulation

TRT: Total retinal thickness

V-CAM: Vascular Cell Adhesion Molecule 1

## 7. Acknowledgement/Danksagung

Mit großer Freude und tiefer Dankbarkeit möchte ich mich bei all denjenigen bedanken, die mich während der Arbeit an meiner Dissertation unterstützt und begleitet haben.

Mein aufrichtiger Dank gilt zunächst dir, Prof. Philipp Albrecht. Deine stetige Begleitung über die Jahre, deine fordernde und fördernde Art sowie deine konstruktive Kritik haben mich zu einem besseren Wissenschaftler gemacht. Du hast mich nicht nur fachlich, sondern auch persönlich weiterentwickelt und mir stets neue Perspektiven eröffnet. Ein besonderer Dank gebührt auch dir, Prof. Sven Meuth, der mir die Möglichkeit eröffnete, in den Laboratorien der Klinik für Neurologie zu arbeiten. Deine Unterstützung und die großartige Zusammenarbeit bei unseren gemeinsamen Projekten waren von großem Wert. Weiterhin möchte ich mich herzlich bei dir, Prof. Bodo Levkau, bedanken für deine Begleitung, dein Mentoring und deine gründliche Begutachtung meiner Dissertation.

Mein Dank geht auch an alle Mitarbeiter der Klinik für Neurologie. Die gute Atmosphäre, die stete Hilfsbereitschaft und die tolle Zusammenarbeit bei den verschiedenen Projekten haben maßgeblich zum Gelingen dieser Arbeit beigetragen. Besonders hervorheben möchte ich Vera, Rajeevan, Joel und Tim, deren Unterstützung und kollegialer Geist für mich sehr wertvoll waren. Ein besonderer Dank gilt meinen Arbeitsgruppenmitgliedern Andrea, Michael, Christina und Diana. Eure Zusammenarbeit und Unterstützung waren von großer Bedeutung für den Fortschritt und Erfolg meiner Arbeit.

Ohne die unermüdliche Unterstützung meiner Familie und insbesondere meiner Mutter, wäre diese Arbeit so nicht möglich gewesen. Eure bedingungslose Unterstützung und Glauben an mich, hat mir den Rücken gestärkt und mir die Kraft gegeben, dieses Projekt zu vollenden. Ich danke euch allen von Herzen.

# 8. Declaration/Erklärung

Ich versichere an Eides Statt, dass die Dissertation von mir selbständig und ohne unzulässige fremde Hilfe unter Beachtung der "Grundsätze zur Sicherung guter wissenschaftlicher Praxis an der Heinrich-Heine-Universität Düsseldorf" erstellt worden ist. Diese Dissertation wurde bei keiner anderen Institution in dieser oder ähnlicher Form bisher eingereicht und es wurden keine erfolglosen Promotionsversuche unternommen

Mustafa Sindi